PARACRINE REGULATION OF GLUCAGON SECRETION FROM PANCREATIC ISLETS

by

Amicia Devin Elliott

Dissertation

Submitted to the Faculty of the

Graduate School of Vanderbilt University

in partial fulfillment of the requirements

for the degree of

DOCTOR OF PHILOSOPHY

in

Molecular Physiology and Biophysics

August, 2014

Nashville, Tennessee

Approved:

Professor Roland Stein

Professor Eric Delpire

Professor Kevin Currie

Professor David Jacobson

To my parents, Deborah and Stephen Elliott, for instilling in me an insatiable love of learning and for challenging me with high expectations.

ACKNOWLEDGEMENTS

The work described in this thesis would not have been possible without the encouragement of several people who deserve special mention. I am very thankful to my advisor, Dave Piston, who provided many challenging opportunities to learn about physiology and introduced me to the wide worlds of quantitative fluorescence microscopy and biophysics. I am also thankful that Dave kept me interested in my work with new projects, collaborations, and learning opportunities. My committee members, Roland Stein, David Jacobson, Eric Delpire, and Kevin Currie have provided fantastic critical feedback and guidance during the course of my dissertation studies. I am grateful for their patience and dedication to developing my project(s) and perspectives.

Furthermore, I would like to acknowledge the Molecular Biophysics Training Program for the first two years of my funding. I must also thank my collaborators at Rice University, Liang Gao, Noah Bedard, and Tomasz Tkaczyk for teaching me so much about optics, spectral imaging, and instrumentation. Additionally, my Vanderbilt collaborators David DeGraff, Magda Grabowska, and Bob Matusik have my thanks for helping me expand my capabilities in experimental design to new biological systems and for partially funding my graduate work.

I am super grateful for the current and past members of the Piston Lab who contributed to my projects both experimentally and with positive encouragement, including Gert Kremers, Richard Benninger, Sylvan Le Marchand, Suba Gunawardana, and JP Baudoin. I am especially thankful for Alessandro Ustione who worked closely with me through the best and worst of the instrumentation project and has been a constant resource and friend. Additionally, a single mouse experiment would not have been done without one of Tara Schwetz, Chris Reissaus, Alessandro, or Troy Hutchens

giving them ketamine/xylazine injections, which I still find myself incapable of doing four years later. We have been a great team; Piston Lab represent! I'd also like to acknowledge the memory of Steve Head, our laboratory manager, who was an integral part of the first year and a half of my time in the Piston Lab.

One of the highlights of my graduate experience has been participating in the Quantitative Fluorescence Microscopy course at Mount Desert Island Biological Laboratories, first as a student and now as course assistant. Dave Piston, Anne Kenworthy, Simon Watkins, Claudette St. Croix, and Gert Kremers, who also worked with me during my rotation in the Piston lab, teach me new things every year and I am grateful for that experience.

Finally, my family and friends have been endlessly patient and encouraging throughout my dissertation research. All I can say is thank you, I couldn't have wished for better, and I love you all. You light up my life…

TABLE OF CONTENTS

Page

LIST OF FIGURES

Figure Page

CHAPTER 1

INTRODUCTION

Introductory comments

The two goals of this work have been to characterize the glucose-dependent paracrine regulation of glucagon inhibition from the pancreatic islet α-cells, and to develop a useful methodology for studying the dynamic molecular processes in these cells. Along the way, these goals have been facilitated by collaborative experiments with a variety of laboratories using different cellular systems, which are described. This document begins with an introduction to the physiology of the pancreatic islet of Langerhans and is followed by two chapters that describe specific materials and methods and the results of work conducted toward the first goal of identifying the paracrine mechanisms of glucagon inhibition. Next, an instrumentation overview follows, discussing the tools used for spectral imaging to monitor multiple molecular events in living cells, some of which were developed during this work. Additionally, the experimental findings and validation of the spectral imaging methodology is presented. This dissertation is then concluded with a discussion about the results, their relevance with respect to current literature as laid out in the introduction, ongoing studies, and future directions.

Glucose homeostasis and metabolic diseases

Metabolic diseases are a class of disorders that can be described as dysfunctions in the conversion of food into energy, or usage of stored energy. These include type 1 and type 2 diabetes mellitus, which are characterized by chronic hyperglycemia, and can lead to severe complications such as coronary artery disease, diabetic retinopathy, kidney disease, and stroke.

The prevalence of metabolic diseases in the world is rising at an alarming rate along with the rapidly increasing rates of obesity, a common comorbidity (Prevention 2011). The purification of insulin and first injections into diabetic patients in the 1920s heralded the end of type 1 diabetes as a conventionally lethal disease, but we now know that insulin is by no means a cure (Bliss 1997).

Diabetes is characterized by chronic hyperglycemia, which leads to other clinical signs including polyuria, polydipsia, and polyphagia. The chronic hyperglycemia is typically attributed to a reduction in glucose-stimulated insulin secretion or a reduction in the responsiveness of target tissues to secreted insulin that results in a loss of glycemic control. In addition to high blood glucose, diabetic patients present with low plasma insulin levels and high plasma glucagon and free fatty acid levels (Berg 2002). Insulin therapy and pharmaceuticals that stimulate insulin secretion drive glucose uptake by relevant tissues to oppose hyperglycemia, but alone, this is not sufficient to counter the effect of elevated plasma glucagon that accompanies diabetes (Cryer 2002).

Patients with type 2 diabetes often have insulin-resistant tissues, and thus require a different strategy for achieving euglycemia. This includes diet changes, exercise, and a rigorous blood glucose-monitoring regime; along with drugs that stimulate insulin secretion from the pancreas (Cryer 2002), or increase the insulin sensitivity of relevant tissues and block hepatic glucose production (Edgerton, Johnson et al. 2009). However, solely manipulating insulin levels or function to treat disease symptoms can have negative consequences as well. In fact, the largest risk factor for diabetic patients undergoing insulin-based treatment strategies is acute hypoglycemia, a condition responsible for 2-4% of deaths in type 1 diabetic patients. This insufficiency of current treatments for diabetes management has encouraged research efforts toward a more detailed understanding of the pathophysiology and associated risk factors, with the goal of preventing the onset of diabetes and developing more effective therapeutics. One of the avenues of this research is the regulation of glucagon secretion from the pancreatic α-cells

that contributes to the chronic hyperglycemia associated with diabetes. Much of this dissertation work has focused on the normal mechanisms of glucose in suppressing glucagon secretion.

Significance of glucagon in regulating blood glucose levels

In addition to a loss of insulin secretion or function, patients of both type 1 and type 2 diabetes have elevated plasma glucagon levels that contribute to the hyperglycemic state. It has even been suggested that glucagon hypersecretion is the primary driver of chronic hyperglycemia (Unger and Cherrington 2012). Often called a "counter-regulatory" hormone, glucagon stimulates the release of glucose into the blood stream when blood glucose levels are low, thus opposing the action of insulin. Though glucagon was identified just a few years before the purification of insulin (Kimball and Murlin 1923), it was not purified until later and comparatively little has been revealed about its regulation (Gromada, Franklin et al. 2007). However, it has become clear that glucagon-secreting islet α-cells play a critical role in glucose homeostasis. The persistence of α-cell function, especially in type 1 and advanced type 2 diabetes, makes the α-cell an important target for therapeutic intervention.

In addition to the chronic hyperglycemia that dysregulated glucagon secretion contributes to, severe hypoglycemia is just as dangerous. Glucose is the primary source of energy for the brain, which is unable to synthesize glucose and stores only small amounts as glycogen. Thus, low plasma levels of glucose can lead to brain damage, and if unaddressed, coma and death. Hypoglycemic episodes are also the primary limiting factor for glycemic control of both type 1 and late-stage type 2 diabetes, which limits the ability to consistently maintain normal blood glucose levels (Cryer 2002).

This has prompted a surge in research targeting glucagon regulation as a treatment for type 2 diabetes that has resulted in the development of glucagon receptor antagonists in varying stages of regulatory approval for treatment (Drucker and Nauck 2006; Christensen, Vedtofte et

al. 2011). Clinical studies with these drugs have demonstrated that accurate suppression of glucagon secretion restores normal glucose homeostasis in diabetic patients (Degn, Juhl et al. 2004; Madsbad 2009; Kielgast, Krarup et al. 2011). However, the off-target molecular effects remain uncharacterized and a number of negative side effects are being noted in some patients (Alves, Batel-Marques et al. 2012). This highlights the importance of understanding the molecular regulation of glucagon secretion, and the infusion of research will hopefully lead to safe and effective therapeutic options that target the α-cell. Additionally, recognizing that multiple tissue types have reciprocal relationships with the endocrine pancreas adds complexity to the healthy and pathological states but may also provide novel targets to pursue for treatment.

The islet of Langerhans

The human pancreas is largely made up of acinar tissue responsible for producing digestive enzymes, which include trypsin, chymotrypsin, RNase A, phospholipase A2, and α-amylase that are secreted into the pancreatic duct for functions in the small intestine. Approximately 1-2% of this tissue is composed of multicellular islands of cells called the islets of Langerhans that provide the endocrine function of the pancreas, which is responsible for maintaining glucose homeostasis. Approximately one million islets are scattered throughout the exocrine tissue separated by a thin collagen layer. They are roughly spherical in shape and exhibit diameters from 40 – 200 μM (with 1000 – 10,000 cells) (Motta, Macchiarelli et al. 1997; Kilimnik, Kim et al. 2009). There are several specialized cell types that make up the islet, including insulin-secreting β-cells, glucagon-secreting α-cells, somatostatin-secreting δ-cells, pancreatic polypeptide-producing cells, and ghrelin-containing ε-cells (Cabrera, Berman et al. 2006). These cell types cooperate in a number of ways including cell adhesions, junctional

protein interactions, via secreted factors, and membrane receptors (Marks, Tan et al. 1990; Ravier, Guldenagel et al. 2005; Konstantinova, Nikolova et al. 2007; Head, Orseth et al. 2012).

Islets are highly vascularized and highly innervated, two properties that are critical to their function. The fenestrated vasculature throughout the islet permits the rapid exchange of gases and facilitates the transport of hormones to other tissues via the blood stream. Additionally, though the endocrine pancreas accounts for 1-2% of the tissue, it receives 10-15% of the blood supply (Jansson and Hellerstrom 1983). It has also been proposed that blood flow through the islet vasculature, via both volume and direction, plays an important role in directing islet function (Bonner-Weir and Orci 1982; Nyman, Wells et al. 2008; Nyman, Ford et al. 2010). For example, studies have shown that blood moves directionally from β-cells toward α-cells, suggesting that proximal α-cells may see a higher concentration of insulin than more distal targets (Maruyama, Hisatomi et al. 1984). Similarly, somatostatin secreted from islet δ-cells, which are juxtaposed to both α- and β-cells, regulates the hormone secretion from both neighboring cell types (Schuit, Derde et al. 1989). In addition to the significant vascularization in the islet, the proximity of nerve terminals allows for parasympathetic and sympathetic nervous system control over the excitable islet cells, which provides another level of regulation for hormone secretion (Ahren 2000).

While many functions of the islets in maintaining blood glucose homeostasis are well conserved in mammals, the cytoarchitecture is quite different between human and mouse islets, which are the most common animal models for research (Cabrera, Berman et al. 2006; Kim, Miller et al. 2009). The differences in cellular composition can be seen in Figure 1-1 and are described in more detail below.

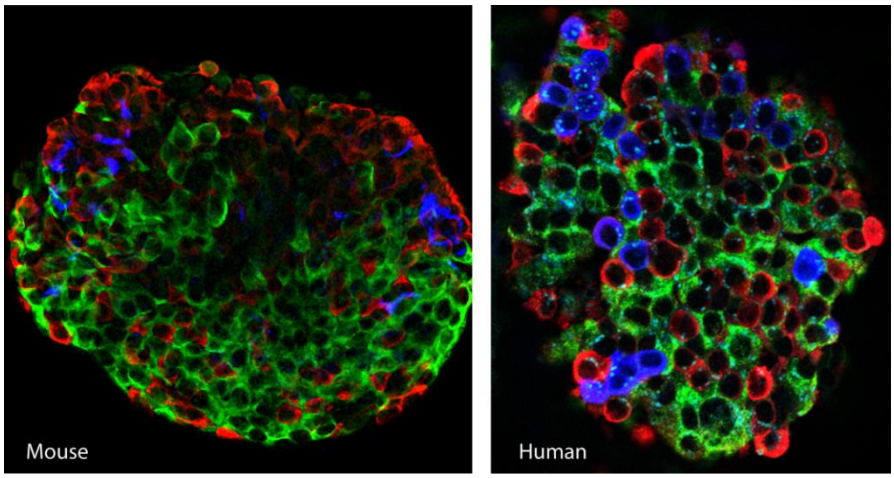

Figure 1-1. Murine and human islet α, β, and δ cell distribution. Immunofluorescence of a single optical section of a murine (left) and human (right) islet fixed and stained with primary antibodies to glucagon (red), insulin (green), and somatostatin (blue).

Human islet composition

While the same primary cell types have been identified in both human and murine islets, there is a greater variability in the composition and relative arrangement of these cell types in human islets. Generally, a human islet may be composed of ~60% β-cells, ~30% α-cells, and ~10% δ-cells, pp-cells, and ε-cells (Brissova, Fowler et al. 2005). The arrangement of the cells within the islet is also heterogeneous and allows a very high percentage of cells access to adjacent blood vessels. It has also been shown that the islet architecture is size-dependent, with larger islets having a larger fraction of α- and δ-cells, and smaller islets exhibiting similar cellular composition to murine islets. Historically, the apparent lack of organization in cellular distribution in human islets was proposed to play a role in the differences in islet function between species. However, recent studies using 3-D reconstruction techniques have provided more quantitative information about the islet cell distribution and populations. By fitting the data to either a model where particular cell-cell contacts have distinct probabilities or a model based on random mixture, this study reported a significantly better fit to the former. Additionally, the distance calculated between cells demonstrated that there was a preferential association

between α- and β-cells and allows for the intermingling of δ-cells (Kilimnik, Jo et al. 2012). The proximity of different cell types to each of the others as reported by both early and recent studies, likely contributes to paracrine regulation from secreted factors among the cells (Cabrera, Berman et al. 2006; Kilimnik, Jo et al. 2012).

There are also differences in gene expression between human and murine islets. For example it has been demonstrated that the glucose transporter expressed in human β-cells is GLUT1 and GLUT3, not GLUT2, which has been well-characterized in the mouse islets (McCulloch, van de Bunt et al. 2011). There are many other such differences between human and mouse islets including developmental transcription factors v-maf musculoaponeurotic fibrosarcoma oncogene homologue (MAF) B, PDX1, and glucose-regulated expression of PDX1, insulin, MAFA, and glucokinase, which suggest potentially significant differences in islet function between species (Dai, Brissova et al. 2012; Guo, Dai et al. 2013). There are also, however, a number of highly conserved regulatory processes that span many species' islets, including the regulation and molecular singling of insulin and glucagon in their target tissues (Noyes, Katz et al. 1995; Leevers 2001). Additionally, the function of pancreatic islets with respect to normalizing blood glucose levels is robust and nearly identical across species.

Murine islet composition

Rodent islets have a larger percentage of β-cells than human islets (> 70%) and fewer α-cells (< 20%), with the remainder (5-10%) made up of δ-cells, pp-cells, and ε-cells. In terms of arrangement about the islet, α-cells are typically found in the periphery, around a core of β-cells. The δ-cells, pp-cells, and ε-cells are distributed sparsely throughout the islet. While the significance of this arrangement is not well understood, extensive studies have been performed on the connectivity of islet β-cells by gap junctional complexes, which contribute greatly to the syncytial function and pulsatility observed in insulin secretion from coupled β-cells (Ravier,

Guldenagel et al. 2005; Head, Orseth et al. 2012). While human and murine islets are both highly vascularized, the cytoarchitecture of mouse islets lends them to directional regulation via blood flow. It is generally accepted that blood moves through islet capillaries toward peripheral α-cells from the core β-cells, which may underlie the paracrine regulation of glucagon secretion by secreted factors from the β-cells (Jansson and Hellerstrom 1983; Nyman, Ford et al. 2010).

Islet endocrine physiology

The peptide hormones insulin and glucagon secreted from islet cells make up the majority of the endocrine function of the pancreas. The integrated network of islet capillaries facilitates the delivery of these hormones to target tissues, which include the liver, muscle, and adipose tissue, depicted in Figure 1-2. Insulin and glucagon have opposing functions in the body; insulin is an anabolic hormone, triggering the uptake and storage of glucose, fatty acids, and amino acids. Glucagon is a catabolic hormone, mobilizing glucose, fatty acids, and amino acids from stores into the blood. Dysregulation of these hormones as the origin of diabetes is termed the "bi-hormonal" hypothesis, posited in the 1970s, which has driven an increase in the attention paid to glucagon in research as well as the clinic (Unger and Orci 1975).

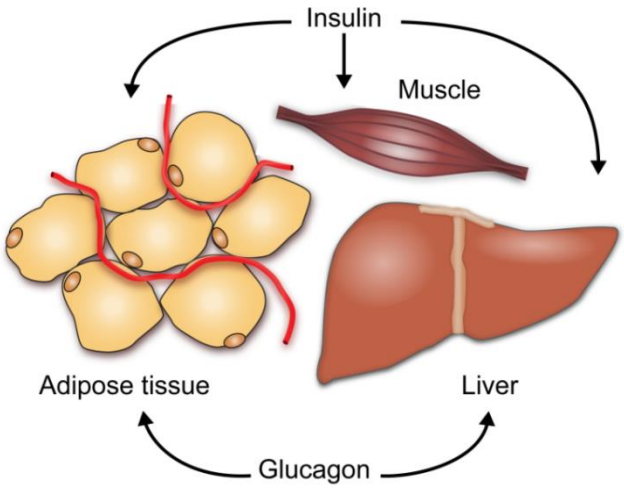

Figure 1-2. Target tissues for secreted islet hormones.

The liver is a critical site of hormone action because the blood flow proceeds directly there from the pancreas and it is one of the major storage locations for glucose. Upon increases in blood glucose levels and insulin-stimulated uptake into the liver, glucose is polymerized into the storage form, called glycogen. This is a branched polymer chain of glucose molecules connected by a α (1→4) linkage that is readily reduced for delivery to the blood stream by glucagon action on the liver when blood glucose levels are low (Berg 2002). Insulin has several functions in the liver including the stimulation of glycogen synthesis and glycolysis and the inhibition of glycogen breakdown and gluconeogenesis. Glucagon also significantly impacts liver function by stimulating amino acid uptake, gluconeogenesis, and glucose release while inhibiting glycolysis and fatty acid synthesis.

The opposing functions of insulin and glucagon on the liver are critical in the maintenance of blood glucose homeostasis, and their respective molecular mechanisms of action will be covered in a later section. Dysregulation of insulin and glucagon during diabetes leads to abnormalities in glycogen function and is the source of inappropriate ketone production characteristic of severe diabetes. The importance of the relationship between the islet hormones and the liver is highlighted by the strong association between many liver diseases and diabetes. There are three categories of associations that have been described: liver disease as a consequence of diabetes, diabetes and dysregulated glucose homeostasis resulting from liver disease, and coincidently occurring diabetes and liver disease (Wraith 1989; Iozzo, Pratipanawatr et al. 2001; Tolman, Fonseca et al. 2007).

Fatty acid metabolism is also regulated by glucagon and insulin in the adipose tissue. Triglycerides are the storage form of fatty acids, which are an important energy source and are readily reduced to provide free fatty acids to the blood (Spector 1975). Decreasing insulin levels during hypoglycemia relieve the inhibition of lipases in adipocytes, allowing the oxidation of triglycerides to free fatty acids (Goldberg, Eckel et al. 2009). Glucagon, as well as epinephrine, stimulates lipase activity to increase available energy during periods of high demand. Diabetic

patients exhibit increased levels of free fatty acids due to impairments in regulated triglyceride turnover, which correlates with hyperglucagonemia and the onset of peripheral and liver insulin resistance (Boden and Shulman 2002). Understanding the relationship between glucagon, insulin, and adipocytes is important for obesity and metabolic disease (Mauriege, Klein Kranenbarg et al. 1996).

Finally, the muscle is a critical target tissue for insulin, as ~80% of glucose uptake is accounted for by this tissue and stimulated by insulin receptor signaling (Thiebaud, Jacot et al. 1982). During diabetes, reduced glycogen synthase activity and impaired glycogen synthesis in the skeletal muscle are the primary defects responsible for insulin resistance in this tissue (DeFronzo and Tripathy 2009). Another interesting observation from studies of skeletal muscle diseases such as inclusion-body myositis, polymiositis, and inflammatory myositis is an association with insulin resistance and diabetes (Broccolini, Ricci et al. 2004; Cuthbertson, Smith et al. 2005; Limaye, Lester et al. 2010; Lopez-Menduina, Martin et al. 2010). The relationship between metabolic target tissues and islet hormone secretion has profound implications for irregularities in whole-body glucose homeostasis, though many questions remain unanswered at the level of cellular and molecular interplay among them.

The roles of insulin and glucagon in regulating metabolic tissue have been a major focus of diabetes research. Another important body of work has been done characterizing the source of these hormones, their molecular function and regulation, and respective roles in metabolic disease. The multi-cellularity and differential cellular function in the islet highlight the complexity of this critical endocrine organ. The primary cell types responsible for glucose homeostasis are the α-, β-, and δ-cells, although there is an increasing appreciation for the contribution of the other cell types to islet disease (Koska, DelParigi et al. 2004; Poykko, Ukkola et al. 2005). The remainder of this section details the primary islet cells, their respective hormones, and molecular regulation.

α-cells and glucagon signaling

Glucagon is a peptide hormone composed of 29 amino acids that is translated as a pre-prohormone and packaged into vesicles after several proteolytic cleavages in the rough endoplasmic reticulum (ER) and Golgi apparatus to form the mature hormone. There are other cleavage products from the same gene that have important biological function including glucagon-like peptide 1 (Glp-1) and gastric inhibitory peptide (GIP) (Bell, Santerre et al. 1983), which will be discussed in a later section. Glucagon is secreted from dense core granules in the pancreatic α-cells and drives an increase in blood glucose levels (Deconinck, Van Assche et al. 1972). Stimulation of glucagon secretion is complex and can arise from a number of states, including exercise, fasting, and trauma, as well as hypoglycemia and high blood glucose levels of amino acids.

Under normal physiological conditions, however, when blood glucose levels decrease below ~4 mM, glucagon is secreted from islet α-cells. In human, glucose transport into the α-cells occurs via the facilitated glucose transporter GLUT1. The GLUT1 transporter is responsible for low-level glucose uptake that is required for maintenance of basal respiration in all cells and has a high affinity for glucose with a Km of 1-2 mM (Gould and Holman 1993). GLUT1 expression is also up-regulated under glucose starvation conditions (Kumagai, Kang et al. 1995; Seidner, Alvarez et al. 1998). Additionally, the effect of glucose on metabolic redox state, as measured by NAD(P)H autofluorescence, is similar to that of the β-cells, but has a higher basal level at low glucose that results in a decreased dynamic range (Le Marchand and Piston 2010). Other studies have shown that the β-cells are more efficient in glucose oxidation and the α-cells rely more on anaerobic glycolysis (Sekine, Cirulli et al. 1994; Schuit, De Vos et al. 1997; Quesada, Todorova et al. 2006). These properties suggest that α-cells are less coupled to glycolytic events and provide an explanation for the metabolic activity in α-cells during hypoglycemia. Glucose is metabolized by the rate-limiting enzyme glucokinase, leading

into glycolysis, oxidative phosphorylation, and the generation of ATP (Heimberg, De Vos et al. 1995; Heimberg, De Vos et al. 1996).

Similar to the well-characterized β-cells, the α-cell cytosolic ATP/ADP ratio increases and K_{ATP} channels are closed, leading to a membrane depolarization. The K_{ATP} channels in α-cells reportedly have a higher ATP sensitivity, allowing for maximal inhibition of K_{ATP} channel conductance at low levels of cytosolic ATP (Leung, Ahmed et al. 2005). Single nucleotide polymorphisms in the K_{ATP} channels identified in genome-wide association studies (GWAS) result in defective channel activity, reviewed in (Denton and Jacobson 2012), which by either direct or indirect action on the α-cell channels, lead to dysregulation of glucagon secretion (Tschritter, Stumvoll et al. 2002; Rorsman, Salehi et al. 2008; Quoix, Cheng-Xue et al. 2009; Unger and Orci 2010). These ion channels are certainly critical in the regulation of glucagon secretion at low glucose levels, but the extent to which they drive glucose-dependent regulation in the α-cells is unknown and under debate (Cheng-Xue, Gomez-Ruiz et al. 2013; Zhang, Ramracheya et al. 2013).

Other ion channels also contribute to membrane potential dynamics, including voltage-dependent Na^+ channels, voltage-gated K^+ channels, and N-, L-, and T-type Ca^{2+} channels that are important for action potential regulation, reviewed in (Quesada, Tuduri et al. 2008). The membrane-level organization and distal steps of glucagon exocytosis are much less well-characterized due to significant challenges in studying native islet α-cells. However, several proteins involved in β-cell vesicle exocytosis are expressed in the α-cells, suggesting the capacity for similar mechanisms. For example, the F-actin modifying Rho-GTPases are key players in regulating insulin exocytosis and will be discussed further in Chapter 3, which addresses the possibility that α-cells share this regulatory function for glucagon secretion.

The metabolic target tissues for glucagon action include the liver, adipose tissue, and the islet itself. In the liver, glucagon stimulates the breakdown of glycogen stores to liberate glucose for delivery to the blood stream, a process called glycogenolysis. The production of

cAMP and activation of PKA in this signaling pathway, via glucagon receptor activation, leads to the phosphorylation and activation of glycogen phosphorylase. This enzyme removes the α (1→4) linkage between glucose units forming glucose-1-phosphate, which in turn is converted to glucose-6-phosphate. Finally, glucose-6-phosphatase removes the phosphate and releases free glucose (Imazu, Strickland et al. 1984; Imazu, Strickland et al. 1984). This process is enhanced in the hyperglucagonemic environment of type 2 diabetes and insulin resistance (Iozzo, Pratipanawatr et al. 2001). In fact, the most prescribed drug for type 2 diabetes patients is the biguanide compound metformin, which decreases hepatic glucose output and counters excessive glucagon stimulation (Leavens and Birnbaum 2011; Miller, Chu et al. 2013).

In adipose tissue, glucagon functions via a similar mechanism to stimulate the release of free fatty acids and glycerol into the blood stream, by increasing cAMP production and PKA activation. The PKA then phosphorylates hormone-sensitive lipase (HSL), which hydrolyzes fatty acids from diacylglycerols. Lastly, the fatty acid is released from monoglycerides via monoglyceride lipase that also liberates glycerol (Berg 2002). The chronic elevation of free fatty acids in circulation is a major risk factor for insulin resistance and metabolic syndrome, which provides a link between obesity and type 2 diabetes. Under normal, healthy conditions the adipose tissue is more heavily influenced by insulin than glucagon (Liljenquist, Bomboy et al. 1974). In a diabetic state, however, the chronic hyperglucagonemia strongly stimulates lipolysis, which insulin signaling is no longer sufficient to overcome due to resistance (Liljenquist, Bomboy et al. 1974; Liljenquist, Bomboy et al. 1974; Boden 1997).

β-cells and insulin signaling

Insulin is also a peptide hormone, composed of 51 amino acids, that is synthesized as pre-proinsulin, which becomes proinsulin following a series of cleavages in the rough ER and Golgi. Once packaged into secretory granules, proinsulin is further cleaved to produce insulin

and c-peptide, which are secreted together from dense-core vesicles by exocytosis from pancreatic β-cells (Rhodes and Halban 1987). The primary role of insulin in normal physiology is to lower blood glucose levels in response to hyperglycemia by acting on the muscle, liver, and adipose tissue to take up glucose from the blood and store it in the form of glycogen (Berg 2002). Additionally, insulin signaling in the liver and adipose tissue inhibits the degradation of glycogen and release of free fatty acids, respectively. Since the β-cells are the only known cells that secrete insulin, no other tissue can provide compensatory function. This is why insulin has been so important for diabetes, which is defined by a profound lack of insulin function.

In terms of glucose-stimulated insulin secretion from β-cells, a wealth of knowledge has been gathered over the last several decades. Glucose is transported into the β-cell by facilitated glucose transporter 2 (GLUT2), which has a Km of ~15 mM (Gould and Holman 1993). Then glucose is converted by glucokinase to glucose-6-phosphate, the leading molecule for glycolysis. The subsequent production of ATP from the normal metabolic cycle leads to an increase in the ATP/ADP ratio, closure of K_{ATP} channels, membrane depolarization, and eventual activation of voltage-gated Ca^{2+} channels that allow Ca^{2+} influx from the extracellular space. Downstream exocytotic events in the β-cell are much better characterized than in the α-cell and the F-actin modifying small Rho-GTPase, Rac1, has been shown to be important in insulin exocytosis (Li, Luo et al. 2004; Konstantinova, Nikolova et al. 2007). This enzyme remodels the F-actin network proximal to the membrane, allowing vesicle fusion and release of insulin and the co-secreted factors (Asahara, Shibutani et al. 2013). Insulin exocytosis is a pulsatile process with Ca^{2+} waves occurring across the β-cells in the islet, which is mediated by gap junctional coupling between the β-cells that allows the islet cells to behave like an electrical syncytium (Head, Orseth et al. 2012). Importantly, the syncytial activity of islet β-cells varies wildly across species.

Once secreted into the bloodstream, insulin acts through the insulin receptor, which is a member of the receptor tyrosine kinase family of enzymes. The insulin receptor is composed of

two extracellular and 2 intracellular subunits that dimerize upon activation by insulin binding. This initiates a transphosphorylation and conformational change that induces phosphorylation of insulin receptor substrates (IRS). There are two primary downstream pathways from this point: activation of PI3K-AKT (AKT is also known as PKB) signaling, or the Ras-mitogen-activated protein kinase (MAPK) pathway, which regulates cell growth. The PI3K-AKT pathway is predominantly critical in metabolic regulation, and is depicted in Figure 1-3. Active PI3K leads to the production of lipid signaling molecule phosphatidylinositol-3,4,5-triphosphate (PIP_3) at the plasma membrane. This second messenger recruits AKT to the membrane along with the activating enzyme phosphoinositide dependent kinase. Upon activation, AKT translocates from the membrane and participates in a number of downstream intracellular signaling pathways depending largely on the tissue, subcellular distribution, and availability of substrates (Taniguchi, Emanuelli et al. 2006).

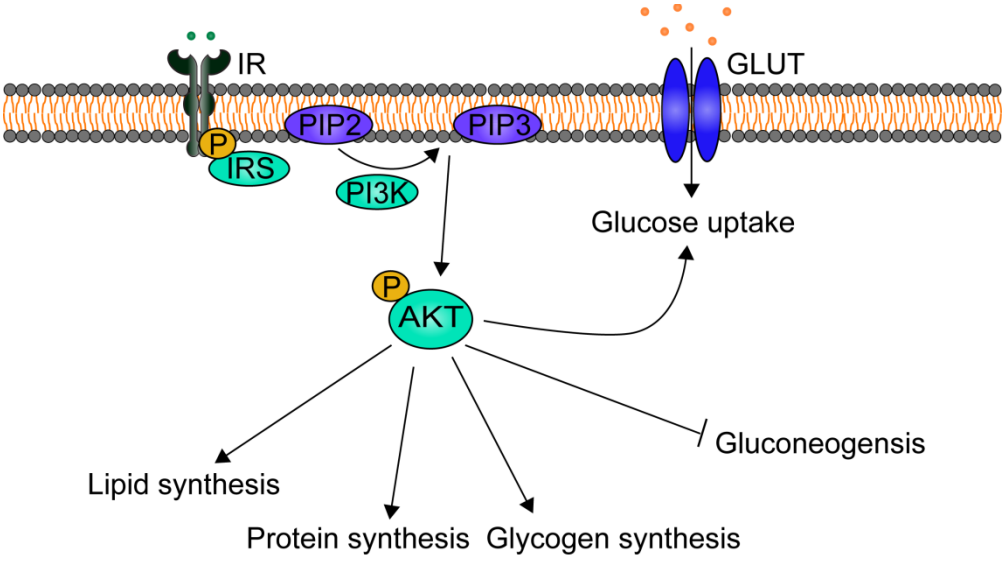

Figure 1-3. Insulin signaling overview.

In the liver, insulin is a multifunctional signaling molecule. Upon AKT activation, insulin stimulates amino acid uptake and protein synthesis via mTORC1 signaling. Glucose uptake via GLUT2 transporter is also stimulated by relieving the inhibition of glycogen synthase kinase (GSK3) and allowing glycogen synthesis. Finally, hepatic fatty acid and triacylglycerol synthesis is increased by lipoprotein lipase activity and transcription of lipogenic genes (Mounier and Posner 2006). Additionally, gluconeogenesis is inhibited by AKT's activation of phosphodiesterase 3B (PDE3B), which catalyzes the degradation of cAMP and reduces the downstream effectors, thus opposing the stimulatory effect of glucagon through its GPCR (Choi, Park et al. 2006). Insulin action is primarily opposed by protein tyrosine phosphatases that dephosphorylate the insulin receptor and reduce its activity (Elchebly, Payette et al. 1999). During diabetes, the loss of insulin signaling is a key defect and leads to dramatic increases in glucose release, poor glycogen synthesis, poor protein synthesis, and dysregulated gluconeogenesis (Michael, Kulkarni et al. 2000). There are also a number of indirect effects of insulin signaling dysfunction during diabetes that ultimately impact the liver, as described briefly in (Cherrington 2005).

In adipocytes, insulin signaling also progresses through the PI3K-AKT-PDE3B pathway to inhibit cAMP production, which reduces lipolysis. Insulin also upregulates lipoprotein lipase and stimulates lipogenic enzymes like acetyl-CoA carboxylase and fatty acid synthase (Kersten 2001). Additionally, AKT stimulates glucose uptake and glucose transporter GLUT4 translocation (Kohn, Summers et al. 1996). In a diabetic state, where insulin signaling is insufficient, there is a significant increase in free fatty acids delivered to the blood stream and a repartitioning of lipid stores to inappropriate tissues, like the skeletal muscle, liver, and islet cells (Yu and Ginsberg 2005). The inhibitory role of insulin signaling on cAMP generation via PDE3B activation in both the liver and adipose tissue was a significant contributor to the experimental design and hypothesis behind the work described in Chapter 2.

δ-cells and somatostatin signaling

Somatostatin is a short 14- or 28-amino acid peptide secreted from multiple cells throughout the body including in the hypothalamus, the gastrointestinal tract, and the pancreatic islet δ-cells. Somatostatin-14 inhibits both insulin and glucagon secretion from the islet. Somatostatin-28, which is produced by an alternate posttranslational cleavage, has neuroendocrine function and may act as a neurotransmitter.

Somatostatin secretion from the δ-cells is stimulated by glucose and amino acids, though comparatively little is known about the molecular mechanisms underlying δ-cell function. This secretion is pulsatile and synchronous with insulin while being asynchronous with glucagon. Additionally, the dose response curve for somatostatin resembles that of insulin while being slightly left-shifted, such that it leads insulin secretion in response to elevating glucose levels (Hellman, Salehi et al. 2009). While somatostatin is known to be a potent inhibitor of insulin and glucagon secretion in the islet, until recently, less attention has been given to studying the intra-islet functions. Furthermore, since somatostatin is locally secreted from other tissues in the body, the relative contributions of circulating and islet-derived hormones on α- and β- cells is another important avenue of research (Cejvan, Coy et al. 2003; Hauge-Evans, King et al. 2009; Kailey, van de Bunt et al. 2012; Schwetz, Ustione et al. 2013).

Somatostatin functions as the ligand for a family of GPCRs that associate with an inhibitory Gαi subunit. There are 5 known subtypes of these receptors, called somatostatin receptors (SSTR) type 1-5 that are encoded by five genes. SSTR1, SSTR2 and SSTR5 are the primary receptors localized in the islet cells, with SSTR2 being predominantly functional in α-cells (Kailey, van de Bunt et al. 2012) and SSTR5 dominating in the β-cells (Strowski, Parmar et al. 2000). The subtype distribution of these receptors appears conserved in both humans and mice, though the subtype specificity data is relatively variable (Kumar, Sasi et al. 1999; Cejvan, Coy et al. 2003; Hauge-Evans, King et al. 2009). The molecular mechanism of somatostatin function is debated, due to the large number of possible downstream effects from GPCR

activation, described below and depicted in Figure 1-4. For example, several studies have shown that the Gαi subunit is responsible for inhibiting adenylyl cyclase and decreasing cAMP levels (Schuit, Derde et al. 1989; Gromada, Hoy et al. 2001; Hauge-Evans, King et al. 2009). However, there are also a number of reports suggesting that the βγ complex plays a role in somatostatin function via activation of K^+ channels that hyperpolarize the membrane to reduce Ca^{2+} activity and exocytosis (Yoshimoto, Fukuyama et al. 1999; Gromada, Hoy et al. 2001; Schwetz, Ustione et al. 2013). These data were instrumental in the hypothesis and experimental design for the studies described in Chapter 2.

Regulators of islet function

There are several peripheral factors and islet factors that participate in regulating islet functions like secretion, protein synthesis, and proliferation. Many of these tissues have directly reciprocal relationships with the islet hormones, such as the adipose tissue, and were described above. The gastrointestinal and nervous system contributions are just as critical, particularly in certain physiological states, such as extreme duress. Additionally, the differences in mechanism for these factors between the islet cells provide multiple levels of physiological specificity for context-dependent stimulation, which are extensively reviewed here (Quesada, Tuduri et al. 2008). The stimulus-dependent molecular regulation of islet cells is facilitated by a number of membrane G-protein coupled receptors (GPCR), including the glucagon and Glp-1 receptors, which are members of Family B, or the secretin receptor family, of GPCRs. These 7-transmembrane domain receptors represent an important paradigm in molecular regulation of intracellular function and feature in a variety of different cellular types and organismal functions including development, sensory perception, and others. Additionally, GPCRs represent the most common class of receptors targeted for pharmaceutical intervention in disease, and recent efforts in designing new drugs for diabetes are targeting the glucagon receptors and Glp-1

receptors (Madsbad 2009; Christensen, Bagger et al. 2011; Christensen, Knop et al. 2011).

Upon activation by a specific ligand, a conformational change in the GPCR leads to the dissociation of the intracellular Gα and Gβγ subunits, which are responsible for the variety of downstream effects (Gilman 1987). There are several types of α subunits that determine their function, and for which the receptors are named, as reviewed in (Kimple, Bosch et al. 2011). GPCRs coupled to a Gαs subunit stimulate the action of adenylyl cyclases to drive the production of cAMP and subsequent signaling events that can lead to ion channel regulation, transcriptional activation, and exocytosis. The Gαi/o subunits inhibit the adenylyl cyclases and reduce cAMP generation. Finally, the Gαq subunit family activates PLC and produces lipid signaling molecules diacylglycerol (DAG) and inositol 1,4,5-triphosphate (IP3), which regulate downstream ion channel function and release of Ca^{2+} from intracellular stores (Neves, Ram et al. 2002).

In addition to α subunit signaling, the βγ complex is also a critical component of GPCR function, which normally inhibits α subunit function. However, upon dissociation with receptor activation, it is also capable of working as a signaling molecule with such downstream effects as ion channel modulation, phosphoinositide3-kinase (PI3K) activation, PLC activation, and inhibition of the exocytotic machinery (Brock, Schaefer et al. 2003). The complexity of these downstream signaling pathways and their effects, particularly under conditions where multiple ligands are binding their receptors, makes it quite challenging to tease apart the signals that drive cellular function for any given cell type. Particularly since the islet cells influence each other only in part via GPCRs (Ahren 2009), and are connected by proximity and junctional complexes (Cirulli, Baetens et al. 1994; Konstantinova, Nikolova et al. 2007), deconvolving the signaling has been challenging research. In Figure 1-4, a schematic of several different GPCR-mediated signaling cascades is shown. The Gαs and Gαi subunit pathways play key roles in the studies presented in Chapter 2 with regard to glucagon secretion.

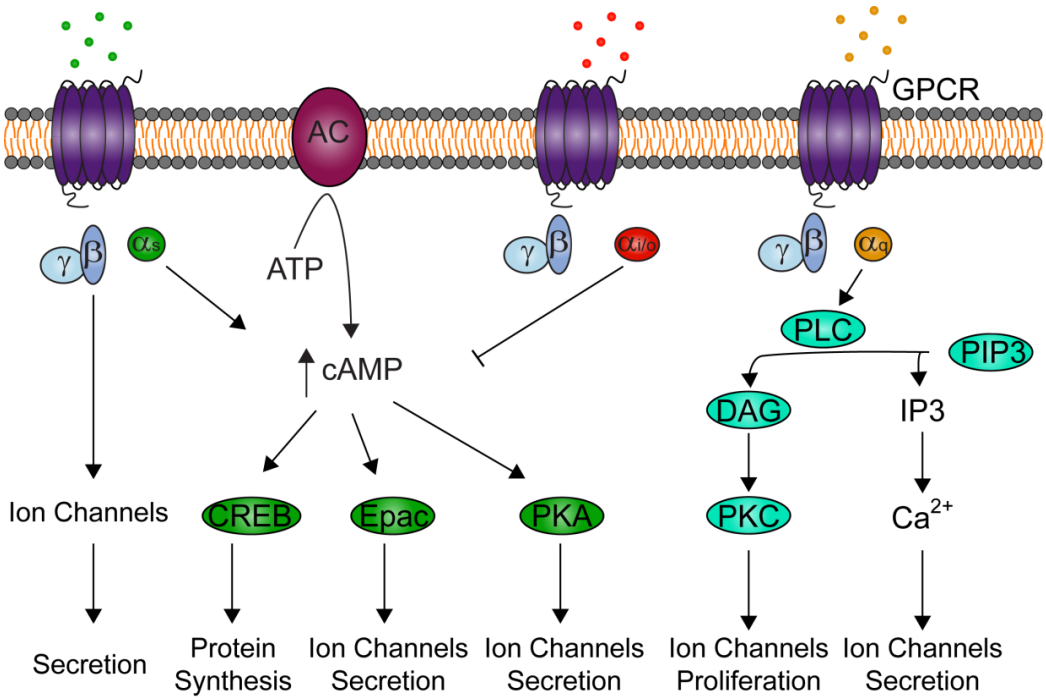

Figure 1-4. GPCR signaling examples by α-subunit specificity and primary downstream targets. These few examples are prevalent in islet tissue, but make up a small fraction of the systemic functions mediated by this family of receptors.

Incretin system

Incretin hormones, like gastric inhibitory peptide (GIP) and glucagon-like peptide-1 (Glp-1), are produced by specialized intestinal cells and regulate insulin secretion and blood glucose in response to a meal. These hormones account for the differences in response to oral glucose load vs intravenous administration. Glucose-dependent insulinotropic polypeptide (GIP), is a 42 amino acid peptide that results from cleavage of the proglucagon gene and is secreted from gastrointestinal K-cells. This hormone stimulates insulin secretion from pancreatic β-cells and may enhance glucagon secretion from the α-cells, though the role of GIP in regulating glucagon is controversial (Lynn, Pamir et al. 2001). GIP is a glucose-dependent insulin secretagogue (Andersen, Elahi et al. 1978). The GIP receptor in β-cells is a GPCR coupled to a Gαs subunit and, thus, stimulates insulin secretion by ramping up cAMP levels in the cytosol and activating

PKA/Epac (Christensen, Vedtofte et al. 2011). This function is lost in type 2 diabetes and in animal models including the diabetic Zucker fatty rat, which have a decreased incretin response and elevated response to oral glucose load (Lynn, Pamir et al. 2001). Additionally, some reports indicate that GIP increases glucagon secretion at low glucose levels (Pederson and Brown 1978; Christensen, Vedtofte et al. 2011), though clinical studies in human subjects show little to no change with oral glucose tolerance tests (Theodorakis, Carlson et al. 2004).

Glp-1, however, has been the focus of much recent research as a potential target for treating diabetes due to its inhibitory effect on glucagon secretion and stimulatory role in insulin secretion. A cleavage product of the proglucagon transcript, this 36-residue peptide is secreted from intestinal L cells in the presence of ingested carbohydrates, lipids, and proteins. Like GIP, this secretion is glucose dependent, which makes it particularly attractive as a therapeutic target for diabetes. In addition to its roles in islet cell secretion regulation, Glp-1 has been shown to inhibit β-cell apoptosis and stimulate proliferation and differentiation (Farilla, Hui et al. 2002). Furthermore, Glp-1 inhibits glucagon secretion and gastric emptying, though it remains unclear whether or not the glucagon inhibition is due to direct action on the α-cells (Dillon, Lu et al. 2005; Tornehave, Kristensen et al. 2008). These functions have led to the development of many Glp-1 mimetics, including exenatide and liraglutide, which are currently on the market as therapeutics for type 2 diabetes.

Glp-1 and GIP are both rapidly degraded by dipeptidyl peptidase-4 (DPP-4), which is a critical enzyme for regulating incretin function. This provides another therapeutic avenue by inhibiting the Glp-1 inhibitor to increase Glp-1 availability. Sitagliptin is a DPP-4 inhibitor that has recently shown clinical significance by inhibiting glucagon secretion in some contexts (DeFronzo, Okerson et al. 2008; Watanabe, Kobayashi et al. 2013). However, data from diabetic patients treated with these drugs have revealed negative side effects such as pancreatitis (Garg, Chen et al. 2010; Singh, Chang et al. 2013) and increased risk for pancreatic cancer (Alves, Batel-Marques et al. 2012). The lack of insight into the molecular mechanisms of

Glp-1 action in the islet, as well as other tissues, requires further scrutiny, though this peptide remains a significant target for type 2 diabetes therapy.

Nervous system

In addition to circulating neural factors that can regulate islet function, islet tissue is highly innervated. Parasympathetic innervation is derived from preganglionic parasympathetic nerves under the control of the vagus. A number of neurotransmitters from this system are relevant to islet function including acetylcholine, vasoactive intestinal polypeptide, NPY, pituitary adenylate cyclase-activating polypeptide, and others. Parasympathetic stimulation increases secretion of insulin, glucagon, somatostatin, and pancreatic polypeptide during hyperglycemia, thus coordinating an increase in whole-islet function (Ahren, Paquette et al. 1986; Ahren and Taborsky 1986).

By contrast, the sympathetic nerves in the islet are postganglionic, with cell bodies located in the celiac ganglion or paravertebral sympathetic ganglia. The sympathetic nervous system and hypothalamic-pituitary-adrenal (HPA) axis are important components of a high stress response in the islets. In the absence of a normal glucagon response or in periods of high stress, the sympathetic nervous system can stimulate glucagon secretion while also inhibiting insulin release. Neurotransmitters secreted from the sympathetic nervous system, like neuropeptide Y (Morgan, Kulkarni et al. 1998; Kulkarni, Wang et al. 2000; Schwetz, Ustione et al. 2013) and galanin (Dunning, Ahren et al. 1986; Lindskog, Dunning et al. 1990; Ahren, Ar'Rajab et al. 1991), inhibit insulin secretion. Norepinephrine also inhibits insulin and somatostatin secretion but simultaneously stimulates glucagon secretion from islets (Ahren, Veith et al. 1987; Kurose, Seino et al. 1990; Kurose, Tsuda et al. 1992; Yajima, Komatsu et al. 2001; Cheng, Straub et al. 2003). Epinephrine release also stimulates glucagon secretion while inhibiting insulin secretion via differential expression of adrenergic receptors, and is discussed in

more length in Chapter 2 (Tian, Sandler et al. 2011). There are also a number of neural peptides that have been shown to affect islet function, but the relative contributions of these factors have yet to be determined (Ahren 2000). The nervous system is, thus, a critical regulator of islet function, as it provides several options for modulating blood glucose levels in order to retain brain function under duress.

Intra-islet regulators

In support of the paracrine model of glucose-inhibited glucagon secretion, there have been a number of identified mechanisms by which the islet cells regulate each other. While none of these has proven a sufficient explanation for glucagon suppression alone, they do show the importance of intracellular signaling within the islets. To begin with the α-cells at low glucose, glucagon secretion stimulates insulin and somatostatin secretion from the β- and δ-cells via increased cAMP signaling. It also exerts an autocrine effect, whereby glucagon potentiates its own secretion (Ma, Zhang et al. 2005). Thus, as glucagon increases, autocrine stimulation decreases, and inhibitory molecules are secreted from neighboring cells. Additionally, acetylcholine is secreted from human α-cells to potentiate glucose-stimulated insulin secretion from β-cells (Rodriguez-Diaz, Dando et al. 2011).

Insulin has a much more controversial role in the regulation of glucagon secretion from α-cells. Studies in insulin receptor knockout mice have demonstrated that insulin is a critical mediator of glucagon secretion but the mechanism by which this occurs is far from agreed upon (Kulkarni, Bruning et al. 1999; Diao, Asghar et al. 2005). Since insulin is insufficient alone to suppress glucagon from α-cells isolated from the islet environment, it is likely that several molecules are required in combination for the cessation of glucagon exocytosis. In the δ-cells, insulin has been suggested to regulate somatostatin secretion. However, while insulin receptor mRNA has been identified in δ-cells, the evidence that there is a direct action these cells is

controversial and varies between rodent and human studies (Brunicardi, Kleinman et al. 2001; Muller, Huang et al. 2007; Hauge-Evans, Anderson et al. 2012). Somatostatin has been shown to inhibit both glucagon and insulin secretion via a couple of different pathways described above in the δ-cells and somatostatin secretion section. One of the major goals of the work presented here aimed to shed light on the molecular mechanism by which insulin and somatostatin participate in the glucose-dependent inhibition of glucagon secretion, and the results are documented in Chapters 2 and 3.

Models of islet hormone secretion

The opposing functions of insulin and glucagon with respect to blood glucose levels are critical in both normal function and the pathophysiology of diabetes, hence the bi-hormonal hypothesis of glucose homeostasis. Because of the therapeutic success of insulin, the majority of diabetes research has focused on the β-cells and how to modulate their function to treat or prevent dysfunctional glucose-stimulated insulin secretion. However, the hyperglucagonemia associated with diabetes suggests dysfunctional inhibitory mechanisms for glucagon secretion from the α-cell as well. While the importance of glucagon secretion from α-cells is now widely accepted, the mechanism by which glucose induces a cessation of glucagon secretion from the α-cells is far from clear and hotly debated (Gromada, Franklin et al. 2007). This debate is at the center of the work described in Chapter 2, and continuing studies toward its resolution.

There are a large number of similarities between α- and β-cells, which have driven the development of one of the prevailing models for glucose-inhibited glucagon secretion, called the electrophysiology model. This model proposes that α-cells intrinsically contain the machinery for inhibiting exocytosis, including many of the similar membrane potential dynamics as seen in the β-cells (Newgard and McGarry 1995; Shiota, Rocheleau et al. 2005; Ramracheya, Ward et al. 2010). Since both cell types metabolize glucose via glucokinase and contain ATP-sensitive

K^+ (K_{ATP}) channels, high-voltage-gated calcium channels, and secretory granules, the molecular tools are available for an analogous mode of regulating exocytosis; though Na^+ channels are proposed to play a different role in α-cell membrane potential (Ramracheya, Ward et al. 2010). As recently reviewed (Zhang, Ramracheya et al. 2013), a number of studies on channel activity in α-cells from isolated islets demonstrate glucose-dependent K_{ATP} channel activity that appears similar to the β-cells. Additionally, some Ca^{2+} channel studies support this model by demonstrating changes in channel activity that are glucose-dependent and decrease with increasing glucose (Gopel, Kanno et al. 2000; Gromada, Ma et al. 2004; MacDonald, De Marinis et al. 2007).

However, there is also a wealth of evidence against a direct, intrinsic inhibition of glucagon secretion. Purified α-cells, for example, in the absence of paracrine factors, are stimulated by glucose and secrete glucagon in a dose-dependent manner (Franklin, Gromada et al. 2005; Olsen, Theander et al. 2005). There are also reports in clonal α-cell lines in support of a direct action of glucose where paracrine factors are negligible (Gromada, Ma et al. 2004; Vieira, Salehi et al. 2007). Unfortunately, the clonal α-cell lines are notoriously poor models of the physiology observed in intact islet α-cells, which makes interpretation of data collected in these cell lines difficult (Hamaguchi and Leiter 1990; Powers, Efrat et al. 1990). Thus, the relative roles of ion channels in regulating glucagon secretion are still unclear, with increasingly complex theories being produced to explain their roles in the stimulation and inhibition of glucagon secretion (Zhang, Ramracheya et al. 2013).

Another hypothesis, known as the store-operated model, has also been recently developed and is based on the observation that inhibiting the sarcoplasmic-endoplasmic reticulum Ca^{2+} ATPase pump (SERCA) causes Ca^{2+} oscillations in α-cells. In this model, a Ca^{2+} dependent store-operated depolarizing current is inhibited as glucose increases, thus decreasing intracellular Ca^{2+} availability for granule exocytosis (Liu, Vieira et al. 2004; Vieira, Salehi et al. 2007). However, inhibiting the SERCA pump by thapsigargin does not affect

glucose-stimulated glucagon secretion from purified α-cells, so the contribution of this mechanism in regulating glucagon secretion is unclear (Olsen, Theander et al. 2005).

Finally, the paracrine model states that secreted islet factors such as Zn^{2+}, γ-aminobutyric acid (GABA), or insulin itself, inhibit glucagon secretion by overcoming the depolarizing effect of glucose metabolism (Starke, Imamura et al. 1987; Unger and Orci 2010; Chen, Philippe et al. 2011; Unger and Cherrington 2012). This model was produced partially by data that did not support the electrophysiology model, as described above. Additionally, several secreted factors have been shown to be required for glucagon suppression (Starke, Imamura et al. 1987; Xu, Kumar et al. 2006; Unger and Orci 2010; Chen, Philippe et al. 2011; Unger and Cherrington 2012). These data strongly suggested a critical role for either a paracrine molecule(s) released from neighboring cells, juxtacrine connections between the islet cells, or both in the suppression of glucagon exocytosis. However, we have shown that several candidate inhibitors, including somatostatin, insulin, and GABA are insufficient alone to inhibit glucagon secretion from purified populations of α-cells, suggesting that a more complex mechanism is involved (Le Marchand and Piston 2010). A promising candidate from this study was Zn^{2+}, which is co-secreted with insulin and c-peptide, and did inhibit glucagon secretion from purified α-cells. Studies done in Zn^{2+} transporter knockout mice have ruled out this factor as a regulator of glucagon inhibition, as glucagon secretion was not altered in those animals or islets (Nicolson, Bellomo et al. 2009).

All of these models commonly assume that a decrease in intracellular Ca^{2+} is required for glucagon inhibition. However, it has been shown that glucose stimulation in α-cells does not reduce global intracellular Ca^{2+} activity, which indicates that suppression of glucagon secretion occurs independent of Ca^{2+} signaling (Le Marchand and Piston 2010; Le Marchand and Piston 2012). A consensus on the molecular mechanism of glucagon suppression has yet to be reached because the data from any given experiment are insufficient to explain all of the observations reported.

CHAPTER 2

ROLE OF SOMATOSTATIN AND INSULIN RECEPTORS IN GLUCOSE-INHIBITED GLUCAGON SECRETION

(Adapted and expanded from Elliott & Piston, Submitted, Diabetes, 2014)

Introduction

Glucagon secretion from pancreatic islet α-cells is inhibited during hyperglycemia, and this inhibition plays a critical role in blood glucose homeostasis. During diabetes, α-cell dysregulation leads to hyperglucagonemia, which in turn over-stimulates liver glucose production and exacerbates chronic hyperglycemia. In spite of the therapeutic success of insulin, it has recently been suggested that glucagon hypersecretion, rather than a lack of insulin, is the primary driver of chronic hyperglycemia (Unger and Cherrington, 2012). Regardless of the root cause of diabetic phenotypes, persistent glucagon secretion during diabetes makes the α-cell an important target for therapeutic intervention. Current glucagon-related therapies address hyperglycemia by mimicking natural glucagon inhibitors (such as GLP-1 mimetics (Drucker and Nauck, 2006)) or antagonizing the glucagon receptor (Christensen et al., 2011). However, data from diabetic patients treated with exenatide have revealed negative side effects such as pancreatitis (Singh et al., 2013) and pancreatic cancer (Alves et al., 2012).

Various hypotheses have been put forth to explain the suppression of glucagon secretion, including paracrine regulation by islet factors (Koh et al., 2012), changes in ion channel activity (Zhang et al., 2013), and others; but they commonly assume that a decrease in intracellular

Ca^{2+} activity ($[Ca^{2+}]_i$) is required. By contrast, our laboratory (Le Marchand and Piston, 2010, 2012) and others (Tian et al., 2011) have shown that glucagon suppression is independent of $[Ca^{2+}]_i$, and none of the current hypotheses explain the loss of glucose inhibition of glucagon secretion from α-cells isolated from the native islet environment (Le Marchand and Piston, 2010).

Under normal physiological conditions, euglycemia is maintained in the face of rising blood glucose by a rise in somatostatin and insulin secretion from islet δ- and β-cells, respectively, accompanied by an inhibition of glucagon secretion. In Type I and advanced Type II diabetes, where β-cells are absent or mostly dysfunctional, somatostatin is believed to play a primary role in the inhibition of glucagon secretion (Cheng-Xue et al., 2013; Hauge-Evans et al., 2010; Kailey et al., 2012; Strowski et al., 2000; Yue et al., 2012). However, a global somatostatin deletion does not lead to increased basal glucagon secretion (Hauge-Evans et al., 2009) and infusion of a specific somatostatin receptor type 2 (SSTR2) antagonist in the absence of insulin does not affect blood levels of glucagon or blood glucose (Yue et al., 2012). Isolated islets from SSTR2 knockout mice show a two-fold increase in glucagon secretion compared with wild type, though, suggesting a role for somatostatin in glucagon inhibition (Strowski et al., 2000). While multiple somatostatin receptors have been identified in islets, SSTR2 is the most abundant in human α-cells (Dorrell et al., 2011), and is the only isoform expressed in murine α-cells (Strowski et al., 2000). Additionally, SSTR2 has been shown to be the functionally dominant isoform in α-cells from both species (Kailey et al., 2012). When somatostatin activates this receptor, the $G\alpha_i$ subunit inhibits adenylyl cyclases to reduce cAMP and glucagon secretion is decreased.

Knockdown of the insulin receptor (IR) in isolated islets leads to changes in glucose inhibition of glucagon secretion, without any effect on insulin secretion, which points to a direct role of the insulin receptor in α-cells (Diao et al., 2005). Tissue-specific insulin receptor knockout mice have also been characterized for both α-cells (αIRKO) and β-cells (βIRKO). The βIRKO mice exhibit normal fasting glucose levels, but have impaired glucose tolerance.

Glucagon secretion from isolated βIRKO islets was not reported (Kulkarni et al., 1999). In contrast, the αIRKO mice exhibit hyperglycemia, hyperglucagonemia, and glucose intolerance, but again, glucagon secretion from these islets was not reported (Kawamori et al., 2009).

While the role of insulin signaling in the α-cell is debated, it has been suggested that insulin reduces KATP channel sensitivity (Franklin et al., 2005; Matsumura et al., 1999), or activates Akt downstream of PI3-kinase to recruit GABA-A receptors to the membrane, which allows for inhibition by secreted GABA (Xu et al., 2006). These mechanisms still rely on a change in Ca^{2+} signaling, which is not observed in α-cells (Le Marchand and Piston, 2010, 2012). However, insulin receptor stimulation can also activate phosphodiesterase 3B, which degrades cellular cAMP (Zmuda-Trzebiatowska et al., 2006). Phosphodiesterase inhibitors have been shown to increase amino-acid stimulated glucagon secretion from isolated islets by increasing cAMP (Jarrousse and Rosselin, 1975), and the phosphodiesterase inhibitors rolipram and cilostazol, have shown efficacy in preventing diabetes in rodents and diabetic complications in humans (Katakami et al., 2010; Liang et al., 1998).

Collectively, experiments from our laboratory in islet α-cells and the work of many others led us to the hypothesis that somatostatin and insulin may be exerting their inhibitory functions by cooperatively decreasing cAMP and PKA signaling to reduce glucagon secretion; rather than by decreasing intracellular Ca^{2+} in the cell. Thus, to determine the role that cAMP and its somatostatin- and insulin-dependent changes play in inhibiting α-cell glucagon secretion, we combined hormone secretion assays, $[Ca^{2+}]_i$ imaging, and immunofluorescence of whole islets and purified α-cells. The results point to a mechanism for glucagon suppression where somatostatin and insulin signaling converge to lower cAMP by both decreasing its production and driving its degradation, leading to reduced phosphorylation of PKA. This chapter includes the detailed results of these studies, methodology employed, and a brief summary of the significance of the findings, which will be expanded upon in Chapter 5: Conclusions and Future Directions.

Materials and Methods

Islet isolation and culture

All animal studies were conducted in compliance with the Vanderbilt University Institutional Animal Care and Use Committee (IACUC). Pancreata from 8-15 week old transgenic male mice (C57BL/6 genetic background) that express tandem-dimer Red Fluorescent Proteins (tdRFP) in α-cells were isolated as described (Le Marchand and Piston 2010; Schwetz, Ustione et al. 2013), and cultured in RPMI 1640 (Invitrogen) supplemented with 10% fetal bovine serum (FBS; Invitrogen), penicillin/streptomycin (Invitrogen), and 11 mM glucose until use. Human islets were kindly provided by Dr. David Jacobson and upon receipt, were hand-picked into RPMI 1640 (Invitrogen) with 11 mM glucose and 2% BSA (Sigma) and allowed to recover for 3-4 hours before use.

Glucagon secretion assay

Isolated islets were cultured overnight inn media, then incubated for 1 hour in buffer consisting of 644.1 mM NaCl, 24 mM KCl, 6 mM KH_2PO_4, 6 mM $MgSO_4$•7H_2O, 12.5 mM $CaCl_2$, 20 mM Hepes, and 5 mM $NaHCO_3$ (pH7.4) with 2.8 mM glucose. 12-15 islets per sample were transferred to buffer with low (1 mM) or high (11 mM) glucose with and without the following drugs: 300 µM 8-Bromoadenosine 3′,5′-cyclic monophosphate (8-Br-cAMP - Sigma), 300 µM 8-(4-Chlorophenylthio)-2′-O-methyladenosine 3′,5′-cyclic monophosphate monosodium hydrate (8-O-Me-CPT - Sigma), 300 µM N6-Benzoyladenosine-3′,5′-cyclic monophosphate sodium salt (6-Bnz-cAMP - Sigma), 100 nM insulin (Sigma), 1 µM insulin, 1 µM somatostatin (sigma), 1 µM epinephrine (Acros Organics), 1 µM S961 (Novo Nordisk), 50 µM forskolin (Sigma), 100 µM IBMX (Sigma), 100 µM Rp-cAMPS (Sigma), cyclosomatostatin (Tocris), and/or 200 nM CYN154806 (Tocris) for 45 minutes with occasional agitation at 37ºC. The samples were centrifuged briefly (Beckman) and supernatants collected as secretion samples. 1.5% HCl/70%

ethanol was added to the remaining islet sample and vortexed for islet content quantification. Glucagon and insulin content and secretion were measured in duplicate with Glucagon ELISA (RayBiotech), Mouse UltraSensitive Insulin ELISA (Alpco), or Human Insulin ELISA (Alpco), and detected on a Spectra Max M5 spectrometer (Molecular Devices). Studies with pertussis toxin (Sigma) were accomplished by an overnight pre-treatment of isolated islets and follow-up secretion experiments as described above.

Immunofluorescence

Islets were treated as for secretion assays described above and then fixed in PBS containing 2% of paraformaldehyde at 4°C. Samples were permeabilized overnight at 4°C in PBS with 0.3% Triton X-100, 5 mM sodium azide, 1% bovine serum albumin, and 5% goat serum (from Jackson ImmunoResearch Laboratories, West Grove, PA). Human islets were incubated with rabbit anti-glucagon (1:250), guinea pig anti-human insulin (1:250), and mouse anti-cAMP (1:250) primary antibodies for 24–48 h at 4°C, washed (2X), and incubated with secondary antibodies conjugated with Alexa Fluor 488 (1:1000), Alexa Fluor 546 (1:1000), and Alexa Fluor 594 (1:1000) or Cy5 (1:1000) for 24 h, and washed (2X) before mounting in gelvatol. Mouse islets were stained similarly, but with rabbit anti-insulin (1:250), guinea pig anti-glucagon (1:250), mouse anti-cAMP (1:250), or rabbit anti-phospho-PKA primary antibodies. All islets were washed overnight between primary and secondary antibodies as an additional blocking step with the permeabilization buffer above. The washing buffer consists of PBS with 0.1% Triton X-100, 5 mM sodium azide, and 1% bovine serum albumin. Immunofluorescence was detected by confocal microscopy using 488 nm (AF488), 561 nm (AF561), or 633 nm (AF594 or Cy5) excitation and corresponding spectral windows (LSM780, Carl Zeiss). All analysis was performed only on raw data, but for display purposes, image look-up tables were compressed equally for gamma and brightness to aid the eye.

Live-cell imaging

Live islets were imaged as described (Le Marchand and Piston 2010). For calcium imaging, islets were incubated with 5 μM of Fluo4-AM for 30 minutes at 2.8 mM glucose. After washing, islets were allowed to equilibrate on the microscope stage for 15 minutes in the same solution. Fluo4 was excited at 488 nm and detected between 490 and 560 nm. Red α-cells were localized by recording tdRFP fluorescence excited by 561 nm. Confocal sections were obtained with an LSM710 or LSM780 (Carl Zeiss) using a Fluar 40x/1.3NA lens and a 2 Airy unit pinhole. Because β-cells constitute ~ 80% of the cells in the islet (Gromada, Bokvist et al. 1997), the Fluo4 signal from non-tdRFP cells in the center of the islet was considered to represent the average β-cell response. Mean intensities were normalized to the first 5 frames of data 8 minutes after reagent change.

Cell dispersion and FACS sorting

Isolated islets were cultured overnight in islet medium with 11 mM glucose and washed in DPBS at pH 7.4 without calcium and magnesium chloride. Accutase (Life Technologies) was used for digestion for 15 minutes at 37ºC (gentle shaking) and cells were pelleted and resuspended in secretion buffer at 11 mM glucose. One to two hours after Accutase dispersion, fluorescent cells were isolated by fluorescence-activated cell-sorting (FACS). The Vanderbilt Flow Cytometry Core facility utilized a BD FACSAria cell sorter (BD Biosciences, San Jose, CA) for purification and DAPI (0.5 μg/ml) was used for exclusion of non-viable cells. Yields were 100-800 viable α-cells per mouse pancreas.

Data analysis and statistics

Data were analyzed with ImageJ, MatLab, or GraphPad Prism software. For all imaging data collected, the background signal was subtracted and the mean fluorescence intensity was

determined by region of interest. Data are reported as mean ± S.E.M. with $p < 0.05$ considered statistically significant as determined by Student's t-test.

Results

There are several challenges with studying islet α-cells, including their identification within the islet and isolation for the purposes of studying pure populations. To address these challenges, we have utilized a mouse model that expresses selectively a red fluorescent protein (tdRFP) in the α-cells by using a Cre-recombinase system driven by the glucagon promoter. This model has facilitated imaging and immunofluorescence studies of theα-cells. It also allows us to use fluorescence-activated cell sorting (FACS) to purify the α-cells upon dispersion of the islets. However, previous studies with the FACS-sorted cells have revealed a large deviation in function from α-cells in the native islet environment, particularly with regard to inhibiting glucagon secretion. None of the known candidate inhibitors of glucagon secretion, except Zn^{2+}, were sufficient to inhibit exocytosis from the isolated cells. Mouse models with deficiencies in Zn^{2+} transport have no phenotype with regard to glucagon secretion, thus ruling it out as the primary mechanism of glucagon suppression. We have concluded from such studies that the junctional contacts between islet cells, which are still being elucidated, and possibly several secreted products from neighboring cells play a major role in the nominal function of α-cells.

Our hypothesis, then, began with the idea that cAMP rather than Ca^{2+} may be the signaling pathway at the heart of glucose-inhibited glucagon secretion. Additionally, there are a number of surface receptors expressed in α-cells that are known to function by modulating cAMP levels, which provided several candidates to test. However, we first needed to identify whether or not cAMP was regulated by increasing glucose levels in the α-cells, as has been reported by other groups, and second, we needed to determine whether or not such a regulation was dependent on changes in Ca^{2+} activity.

Glucose regulation of cAMP in human and mouse islets

To establish the effect of glucose on α-cell cAMP levels, we used semi-quantitative immunofluorescence to measure cAMP in human and murine islets that were stimulated with low (1 mM) or high (11 mM) glucose. While there are several drawbacks to using immunofluorescence as a quantitative measuring system, reviewed in (Taylor and Levenson 2006), it was the most practical technique available for studying α-cells in their native islet environment. However, in addition to the standard challenges with immunofluorescence measures, fixing the islets after stimulation to capture the transient changes in cAMP levels was another potential concern. The localized cAMP measured by this technique is likely bound to receptors, as the washing and fixation process may result in the loss of free, soluble nucleotides (Greene, Shanfeld et al. 1980). However, the bound cAMP is still in equilibrium with the free cAMP and thus, provides a semi-quantitative means of comparing control and treatment groups. It has been shown that a as a semi-quantitative method, relative changes in cyclic nucleotides can be addressed with immunostaining and provide informative results (Dousa, Barnes et al. 1977; Ong and Steiner 1977; Ortez 1978).

Using whole islets, this method also allowed us to measure the cAMP in β-cells, where it is much better characterized, and this provided an intrinsic control for all of our experiments in α-cells using this method. Thus, assuming our hypothesis was correct; we expected to see a decrease in cAMP levels in the α-cells at 11 mM glucose as compared to 1 mM glucose. Representative images for one human islet and one murine islet are displayed in Figure 2-1, where islet α-cells were identified via primary antibodies to glucagon and mean intensities for each channel were background-corrected by pre-immune control images. By eye, the differences in cAMP levels (green channel) are more evident in the murine tissue; however our conclusions were drawn from the quantitative results shown in Figure 2-3, below.

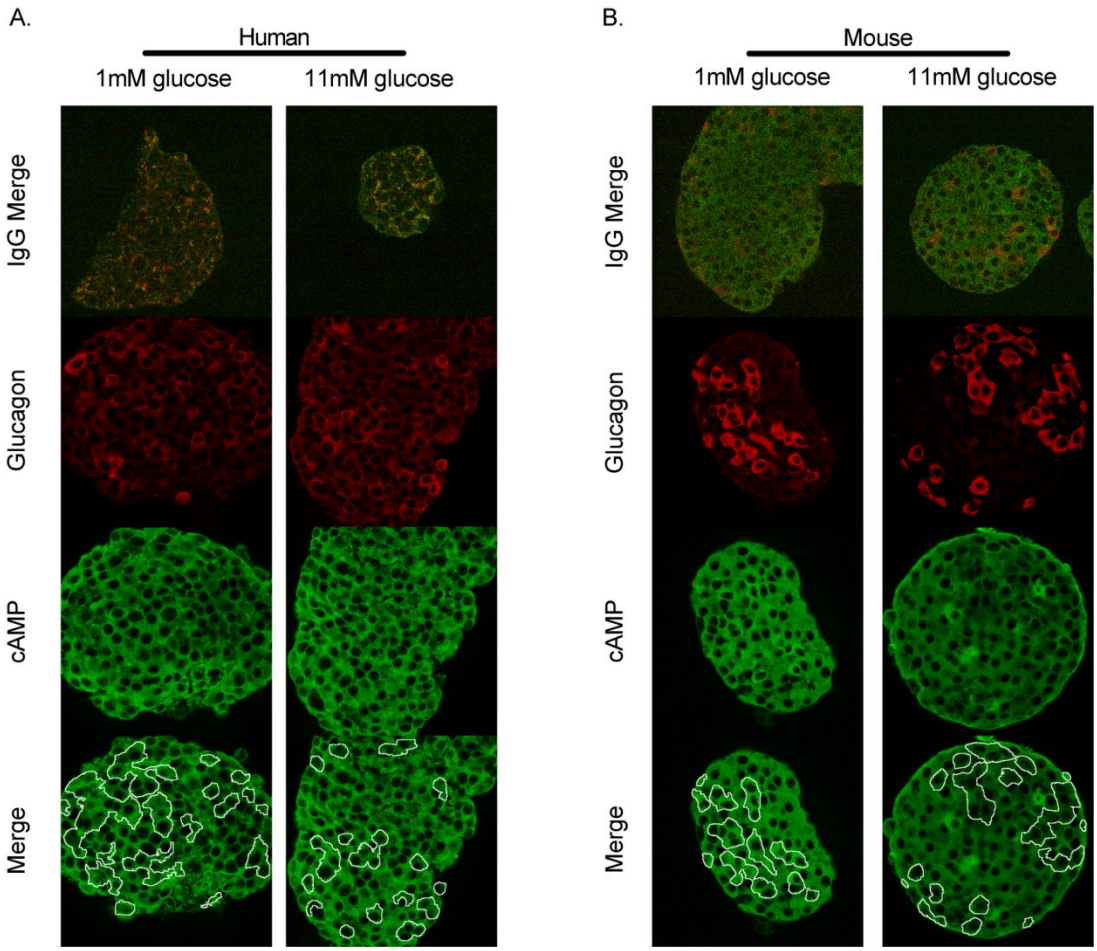

Figure 2-1: cAMP is decreased with high glucose in human and murine α-cells. (A-B) Immunofluorescence from donor human or isolated murine islets statically incubated with 1 or 11 mM glucose before fixing and staining for glucagon and cAMP; cAMP in green, glucagon in red and glucagon-positive cells outlined in white. Images from representative (A) human islets and (B) murine islets shown with merged pre-immune control images (top).

As mentioned, primary antibodies against insulin were also used to identify the effect of glucose on cAMP levels in β-cells. Based on a wealth of previous literature, we expected to see an increase in cAMP with glucose. This parallel experiment provided a very nice control for the immunofluorescence; as a way to be sure the cAMP antibody would exhibit differences in cAMP levels in the islet cells, and also to demonstrate that the protocol used for stimulation, fixing, and staining was effective. Figure 2-2 shows representative immunofluorescence images from the same islets as in 3-1, with the β-cells labeled in blue and cAMP again in green.

Importantly, the antibody used to measure cAMP exhibited enough dynamic range to identify differences in cAMP levels in the islets with a variety of experimental treatments. Standardizing the imaging settings allowed us to compare directly the mean intensity from the α- and β-cells from many islets after normalizing to pre-immune controls. The paradigm developed with these first studies using the immunofluorescence was carried on throughout the remainder of the work in this chapter, though for simplicity, only representative merged (cAMP and glucagon or insulin) images will be shown along with the quantification, from which we drew our conclusions.

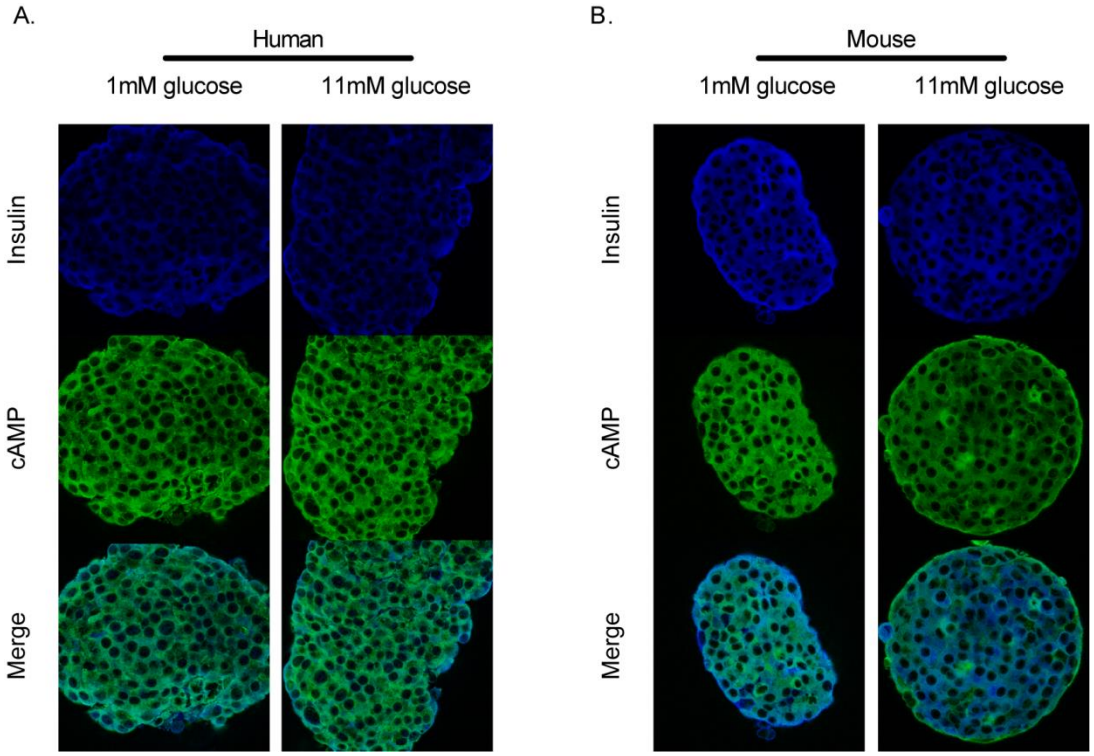

Figure 2-2: In islet β-cells, cAMP increases with increasing glucose levels in humans and mice. Representative images from (A) human islets and (B) murine islets; cAMP in green, insulin in blue.

Figure 2-3 shows the quantification of mean intensities for cAMP from the α- and β-cells treated with either low or high glucose averaged across isolated islets from 4 human donors and

10 mice, including those represented in Figures 3-1 and 3-2. We found that islets treated with 11 mM glucose showed reduced cAMP in both human (32.6% ± 3.43) and murine (24.4% ± 3.98) islet α-cells compared with islets stimulated with 1 mM glucose. In contrast, islet β-cells displayed an increase in cAMP at high glucose in human (27% ± 4.6) and murine (21.5% ± 3.7) islets, as expected from the literature. These studies lent credence to our initial hypothesis, but we did some additional control experiments to convince ourselves that the immunofluorescence method would be fruitful for testing the other components of our theories.

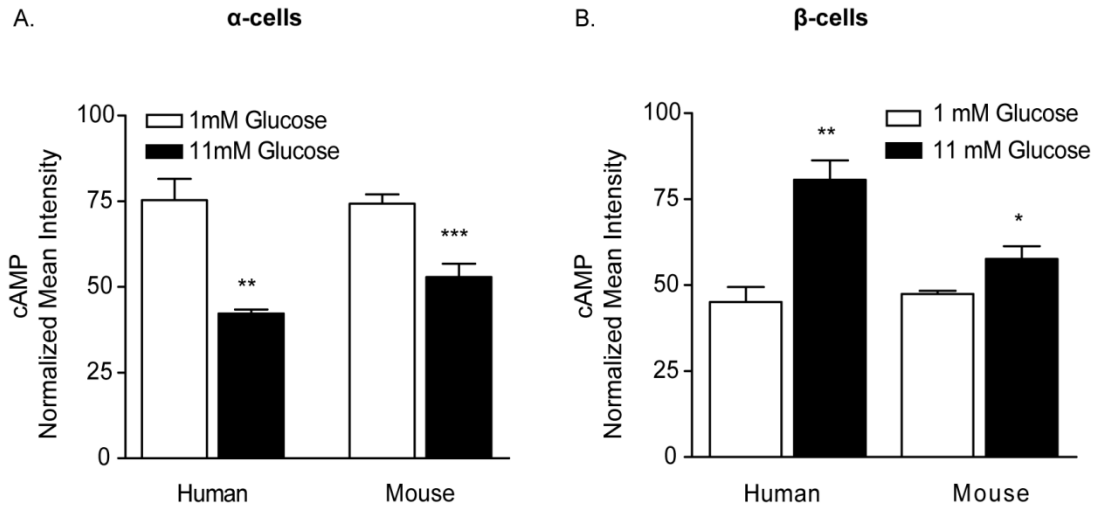

Figure 2-3: cAMP is differentially regulated between α- and β-cells in human and murine islets. Quantification of mean intensity normalized to pre-immune controls from the immunofluorescence images in 3-1 (A) and 3-2 (B). Error bars represent the S.E.M. across islets from 4-6 human donors or 4-10 mice and p values were determined by Student's t-test. * indicates $p < 0.05$, ** $p < 0.01$, *** $p < 0.0001$.

Thus, we also used this technique to confirm that phosphodiesterase inhibitor 3-isobutyl-1-methylxanthine (IBMX) and adenylyl cyclase activator (forskolin) would exhibit the known stimulatory effects on cAMP levels. We expected that maximizing the activity of cAMP in the α-cells would relieve the observed inhibition due to high glucose levels. Since the treatment with IBMX and forskolin maximized the amount of cAMP available for the primary antibodies to bind,

we used this experiment to identify the upper bound of expected signal and dynamic range of the assay. We found that murine islet α-cells treated with IBMX/forskolin showed no significantly differences between those stimulated at 1 mM or 11 mM glucose. However, compared with control islets (11 mM glucose alone), cAMP intensity was increased 21.6% ± 5.8 across islets isolated from 6-10 mice, as shown in Figure 2-4.

Of note, the similarity in the cAMP levels in α-cells treated with IBMX/forskolin is consistent with a maximal level that can be produced, which should be limited, in part, by the amount of ATP available for the reaction by adenylyl cyclases. Additionally, the lack of further stimulation in cAMP levels at 1 mM glucose in the presence of IBMX/forskolin suggests that this pathway is already maximally being utilized by the α-cells in response to low glucose, which implies that these cells rely heavily on this signaling pathway for normal function.

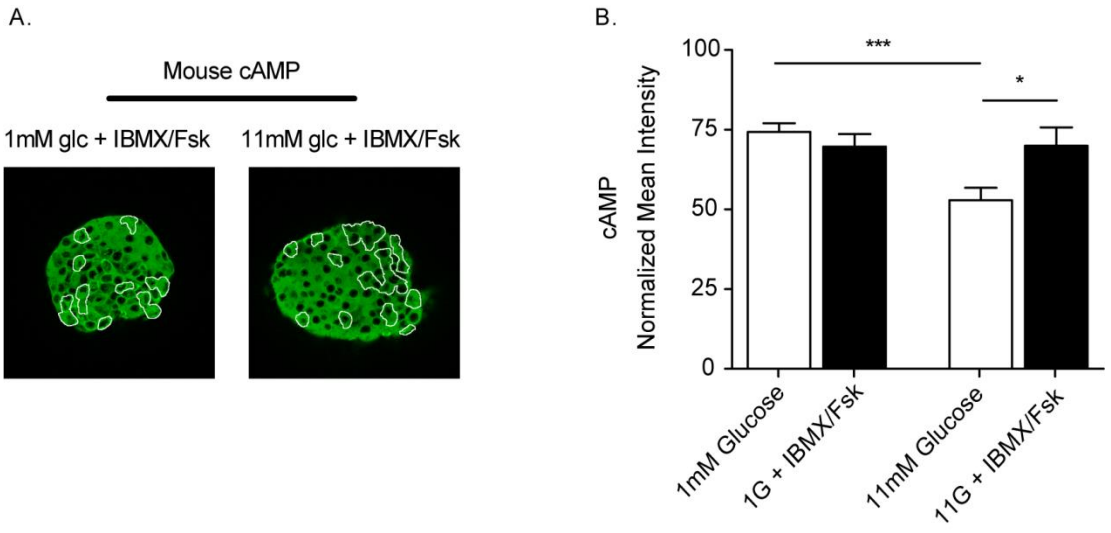

Figure 2-4: Glucose-inhibition of cAMP can be overcome by stimulating production and inhibiting degradation of cAMP. (A) Representative images of islets treated with 100 μM IBMX and 50 μM forskolin at 1 (left) and 11 (right) mM glucose. (B) Quantification of mean intensity normalized to pre-immune controls from the immunofluorescence images. Error bars represent the S.E.M. across 6-10 mice in each experiment and p values were determined by Student's t-test. * indicates $p < 0.05$, ** $p < 0.01$, *** $p < 0.0001$.

Effect of forced cAMP elevation on glucagon secretion

In several endocrine cell types, including islet α- and β-cells, stimulating cAMP has been shown to increase secretion. Thus, to determine if forcibly elevating cAMP is sufficient to overcome the glucose inhibition of glucagon secretion from α-cells, we measured glucagon secretion from donor human islets and isolated murine islets treated with IBMX and/or forskolin. In human islets, we observed a 3.22 ± 0.14 fold increase in glucagon secretion following IBMX/forskolin treatment compared to glucose alone at 11 mM glucose; but no significant difference was found at 1 mM glucose. Similarly, in murine islets at 11 mM glucose, the forskolin-treated samples exhibited a 2.1 ± 0.06 fold increase in glucagon secretion over 11 mM glucose alone, with no difference at 1 mM glucose, as shown in Figure 2-5. From these data, we conclude that modulating cAMP levels exerts a glucose-dependent effect on glucagon secretion in the islet α-cells.

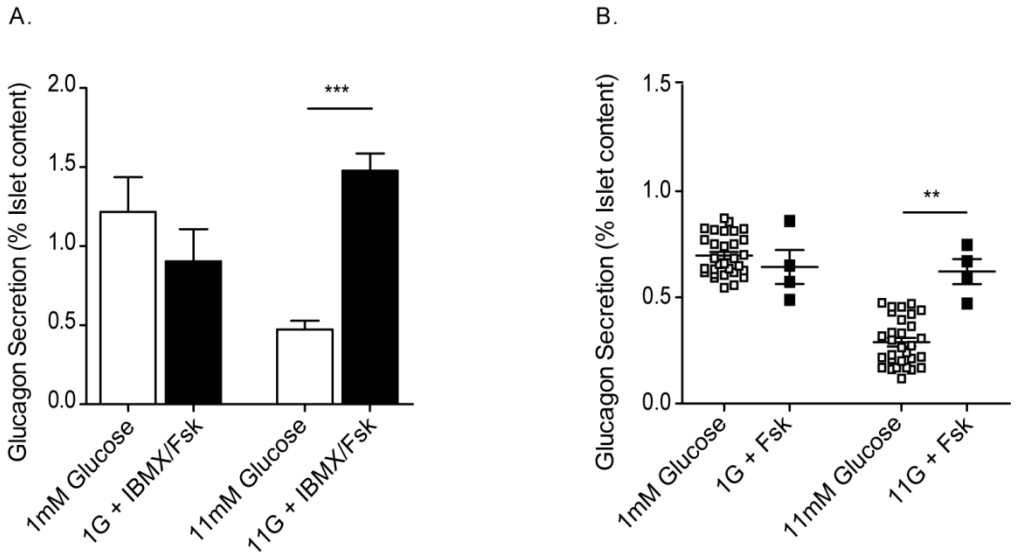

Figure 2-5: Forced elevation of cAMP overcomes glucose-inhibition of glucagon secretion. (A) Glucagon secretion from islets treated with 100 μM IBMX and 50 μM forskolin from the islets of 4 human donors. (B) Glucagon secretion from isolated murine islets treated with forskolin. Error bars represent the S.E.M. and p values were determined by Student's t-test. * indicates $p < 0.05$, ** $p < 0.01$, *** $p < 0.0001$.

We know from the literature that IBMX/forskolin stimulation of cAMP also strongly stimulates β-cells and insulin secretion (and possibly somatostatin secretion from δ-cells), particularly at high glucose levels, so we concluded that the rise in cAMP and glucagon secretion that we observed in the α-cell were due to direct action upon them. However, to control for possible cAMP-mediated effects on β-cell regulation, we also measured insulin secretion from the same islets. Insulin secretion from cAMP-stimulated islets was increased 1.78 ± 0.61 and 15.3 ± 2.8 fold in humans and mice, respectively, at 11 mM glucose, as shown in Figure 2-6. Since we still see a loss of glucagon inhibition from the α-cells after cAMP stimulation in spite of the increase in available insulin, we maintain that cAMP must be decreased in the α-cell for proper suppression of glucagon exocytosis and that this effect is not mediated by the β-cells.

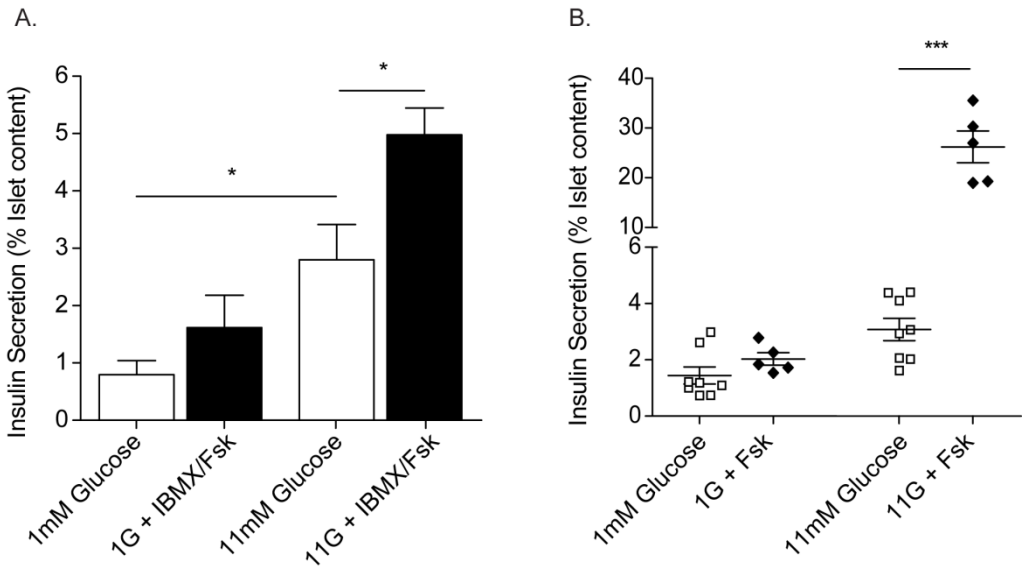

Figure 2-6: cAMP stimulation increases insulin secretion from islet β-cells. (A) Insulin secretion from islets treated with 100 μM IBMX and 50 μM forskolin from the islets of 3 human donors. (B) Insulin secretion from isolated murine islets treated with forskolin. These data are from the same samples as those in Fig. 2-5). Error bars represent the S.E.M. and p values were determined by Student's t-test. * indicates $p < 0.05$, ** $p < 0.01$, *** $p < 0.0001$.

The maximal stimulation of cAMP by forcibly activating adenylyl cyclase and inhibiting degradation by phosphodiesterases can be expected to have many effects, particularly at high glucose levels, where a superfluity of events are occurring across the islet cells. To determine if activating cAMP signaling could overcome the inhibition of glucagon in a more physiological manner, we treated islet cells with a cell-permeant cAMP analog, which has a slight phosphodiesterase resistance, at low and high glucose. We expected this molecule to elicit the same effects as treatment with IBMX/forskolin, and that is what we observed. Islet stimulation with the cAMP analog 8-Br-cAMP caused a 2.48 ± 0.05 fold increase in glucagon secretion over glucose-only controls at 11 mM glucose, with no significant effect at 1 mM glucose, as shown in Figure 2-7. This confirms that there is a glucose-dependent effect on glucagon secretion via cAMP pathway modulation that is detectable without maximally stimulating this pathway.

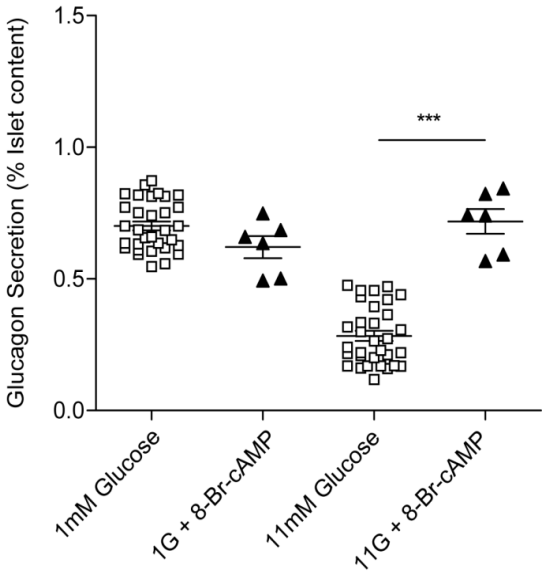

Figure 2-7: A cAMP analog overcomes glucagon inhibition at high glucose. Glucagon secretion from isolated murine islets treated with 300 μM 8-Br-cAMP at 1 and 11 mM glucose. Error bars represent the S.E.M. and p values were determined by Student's t-test. * indicates $p < 0.05$, ** $p < 0.01$, *** $p < 0.0001$.

Glucose-dependent α-Cell cAMP signaling is independent of intracellular calcium

The prevailing models of glucose-inhibited glucagon secretion all rely on a decrease in intracellular Ca^{2+} ($[Ca^{2+}]_i$)as the primary mechanism for suppressing exocytosis. However, we and other have demonstrated that this is not the case and part of the motivation for looking at the role of cAMP in glucagon inhibition was to identify a mechanism that explained the previous data. Since cAMP and Ca^{2+} signaling often cross-talk, and several cAMP-related signaling cascades lead to a modulation of $[Ca^{2+}]_i$, we tested the effect of stimulating cAMP signaling on $[Ca^{2+}]_i$. The expected candidate system for suppressing glucagon secretion with increasing glucose must not rely on a decrease in $[Ca^{2+}]_i$ to be consistent with our previous findings.

To determine whether modulating cAMP affects $[Ca^{2+}]_i$ in α-cells, we utilized loaded islets isolated from mice with tdRFP-expressing α-cells (Le Marchand and Piston 2010) with the fluorescent Ca^{2+} indicator dye Fluo4. Using a microfluidic device (Rocheleau, Walker et al. 2004), Fluo4 intensity was monitored over time in islets treated with IBMX and forskolin. No significant differences in $[Ca^{2+}]_i$ were observed between either 1 and 11 mM glucose, nor between the IBMX/forskolin treated and untreated groups. Additionally, the percentage of α-cells that were oscillating was unaffected by change in glucose concentration and treatment with IBMX/forskolin, as demonstrated by single cell time-course traces of Fluo4 intensity, consistent with other published observations (Quesada, Todorova et al. 2006; Le Marchand and Piston 2010). Figure 2-8 displays the results from measuring $[Ca^{2+}]_i$ in 2-6 isolated islets from 4 mice.

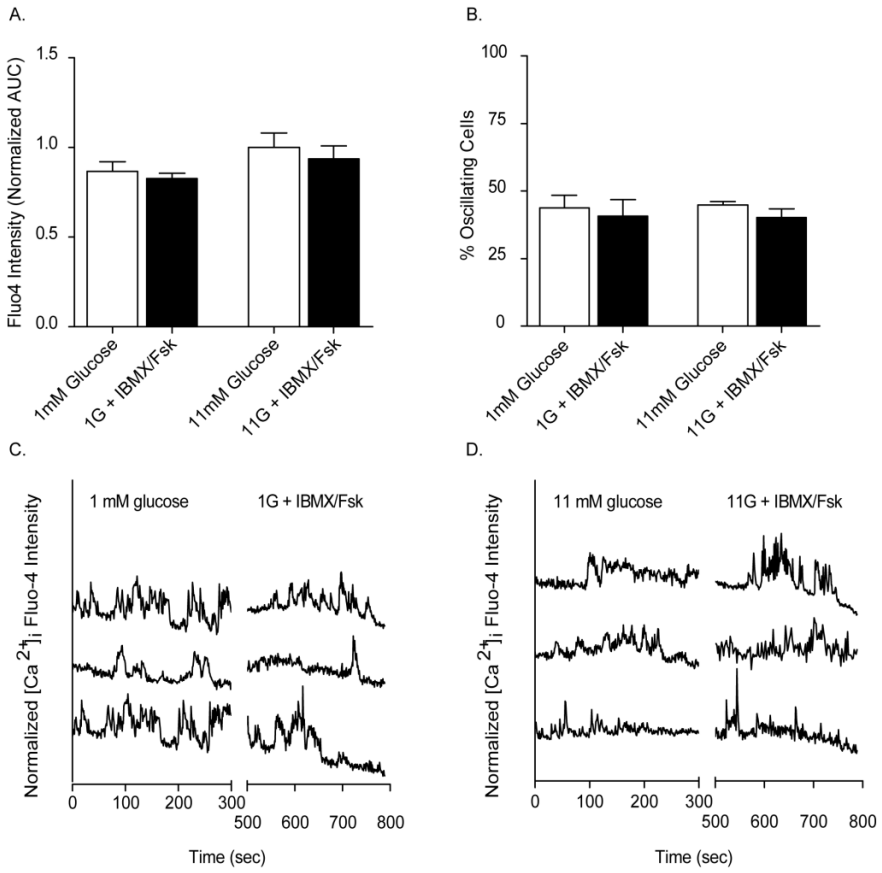

Figure 2-8: cAMP stimulation is independent from changes in α-cell $[Ca^{2+}]_i$. Isolated murine islets were exposed to 1 mM or 11 mM glucose in the absence (white bars) and presence (black bars) of 100 µM IBMX and 50 µM forskolin (Fsk) and subjected to Ca^{2+} imaging via Fluo4 intensity. (A) $[Ca^{2+}]_i$ as measured by Fluo4 intensity (AUC) in murine isolated islets treated with glucose alone or in the presence of IBMX and Fsk. (B) Mean percent of cells with oscillations in Ca^{2+} as a function of glucose, where α-cells were identified by td-RFP expression in islets from 4 mice. Representative $[Ca^{2+}]_i$ response to glucose alone or IBMX/Fsk stimulation at 1 mM (C) and 11 mM (D) glucose. Timecourse traces are offset for clarity. Error bars represent the S.E.M.

As the role of $[Ca^{2+}]_i$ in the glucose-dependent suppression of glucagon secretion is debated in the field, we also analyzed the β-cells to determine the effect of stimulating cAMP, expecting an increase in activity and number of active cells based on a wealth of previous reports. We observed that 11 mM glucose drove a 33.3% ± 0.12 and IBMX/forskolin a 62.1% ± 0.2 increase in $[Ca^{2+}]_i$, respectively, over 1 mM glucose alone in the β-cells from the same islets as in Figure 2-7. The number of oscillating cells was also increased 58.3% ± 3.8 by 11 mM

glucose and 63.5% ± 4.5 with IBMX/forskolin stimulation over 1 mM glucose alone. Additionally, treatment with IBMX/forskolin at 11 mM glucose further significantly increased $[Ca^{2+}]_i$ and the percentage of oscillating cells, which supports previous observations (Dyachok, Isakov et al. 2006) of β-cell activity, and confirmed that our assay was effective for identifying any effects of cAMP stimulation on $[Ca^{2+}]_i$ in the islets. The β-cell data is shown below in Figure 2-9.

From the collected data on $[Ca^{2+}]_i$ and cAMP elevation in the islet α-cells, we conclude that, in contrast to β-cells, stimulating cAMP does not modulate global $[Ca^{2+}]_i$ in the α-cells.

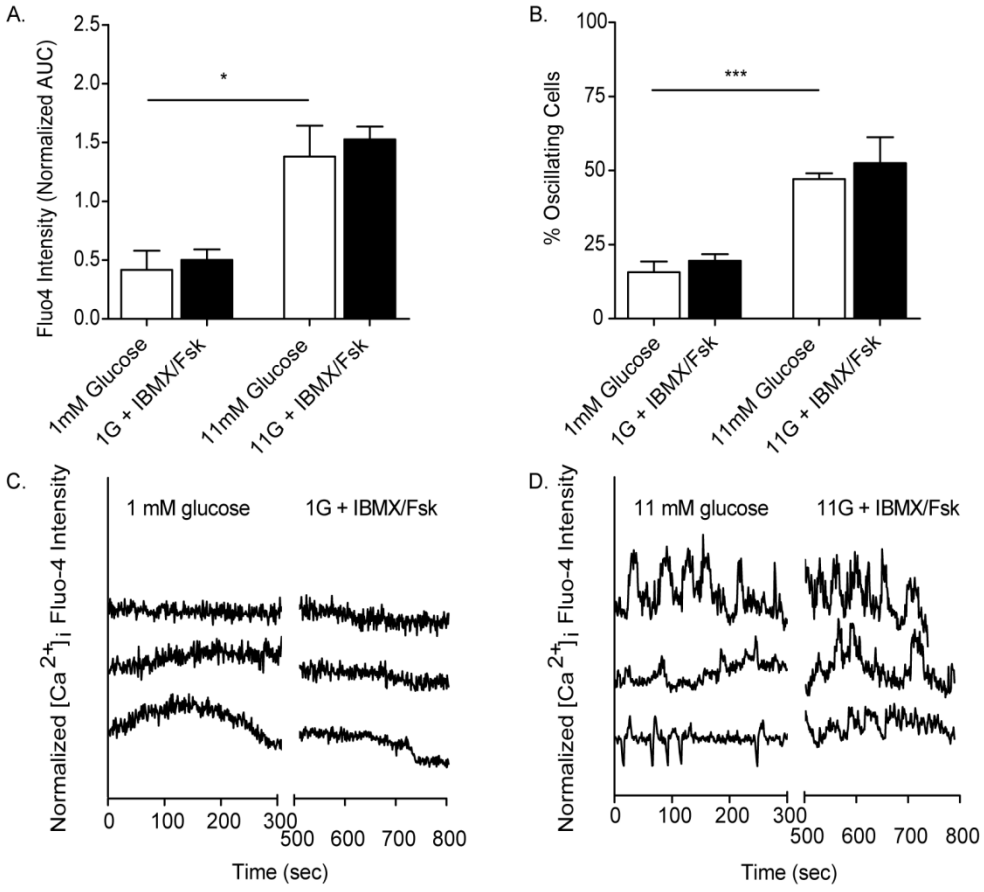

Figure 2-9: Modulating cAMP signaling differentially affects insulin and glucagon signaling in human and murine islets. (A) $[Ca^{2+}]_i$ as measured by Fluo4 intensity (AUC) in murine isolated islets treated with 1 and 11 mM glucose alone (white bars) or in the presence of 100 µM IBMX and 50 µM forskolin (black bars). (B) Mean percent of cells with oscillations in Ca^{2+} as a function of glucose, where β-cells were identified as those not expressing td-RFP in islets from 4 mice. (C) Representative intracellular free-calcium response to glucose alone or IBMX/forskolin at 1 mM and (D) 11 mM glucose. Timecourse traces are offset for clarity.

Epinephrine increases cAMP across glucose levels in islet α-cells

Another important mechanism for increasing glucagon secretion is via the catecholamine epinephrine (a.k.a. adrenaline), which is a hormone and neurotransmitter produced by the adrenal medulla. Epinephrine binds to G-protein coupled adrenergic receptors of either the α- or β- family and typically acts by increasing cAMP production by adenylyl cyclases. The opposing functions by receptor subtype are a critical feature for islet biology. Islet α-cells express β-adrenergic receptors, which when stimulated, increase production of cAMP by activating adenylyl cyclases. By contrast, the β-cells express α_2-adrenergic receptors, which are coupled to an inhibitory $G\alpha_i$ subunit that reduces cAMP production and Ca^{2+} channel activity and leads to decreased insulin secretion. In our studies, we treated isolated murine islets with epinephrine and measured the cAMP by immunofluorescence as with previous studies. As expected, we found a significant increase in cAMP mean intensity in the α-cells at both low and high glucose in islets treated with epinephrine compared with glucose-only treated islets, as shown in Figure 2-10. Since glucagon secretion has been heavily characterized with epinephrine treatment, we did not perform those experiments. However, several publications (Gromada, Bokvist et al. 1997; Kawamori, Kurpad et al. 2009; Hauge-Evans, King et al. 2010; Tian, Sandler et al. 2011) demonstrate the glucose-independence of epinephrine in stimulating glucagon secretion from islets.

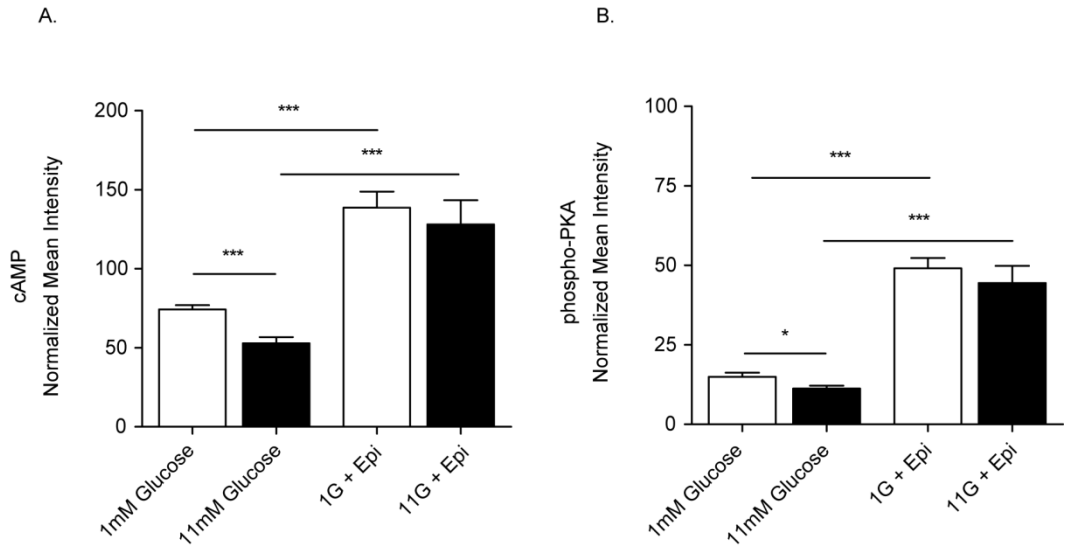

Figure 2-10: Epinephrine stimulates cAMP independently of glucose levels in islet α-cell. (A) Normalized cAMP intensities from isolated islets of 4 mice treated with either 1 mM glucose (white bars) or 11 mM glucose (black bars) in the presence and absence of epinephrine. (B) Normalized phospho-PKA intensities from (A). Error bars represent the S.E.M. and p values were determined by Student's t-test. * indicates $p < 0.05$, ** $p < 0.01$, *** $p < 0.0001$

We also analyzed the β-cells from the same islets treated with epinephrine to confirm that there is no increase in cAMP levels in epinephrine-treated vs glucose-only treated islets. Consistent with the literature, we find no increase in cAMP with epinephrine treatment of isolated islets, as compared with glucose alone, which is shown in Figure 2-11. Treatment with epinephrine significantly blunted the normal stimulation of cAMP by glucose in the β-cells and produced no significant affect at low glucose. These experiments confirmed that cAMP signaling can be regulated in glucose-dependent and independent ways in the α-cells, which is an important factor in stimulus-secretion coupled systems. Finally, while $[Ca^{2+}]_i$ is a known downstream target of epinephrine signaling, we did not see a glucose-dependent change in Ca^{2+} with forced elevation of cAMP (Fig. 3-8). These data demonstrate the different mechanisms by which second messengers can be utilized by various stimuli in the islet cells to control hormone secretion differentially among the specific cell types.

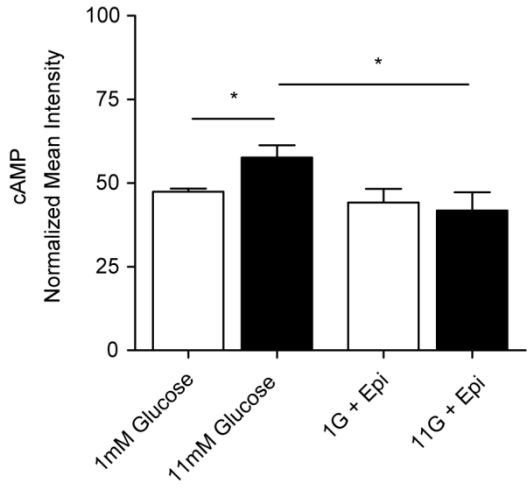

Figure 2-11: Epinephrine does not stimulate cAMP in islet β-cells. (A) Normalized cAMP intensities. Error bars represent the S.E.M. and p values were determined by Student's t-test. * indicates $p < 0.05$, ** $p < 0.01$, *** $p < 0.0001$

These data solidified cAMP signaling as a candidate pathway whose activity must be decreased in mediating the inhibition of glucagon secretion with glucose. Additionally, there are a number of G-protein coupled receptors present in the α-cells, with at least one, the somatostatin receptor, having an inhibitory Gαi subunit that might explain how cAMP is being reduced with glucose. This was the basis for the following line of enquiry in our studies: to determine if somatostatin is driving the decrease in cAMP at high glucose that we observed in the α-cells.

Somatostatin prevents cAMP production via the $G\alpha_i$ subunit of SSTR2

Another important regulator of glucagon secretion is the δ-cell product somatostatin, which has been shown also to affect intracellular cAMP levels. Somatostatin is a potent inhibitor of glucagon secretion and the most highly expressed somatostatin receptor in the α-cells is somatostatin receptor type 2 (SSTR2). We hypothesized that somatostatin exerts its inhibitory effect on glucagon secretion via SSTR2 by decreasing the production of cAMP from

adenylyl cyclase activity. To test this, we measured cAMP using the immunofluorescence methodology to identify if somatostatin decreased cAMP levels at low glucose, and if antagonizing the SSTR2 would prevent such a decrease at high glucose. In murine islets treated with somatostatin at 1 mM glucose, cAMP was reduced by 39.8% ± 3.1 compared with glucose alone. SSTR2 antagonism by CYN154806 elicited a 39.4% ± 4.6 increase in cAMP over 11 mM glucose alone, as shown in Figure 2-12.

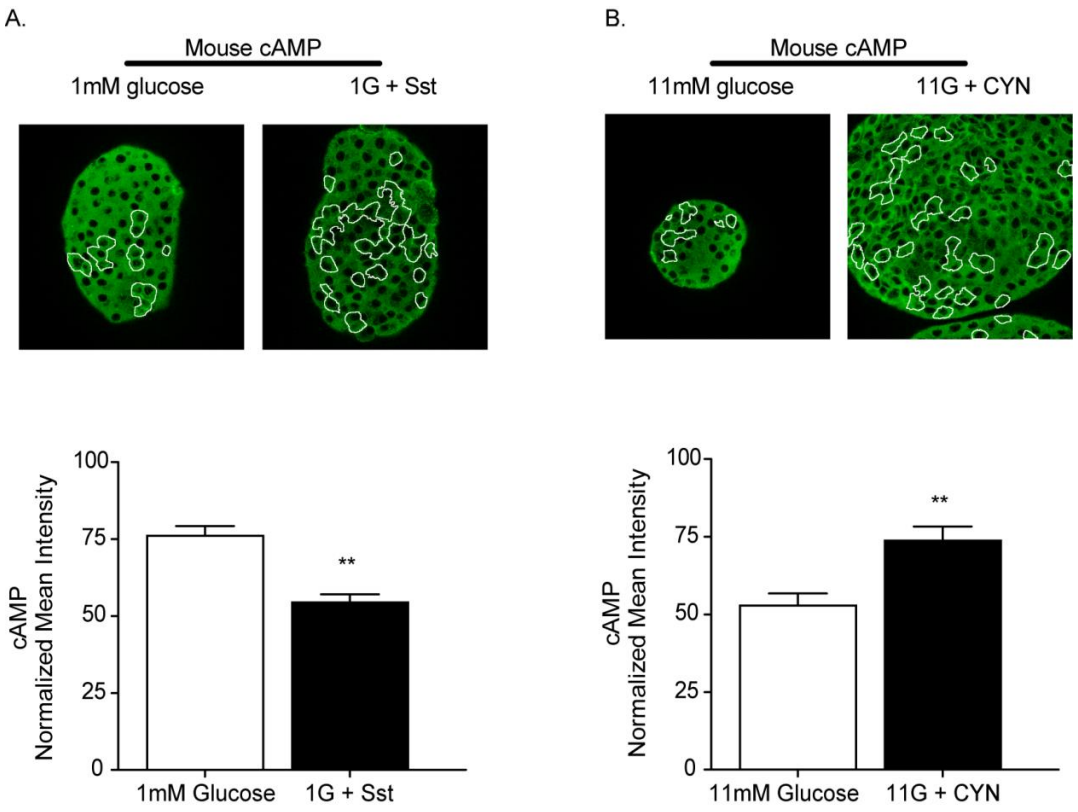

Figure 2-12: Somatostatin inhibits cAMP production via the Gαi subunit of SSTR2. (A-B) Mean intensities from immunofluorescence studies where murine islets were fixed after treatment and stained for cAMP and glucagon and normalized to pre-immune control images; cAMP in green, glucagon positive-cells outlined in white. (A) Islets were treated with 100 nM somatostatin (Sst) at 1 mM glucose (N = 6) or with glucose alone (N = 13). (B) Islets were treated with 200 nM SSTR2 antagonist CYN154806 (CYN) at 11 mM glucose (N = 8) or with glucose alone (N = 10). Error bars represent the S.E.M. and p values were determined by Student's t-test. * indicates $p < 0.05$, ** $p < 0.01$, *** $p < 0.0001$

From these immunofluorescence studies, we concluded that somatostatin inhibits adenylyl cyclases responsible for cAMP production via the action of SSTR2. We next measured glucagon secretion from islets treated with SSTR2 antagonist CYN154806 at 1 and 11 mM glucose to determine if the effect on cAMP was mirrored by a loss of glucagon suppression at high glucose. SSTR2 antagonism in human islets exhibited no difference in secretion at 1 mM glucose and a 2.5 ± 0.41 fold increase over 11 mM glucose alone. Similarly, glucagon secretion from murine islets exhibited a 2.61 ± 0.04 fold increase in glucagon secretion upon addition of CYN154806 at 11 mM glucose, and no significant difference was observed at 1 mM glucose, shown in Figure 2-13. This confirms a glucose-dependent effect of somatostatin on both cAMP production and glucagon secretion that is mediated by the SSTR2.

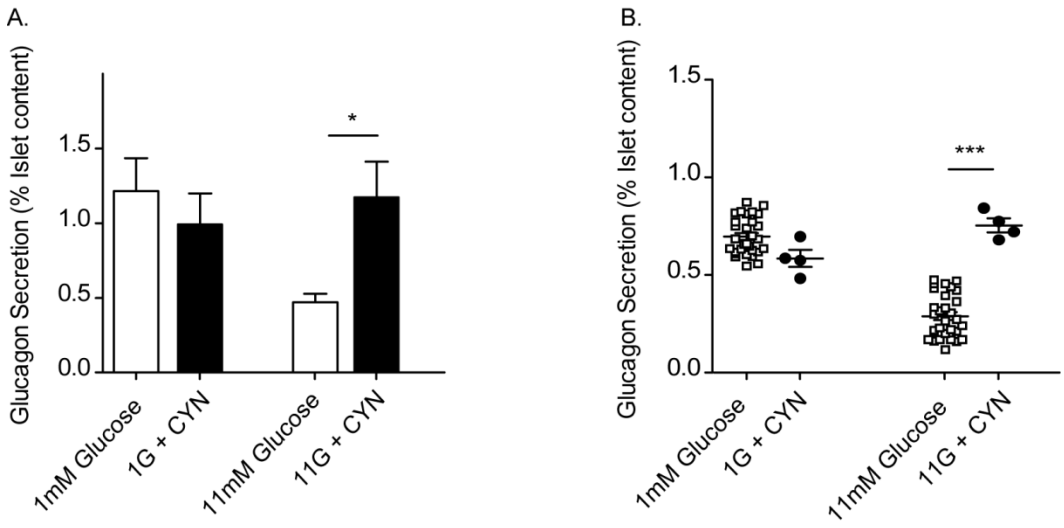

Figure 2-13: Somatostatin inhibits glucagon secretion via SSTR2 activation. (A) Human islet glucagon secretion (N = 3-5 donors) with glucose alone (white bars) or with glucose and CYN (black bars) after static incubation. (B) Isolated murine islet glucagon secretion with glucose alone in white squares and CYN-treated islets in black circles. Error bars represent the S.E.M. and p values were determined by Student's t-test. * indicates $p < 0.05$, ** $p < 0.01$, *** $p < 0.0001$

Since the CYN154806 only specifically antagonized the SSTR2, we repeated the secretion experiment with a broad somatostatin receptor antagonist to both account for the possibility of compensatory function from another SSTR subtype, and also to test the hypothesis that SSTR2 sufficiently explains the effects we observe with glucagon secretion. Treating islets with a putative SSTR antagonist, cyclosomatostatin (cSST), we observed a 2.02 ± 0.05 increase in glucagon secretion over glucose-alone control islets, as shown in Figure 2-14. Additionally, the SSTR2-specific antagonist produced a significantly stronger effect on glucagon secretion than the cSST ($p < 0.05$). These data support the SSTR2 being functionally dominant in the α-cells, suggest that glucagon inhibition with glucose requires somatostatin, and shows that SSTR2 accounts for this effect.

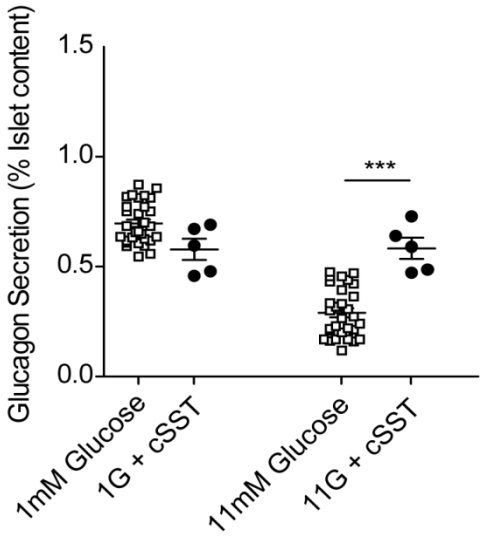

Figure 2-14: A broad somatostatin receptor antagonist also relieves glucagon inhibition at high glucose. Glucagon secretion from murine islets treated with somatostatin receptor antagonist cyclosomatostatin (cSST) at 1 and 11 mM glucose. Error bars represent the S.E.M. and p values were determined by Student's t-test. * indicates $p < 0.05$, ** $p < 0.01$, *** $p < 0.0001$

As somatostatin is expected to act via the inhibitory Gα ($G\alpha_i$) subunit of the G-protein coupled receptor, we next measured glucagon secretion after pertussis toxin (PTX) treatment to

inactivate the $G\alpha_i$ subunit, shown in Figure 2-15 below. At 1 mM glucose, pretreatment with PTX led to a 2.10 ± 0.05 fold increase in glucagon secretion over somatostatin-treated control islets. At 11 mM glucose, PTX caused a 2.35 ± 0.08 fold increase in secretion over glucose alone. To test whether the effect of PTX is due to a direct inhibition of $G\alpha_i$ signaling in α-cells rather than an indirect effect through β-cells, we also measured insulin secretion. As previously reported (Cawthorn and Chan 1991), somatostatin did not inhibit insulin secretion from these islets, which was increased 5.91 ± 0.34 fold and 5.95 ± 0.58 fold at 1 and 11 mM glucose, respectively, with PTX pretreatment. Presumably, the PTX would prevent any $G\alpha_i$ signaling in the δ-cells as well, which further supports the hypothesis that the effect we observe in the α-cells is due to a direct effect.

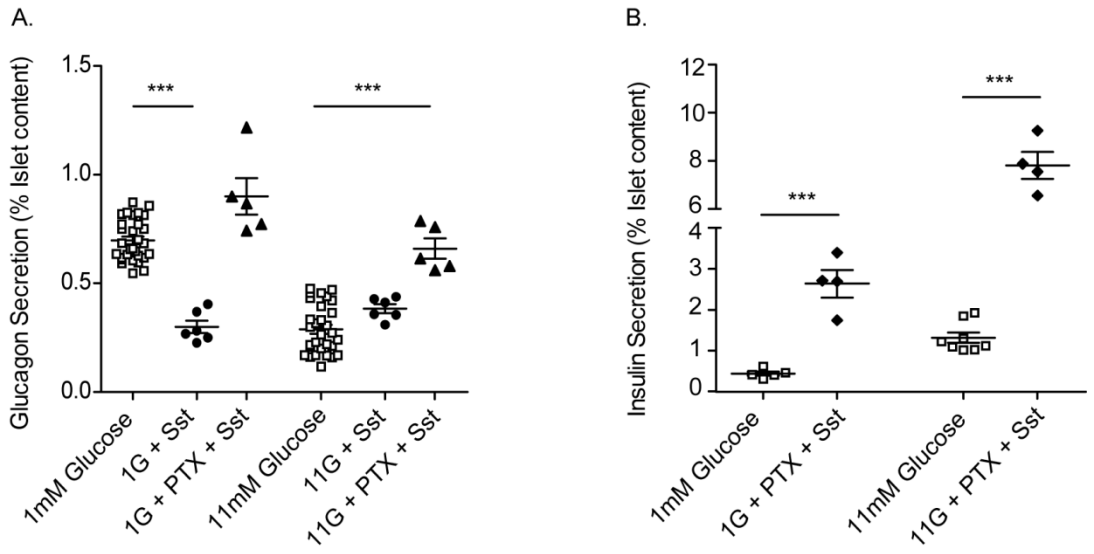

Figure 2-15: Somatostatin inhibits glucagon secretion via Gαi subunit of SSTR2. (A) Murine islets were pretreated with 1 mg/ml pertussis toxin (PTX) for 18 hours, and then stimulated with 100 nM Sst (black triangles) at 1 mM glucose or 11 mM glucose. Control islets treated with glucose alone (white squares) or with 100 nM Sst (black circles) are also displayed. (B) Insulin secretion from isolated murine islets from (A) with PTX-pretreated islets in black diamonds and glucose-only controls in white squares. Error bars represent the S.E.M. and p values were determined by Student's t-test. * indicates $p < 0.05$, ** $p < 0.01$, *** $p < 0.0001$

These data demonstrate that somatostatin's primary inhibitory mechanism in glucagon-secreting α-cells is by Gαi submit-mediated inhibition of adenylyl cyclase. We further conclude that it is a direct effect on the α-cells due to the concomitant increase in insulin secretion from β-cells that we measured. Since PTX pretreatment prevents somatostatin from inhibiting insulin as well as glucagon at high glucose, we next wanted to see if a high enough concentration of insulin could compensate for the lack of somatostatin and drive down glucagon secretion. As insulin signaling does not proceed via GPCRs, we reasoned that the PTX should not prevent the mechanism of insulin's inhibition. Thus, islets pretreated with PTX were subsequently stimulated with 1 mM or 11 mM glucose with and without 100 nM insulin, as shown in Figure 2-16. Interestingly, the added insulin was still unable to rescue glucagon inhibition at 11 mM glucose in PTX-pretreated islets. At 1 mM glucose, pretreatment with PTX led to a 2.30 ± 0.08 fold increase in glucagon secretion over insulin-treated control islets. At 11 mM glucose, PTX caused a 3.32 ± 0.06 fold increase in secretion over insulin-treated control islets. These values are comparable to those observed with somatostatin treatment after PTX pretreatment.

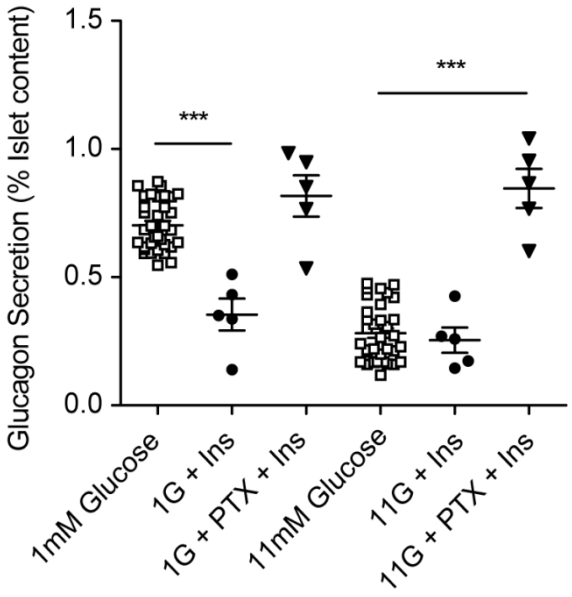

Figure 2-16: Excess insulin cannot inhibit glucagon secretion in the absence of somatostatin. Murine islets were pretreated with 1 mg/ml pertussis toxin (PTX) for 18 hours, and then stimulated with 100 nM Insulin (Ins - black inverted triangles) at 1 mM glucose or 11 mM glucose. Control islets treated with glucose alone (white squares) or with 100 nM Ins (black circles) are also displayed. Error bars represent the S.E.M. and p values were determined by Student's t-test. * indicates $p < 0.05$, ** $p < 0.01$, *** $p < 0.0001$

Taken together these data demonstrate that even an excess of insulin is insufficient for glucose-inhibited glucagon secretion in the absence of somatostatin, which decreases cAMP production by the activity of the SSTR2 Gαi subunit on adenylyl cyclases. This suggests that insulin is an insufficient inhibitor of glucagon secretion in the absence of somatostatin, which previous studies have shown in purified populations of α-cells (Le Marchand and Piston 2010). Another interesting observation we made while studying the effects of IBMX and forskolin on glucagon secretion was that, when used independently, IBMX had a more significant effect than forskolin. At low glucose, IBMX increased glucagon secretion 1.36 ± 0.08 fold compared with forskolin-treated islets. Additionally, at 11 mM glucose, IBMX increased glucagon secretion 1.8 ± 0.06 fold over forskolin-treated islets, as shown in Figure 2-17. From this data, we concluded that phosphodiesterase activity may be a critical factor in the glucose-dependent regulation of

cAMP and glucagon secretion from the α-cells. Combined with the observation that insulin was incapable of exerting an inhibitory effect when somatostatin activity was blocked by PTX, we were encouraged to take a look at the possible role of insulin in the glucose-inhibition of glucagon secretion.

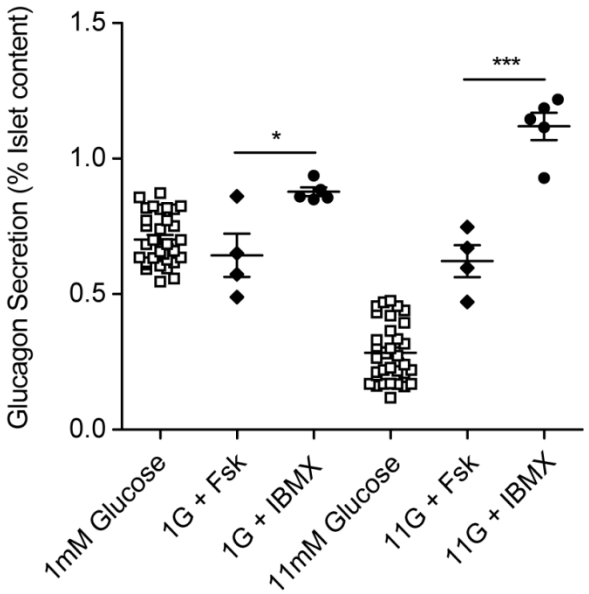

Figure 2-17: Phosphodiesterase activity is critical in the suppression of glucagon exocytosis. Glucagon secretion from murine islets treated with glucose alone at 1 or 11 mM, or stimulated with 50 µM Forskolin (Fsk), or 100 µM IBMX. Error bars represent the S.E.M. and p values were determined by Student's t-test. * indicates $p < 0.05$, ** $p < 0.01$, *** $p < 0.0001$

Insulin mediates α-Cell cAMP degradation by phosphodiesterase 3B

The insulin receptor is known to play a role in α-cell physiology (Kawamori, Kurpad et al. 2009), and insulin receptor signaling can lead to phosphorylation of phosphodiesterases, driving degradation of cAMP (Zmuda-Trzebiatowska, Oknianska et al. 2006). To test the regulatory role of insulin in α-cells, we utilized immunofluorescence as for the somatostatin studies above to identify if insulin affects cAMP levels. Islets treated with insulin exhibited a 23.1% ± 7.2 reduction in α-cell cAMP as compared with 1 mM glucose alone. α-cell cAMP in islets treated

with insulin receptor antagonist S961 (Vikram and Jena 2010) showed a 30% ± 7.8 increase in cAMP over 11 mM glucose, as shown in Figure 2-18.

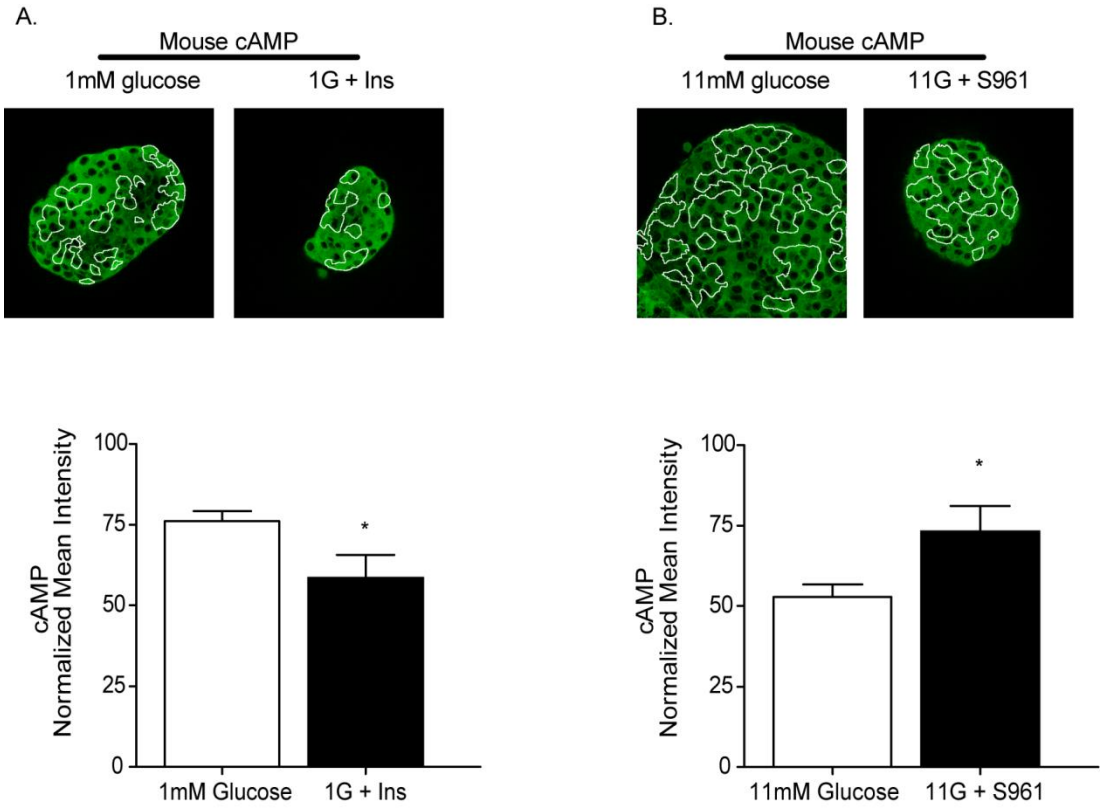

Figure 2-18: Insulin decreases cAMP in the α-cells. (A-B) Mean intensities from immunofluorescence studies where murine islets were fixed after treatment and stained for cAMP and glucagon and normalized to pre-immune control images; cAMP in green, glucagon positive-cells outlined in white. (A) Islets were treated with 100 nM insulin at 1 mM glucose (N = 5), glucose alone (N = 13); or (B) with 1 µM insulin receptor antagonist S961 (N = 6) at 11 mM glucose or with glucose alone (N = 10). Error bars represent the S.E.M. and p values were determined by Student's t-test. * indicates $p < 0.05$, ** $p < 0.01$, *** $p < 0.0001$

We also measured glucagon secretion from islets treated with S961, expecting the loss of insulin receptor signaling to drive an increase in glucagon secretion, which has been demonstrated previously. In human islets, antagonism of the insulin receptor increased glucagon secretion 2.42 ± 0.39 fold over 11 mM glucose alone, with no significant difference in secretion at 1 mM glucose between control and treated islets. In murine islets treated with

S961, glucagon secretion showed a 3.35 ± 0.1 fold increase at 11 mM glucose, and no significant difference at 1 mM glucose, as shown in Figure 2-19.

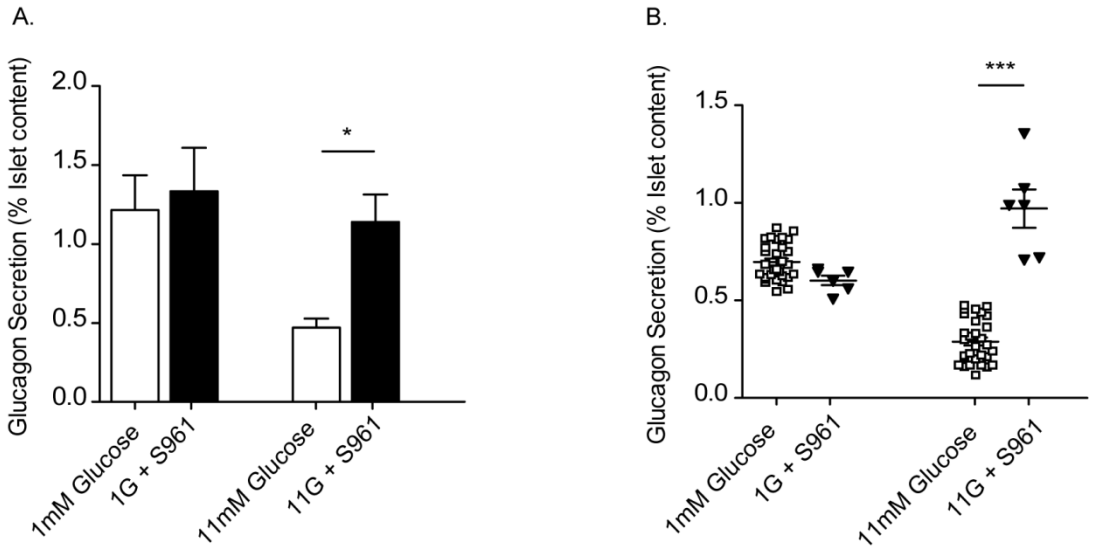

Figure 2-19: Insulin receptors mediate glucagon inhibition with glucose in human and murine islets. (A) Glucagon secretion from islets of 4 human donors incubated with 1 μM insulin receptor antagonist S961 at 1 or 11 mM glucose (black bars) and glucose alone (white bars). (B) Glucagon secretion from isolated murine islets treated with S961 at 1 or 11 mM glucose (black inverted triangles) or glucose alone (white squares). Error bars represent the S.E.M. and p values were determined by Student's t-test. * indicates $p < 0.05$, ** $p < 0.01$, *** $p < 0.0001$

Importantly, one of the caveats of antagonizing the insulin receptor is that the β-cells are also affected and they rely upon positive feedback for glucose-stimulated insulin secretion. Thus, blocking the insulin receptor, including by use of genetic knockout animals, prevents the standard increase in insulin secretion seen with increasing glucose. To be sure that the S961 antagonist was working as reported, we measured insulin secretion from islets treated with the S961. As expected, while there was no effect at 1 mM glucose in the β-cells, insulin secretion was blunted 3.28 ± 0.05 fold in islets treated with S961 compared with glucose-alone controls, shown in Figure 2-20. Additionally, there have been reports of this peptide having selectively agonistic activity at very low concentrations [31] in human islets. Thus, even though its affinity

for the insulin receptor is in the nanomolar range, we utilized a concentration of 1 μM for our studies both to ensure antagonistic properties and also with the expectation of low diffusion through the core of the islets. Collectively, from these data, we conclude that the insulin receptor plays a critical role in the glucose-dependent suppression of glucagon secretion.

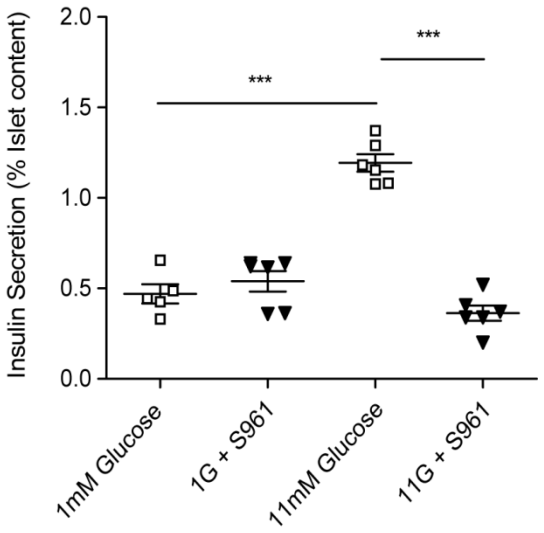

Figure 2-21: S961 blunts glucose-stimulated insulin secretion. Insulin secretion from islets treated with glucose alone (white squares), or with 1 μM insulin receptor antagonist S961 at 1 and 11 mM glucose. Error bars represent the S.E.M. and p values were determined by Student's t-test. * indicates $p < 0.05$, ** $p < 0.01$, *** $p < 0.0001$

Our next goal was to identify the mechanism by which insulin is acting in the α-cells. As mentioned in the introduction to this chapter, there are a number of hypothesis regarding this mechanism. However, the only one that reconciled all of our data with the phosphodiesterase inhibitor was the possibility that insulin is activating phosphodiesterases to degrade cAMP. Turning to the literature on insulin signaling in other cell types, we found that in hepatocytes and adipocytes, insulin decreases cAMP by activating phosphodiesterase 3B (PDE3B) and this leads to the inhibition of gluconeogenesis and lipolysis. Thus, we began our experiments with this idea in mind.

To test the hypothesis that insulin decreases glucagon secretion via phosphodiesterase activation, we measured glucagon secretion from islets at 1 and 11 mM glucose in the presence of insulin and the non-specific phosphodiesterase inhibitor IBMX, displayed in Figure 2-21. While there are at least two IBMX resistant phosphodiesterases (PDE8 and PDE9), neither of them have been reported to be expressed in the α-cells (Bramswig, Everett et al. 2013). We found that at 1 mM glucose, treatment with IBMX and insulin yielded no significant differences in secretion when compared to glucose alone. However, when compared to insulin treatment at 1 mM glucose in the absence of IBMX, glucagon secretion was increased 2.23 ± 0.11. Additionally, 11 mM glucose, IBMX with exogenous insulin increased glucagon secretion 3.17 ± 0.12 fold compared with glucose alone, and 3.61 ± 0.05 compared with glucose with exogenous insulin. These data demonstrate that insulin is ineffective at inhibiting glucagon secretion when phosphodiesterases are blocked.

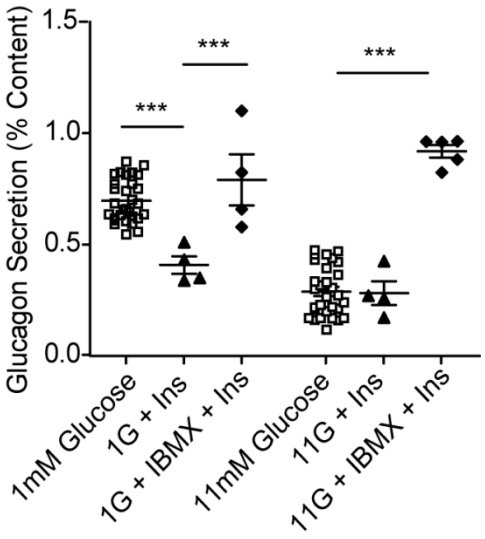

Figure 2-21: Excess insulin cannot inhibit glucagon secretion in the presence of phosphodiesterase inhibitors. Glucagon secretion from murine islets stimulated with 100 nM Insulin (Ins - black inverted triangles) at 1 or 11 mM glucose in the presence and absence of 100 μM IBMX. Error bars represent the S.E.M. and p values were determined by Student's t-test. * indicates $p < 0.05$, ** $p < 0.01$, *** $p < 0.0001$

We measured glucagon secretion in the presence of either a hydrolyzable (8-Br-cAMP) or non-hydrolyzable (6-Bnz-cAMP) cAMP analog together with insulin at 1 mM glucose and 11 mM glucose. While the 8-Br-cAMP does have a slight phosphodiesterase resistance, we still expected to see that a high enough dose of insulin would be able to degrade enough to detect a difference if this was the mechanism by which insulin is functioning in the α-cells. We found that in islets treated with 100 nM insulin, glucagon secretion was not significantly different from glucose alone for either the 8-Br-cAMP or 6-Bnz-cAMP. However, with 1 µM insulin, glucagon secretion from islets treated with 8-Br-cAMP was reduced 1.5 ± 0.15 fold, as we expected. The addition of even a high concentration of exogenous insulin did not have a statistically significant impact on glucagon secretion from islets treated with the non-hydrolyzable 6-Bnz-cAMP, as demonstrated in Figure 2-22.

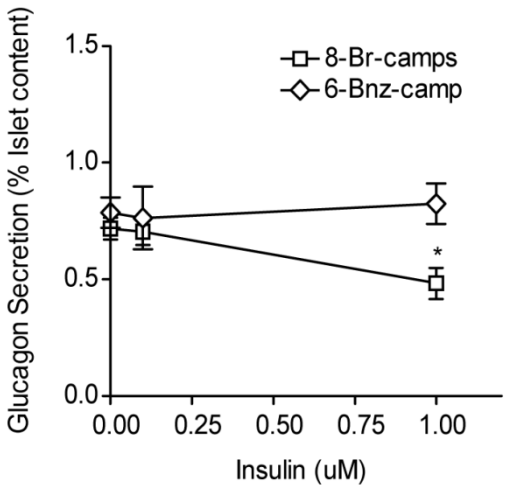

Figure 2-22: Insulin decreases glucagon secretion by activating phosphodiesterases to break down cAMP. At 11 mM glucose, murine islets were incubated with hydrolyzable 100 nM 8-Br-cAMP (white squares) in the presence of no exogenous insulin (N = 6), 100 nM insulin (N = 6), or 1 µM insulin (N = 5). 300 µM non-hydrolyzable 6-Bnz-cAMP (white diamonds) was also tested with no insulin (N = 6), 100 nM insulin (N = 4), or 1 µM insulin (N = 4). Error bars represent the S.E.M. and p values were determined by Student's t-test. * indicates $p < 0.05$, ** $p < 0.01$, *** $p < 0.0001$

Our next goal was to identify the specific phosphodiesterase responsible for the observed effects. From the literature, we expected that PDE3B would be the enzyme of choice for insulin receptor signaling. However, there are other phosphodiesterases in the islet cells. PDE3B and PDE4 have been shown to be expressed in α-cells (Pyne and Furman 2003; Zmuda-Trzebiatowska, Oknianska et al. 2006). To test the hypothesis that one or both of these phosphodiesterases are involved in glucose suppression of glucagon, we measured glucagon secretion in the presence of specific inhibitors for PDE3B (cilostamide) and PDE4 (rolipram). Cilostamide treatment showed a 2.65 ± 0.86 fold increase in glucagon secretion at 11 mM glucose with no significant difference between treated and control islets (glucose alone) at 1 mM glucose. By contrast, rolipram increased glucagon secretion at both 1 mM and 11 mM glucose, with a fold increase of 1.51 ± 0.1 and 2.98 ± 0.06, respectively. Looking at Figure 2-23, only the cilostamide data show significant glucose dependence, which points toward a primary role for PDE3B in insulin-dependent degradation of cAMP and inhibition of glucagon secretion.

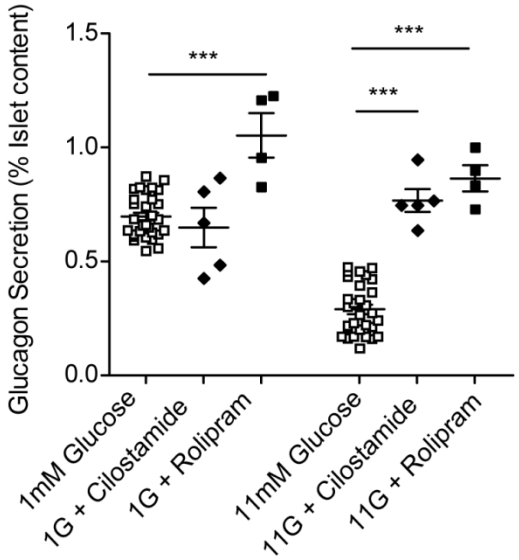

Figure 2-23: PDE3B mediates insulin's effect on cAMP and glucagon secretion. Glucagon secretion from islets treated with glucose alone (white squares), or with phosphodiesterase inhibitors 250 nM cilostamide (PDE3B; N = 5; black diamonds) or 400 nM rolipram (PDE4; N = 4; black squares) at 1 and 11 mM glucose. Error bars represent the S.E.M. and p values were determined by Student's t-test. * indicates $p < 0.05$, ** $p < 0.01$, *** $p < 0.0001$

Insulin signaling proceeds via Akt to activate PDE3B

Several studies have reported the importance of the insulin receptor in regulating glucagon secretion from the α-cells (Kaneko, Shirotani et al. 1999; Kulkarni, Bruning et al. 1999; Ishihara, Maechler et al. 2003; Franklin, Gromada et al. 2005; Xu, Kumar et al. 2006; Kawamori and Kulkarni 2009; Kawamori, Kurpad et al. 2009). However, there is little agreement between them about the mechanism by which this occurs. Despite the disparity, these mechanisms have in common the core insulin signaling pathway. This includes insulin binding its receptor, triggering the activation of PI3 kinase, a promiscuous kinase with several downstream phosphorylation targets, and subsequent activation of Akt/Protein Kinase B (PKB). Akt/PKB is a key component of insulin's regulatory mechanism in α-cells and has been shown to activate phosphodiesterase 3B in hepatocytes. Furthermore, an increase in Akt/PKB activity has been shown in islets and cultured α-cells at high glucose (Kulkarni, Bruning et al. 1999; Xu, Kumar et al. 2006). Since this data agrees with our results on the role of insulin and PDE3B in regulating glucagon secretion, we expected that insulin signaling would lead to the activation of Akt/PKB upstream of PDE3B.

To test this idea, we used a well-regarded antibody against phosphorylated Akt/PKB and immunofluorescence to characterize the response to glucose, as done with previous experiments. We found that phospho-Akt was increased at 1 mM glucose in the presence of exogenous insulin when compared with 1 mM glucose-alone in the islet α-cells. Insulin caused a 199% ± 9.4 increase in phospho-Akt mean intensity, as depicted in Figure 2-24.

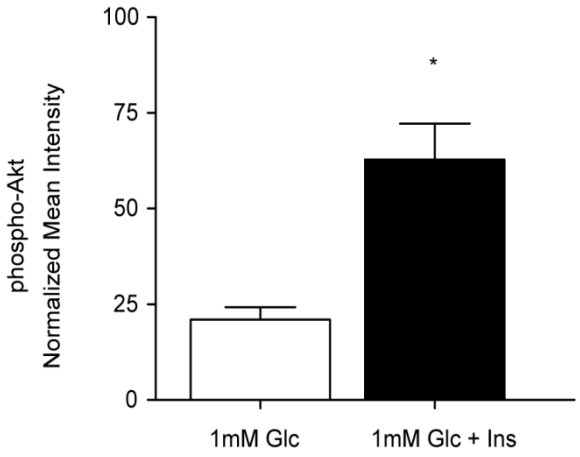

Figure 2-24. Phosphorylated Akt is increased by insulin at low glucose in the alpha cells. Mean intensities from immunofluorescence studies where murine islets were fixed after treatment with low glucose alone (white bar) or low glucose in the presence of 1 μM insulin (black bar), and stained for phospho-Akt and glucagon and normalized to pre-immune control images.

A concomitant decrease of cAMP and PKA is required for glucagon suppression

At this point, our data suggest that somatostatin and insulin are both decreasing cAMP as a means of regulating glucose-inhibition of glucagon secretion. To flesh out the cAMP-dependent signaling pathway that is being inhibited, we next needed to identify the downstream activator that cAMP is targeting to promote secretion. The two proximal targets for cAMP signaling are protein kinase A (PKA) and exchange protein activated by cAMP (Epac). To determine if one or both of these targets may be involved in glucose-inhibited glucagon secretion, we measured secretion from murine islets in the presence and absence of a PKA (6-Bnz-cAMP) or Epac (8-pCPT-2′-O-Me-cAMP**)** specific agonist. Epac activation produced a 1.68 ± 0.03 fold increase in glucagon secretion over 1 mM glucose alone and a 4.0 ± 0.10 fold increase over 11 mM glucose alone. PKA activation, however, increased glucagon secretion by 2.77 ± 0.08 fold only at 11 mM glucose, with no significant difference at 1 mM glucose, over glucose alone, as shown in Figure 2-25.

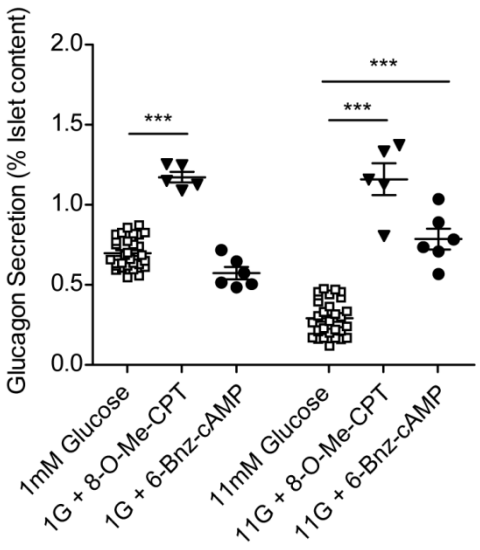

Figure 2-25: PKA activation glucose-dependently stimulates glucagon secretion. Glucagon secretion from murine islets after static incubation with glucose alone (white squares), 300 μM Epac agonist 8-pCPT-2′-O-Me-cAMP (8-O-Me-CPT; black inverted triangles), or 300 μM PKA agonist 6-Bnz-cAMP (black circles) at 1 and 11 mM glucose. Error bars represent the S.E.M. and p values were determined by Student's t-test. * indicates $p < 0.05$, ** $p < 0.01$, *** $p < 0.0001$

We also tested the effect of the PKA-specific agonist on glucagon secretion in human islets and found a similar result. There was no significant difference in glucagon secretion when treated with 6-Bnz-cAMP at 1 mM glucose, but at 11 mM glucose, we observed a 1.79 ± 0.12 increase in glucagon secretion, shown in Figure 2-26, consistent with our murine results

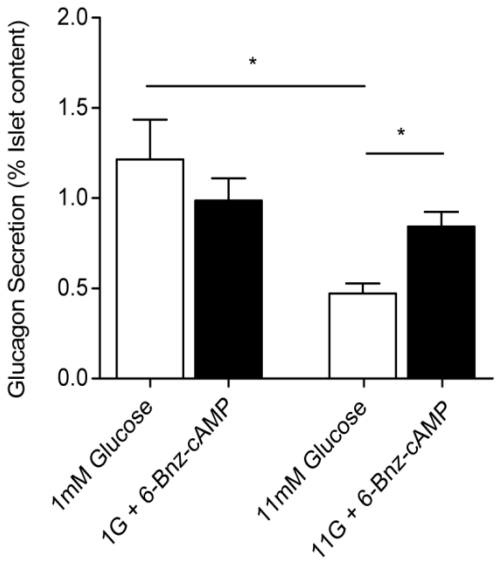

Figure 2-26: PKA activation glucose-dependently stimulates glucagon secretion in human islets. Glucagon secretion from donor human islets after static incubation with glucose alone (white bars) or 300 µM PKA agonist 6-Bnz-cAMP (black bars) at 1 and 11 mM glucose. Error bars represent the S.E.M. and p values were determined by Student's t-test. * indicates $p < 0.05$, ** $p < 0.01$, *** $p < 0.0001$

We next needed to determine whether PKA activity must be decreased for glucose-inhibited glucagon secretion, so we measured secretion from murine islets treated with the specific PKA inhibitor Rp-cAMPS in the presence of forskolin. With this experiment, we expected the Rp-cAMPS to counter the increase in cAMP promoted by forskolin if PKA was the dominant signaling pathway mediating glucose-inhibited glucagon secretion at high glucose. We observed at 1 mM glucose that PKA inhibition did not cause a significant difference in glucagon secretion compared with glucose alone. However, inhibiting PKA partially rescued glucagon suppression at 11 mM glucose, producing a 1.84 ± 0.61 ($p < 0.0001$) fold decrease compared to 1 mM glucose, which is not significantly different from 11 mM glucose alone. Unlike the effects seen with PKA inhibition, inhibiting Epac with Brefeldin-A did not affect the forskolin-stimulated glucagon secretion at either 1 mM or 11 mM glucose, as shown in Figure 2-27. Importantly, this mimics the results from stimulating islets with the Epac-specific agonist

shown earlier. We conclude from these studies that PKA, rather than Epac, is glucose-dependently inhibited as a result of decreasing cAMP levels.

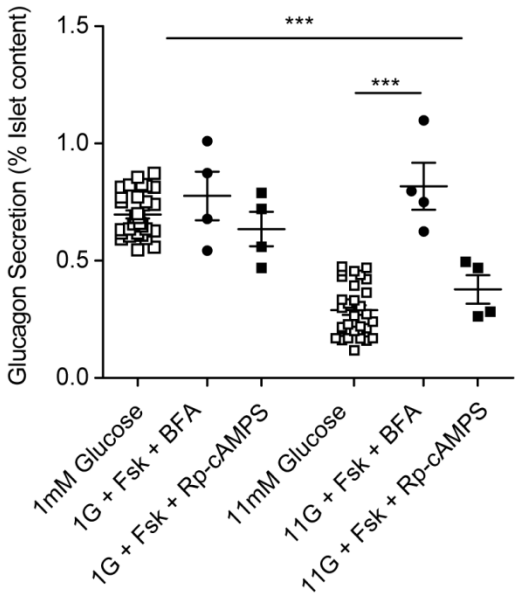

Figure 2-27: Glucagon inhibition is partially rescued by PKA inhibition. Glucagon secretion from murine islets treated with glucose alone (white squares) or 50 µM forskolin (Fsk) and 250 µM Brefeldin A (BFA – black circles) to inhibit Epac or 100 µM PKA-specific antagonist Rp-cAMPS (black squares). Error bars represent the S.E.M. and p values were determined by Student's t-test. * indicates $p < 0.05$, ** $p < 0.01$, *** $p < 0.0001$

We next wanted to directly measure PKA activity in the α-cells to determine if the effects observed with somatostatin and insulin on cAMP would translate to the same decrease in PKA activity, as our secretion data suggested that it should. Thus, to measure PKA activity from islet α-cells after modulation of cAMP, we imaged immunofluorescence of an antibody against phosphorylated PKA (phospho-PKA) after exposure to 1 and 11 mM glucose in the absence and presence of IBMX/forskolin. We found that phospho-PKA was reduced 24.5% ± 1.3 in islets treated with 11 mM glucose compared with 1 mM glucose alone. Furthermore, phospho-PKA in islet α-cells stimulated with IBMX/forskolin was increased 28.9% ± 1.3 at 1 mM glucose and 73.8% ± 3.1 at 11 mM glucose compared with glucose alone, as shown in Figure 2-28.

This is consistent with what we found for cAMP in the same type of study shown earlier in the chapter.

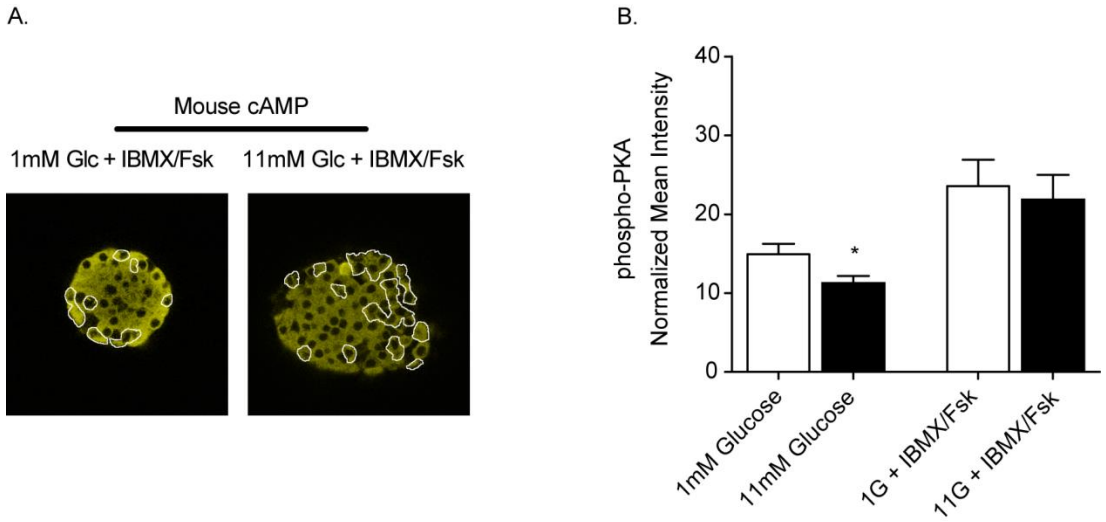

Figure 2-28: Phosphorylated PKA is decreased at high glucose. Mean intensities from islets or purified α-cells treated as described and then fixed and stained for phospho-PKA and glucagon and normalized to pre-immune control images. (A) Images from islets treated and stained for phospho-PKA; p-PKA in yellow, glucagon-positive cells outlined in white. (B) Normalized phospho-PKA intensity from islet α-cells treated at 1 mM glucose (white bars) or 11 mM glucose (black bars) with IBMX/Fsk (N = 6) or glucose alone (N = 7). Error bars represent the S.E.M. and p values were determined by Student's t-test. * indicates $p < 0.05$, ** $p < 0.01$, *** $p < 0.0001$

Our initial hypothesis was based on the observation that the glucagon inhibition pathway should function independently of Ca^{2+} and yet significant crosstalk between cAMP/PKA signaling and Ca^{2+} signaling has been reported in many cell types. To address this question, we measured intracellular Ca^{2+} activity in islet α-cells stimulated with the same PKA-specific agonist, 6-Bnz-cAMP, that we used in our secretion studies. Had PKA been exerting its effect on secretion by directly affecting $[Ca^{2+}]_i$, we would have expected to see an increase in $[Ca^{2+}]_i$ at high glucose in the presence of the agonist. However, at low glucose, where secretion is already dominated by $[Ca^{2+}]_i$, the PKA stimulation may not have a detectable effect.

We found no statistically significant differences in $[Ca^{2+}]_i$ as determined by area under the curve from time-lapse imaging or the number of cells that displayed active Ca^{2+} oscillations, in the control glucose only-treated islets nor the 6-Bnz-cAMP stimulated islets. We conclude from the data in Figure 2-29 that at low glucose, $[Ca^{2+}]_i$ is already maximal to drive the rapid exocytosis of glucagon-containing vesicles and thus increasing PKA activity does not have a measurable effect. Furthermore, the lack of response in $[Ca^{2+}]_i$ at high glucose mimics the IBMX/Fsk data above and supports the hypothesis that cAMP/PKA signaling and $[Ca^{2+}]_i$ are decoupled at high glucose concentrations in the α-cells.

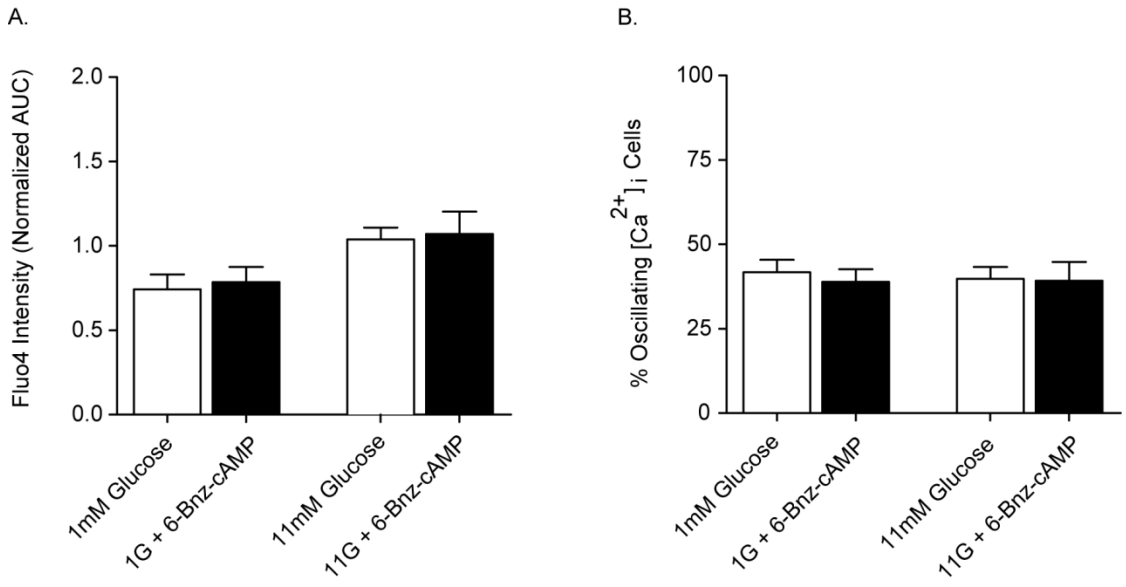

Figure 2-29: PKA activation does not significantly affect $[Ca^{2+}]_i$ in islet α-cells. (A) Intracellular Ca^{2+} ($[Ca^{2+}]_i$) as measured by Fluo4 intensity (AUC) in murine isolated islets treated with glucose alone or in the presence of 6-Bnz-cAMP. (B) Mean percent of cells with oscillations in Ca^{2+} as a function of glucose, where α-cells were identified by td-RFP expression in islets from 4 mice. Error bars represent the S.E.M. and p values were determined by Student's t-test. * indicates $p < 0.05$, ** $p < 0.01$, *** $p < 0.0001$

Somatostatin and insulin lower islet α-Cell cAMP and inhibit glucagon secretion

Earlier studies with the Pertussis toxin suggested that when somatostatin signaling was inhibited, insulin was rendered incapable of inhibiting glucagon secretion suggested a requirement for both paracrine regulators. Additionally, we have shown in previous work that neither somatostatin nor insulin is sufficient to suppress glucagon in isolated α-cells. Thus, we wanted to pursue the possibility that these two paracrine molecules are working together to decrease cAMP/PKA and inhibit glucagon secretion. We tested whether the combination of somatostatin and insulin synergistically lowers cAMP in α-cells. In murine islets treated with both somatostatin and insulin, cAMP was reduced by 56.8% ± 3.07 compared with 1 mM glucose alone, and by 39.6% ± 4.6 and 43.8% ± 7.18 compared to somatostatin and insulin alone, respectively. Additionally, phosphorylated PKA was reduced 41% ± 1.3, 34.4% ± 1.25, and 39.2% ± 1.83 compared with 1 mM glucose alone, respectively, when treated with somatostatin, insulin, or somatostatin with insulin, displayed in Figure 2-30.

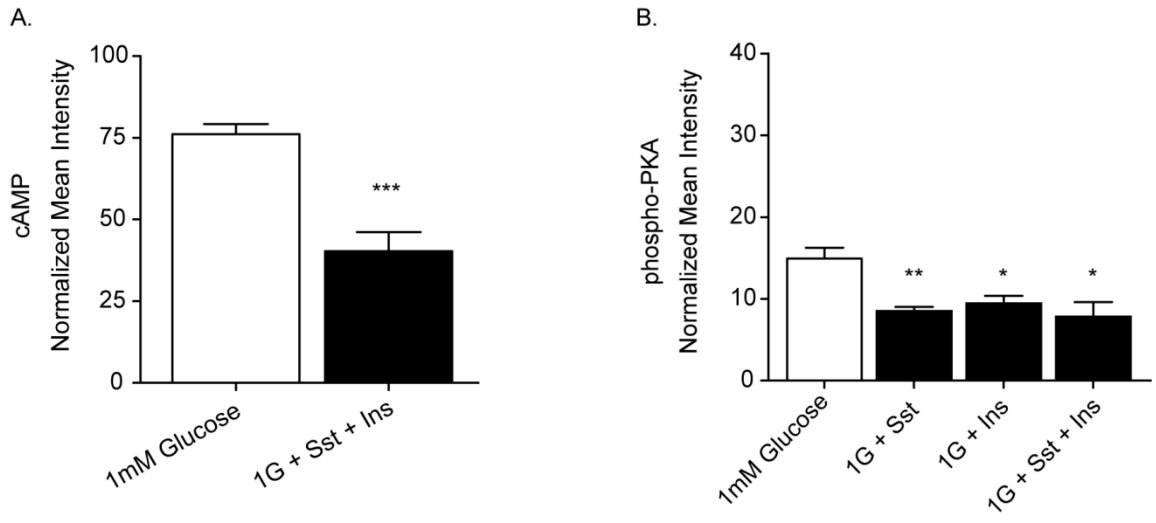

Figure 2-30: Somatostatin and insulin significantly decrease cAMP and phosphorylated PKA at high glucose. (A) Normalized cAMP intensity from islet α-cells treated with 1 mM glucose (N = 13) or somatostatin (Sst) with insulin (Ins) at 1 mM glucose (N = 7). (B) Normalized phospho-PKA (N = 6) intensity from islet α-cells incubated with 1 mM glucose alone (N = 7; white bar) or in the presence of Sst, Ins, or Sst with Ins (N = 5, 4, 5; black bars). Error bars represent the S.E.M. and p values were determined by Student's t-test. * indicates $p < 0.05$, ** $p < 0.01$, *** $p < 0.0001$

These data demonstrate a synergistic relationship between insulin and somatostatin on decreasing cAMP levels. We next wanted to test the hypothesis by the inverse experiments, shown in Figure 2-31. We treated islets with receptor antagonists against somatostatin (CYN154806) and insulin (S961), and observed an 80.4% ± 11.8 increase in mean intensity for cAMP compared with 11 mM glucose alone. Additionally, this was a 40.8% ± 4.6 and 45.6% ± 7.1 increase in cAMP compared to CYN154806 and S961 alone, respectively. Inhibiting both somatostatin and insulin receptors also yielded an increase in phospho-PKA of 130% ± 3.93 over 11 mM glucose alone (data shown in above sections).

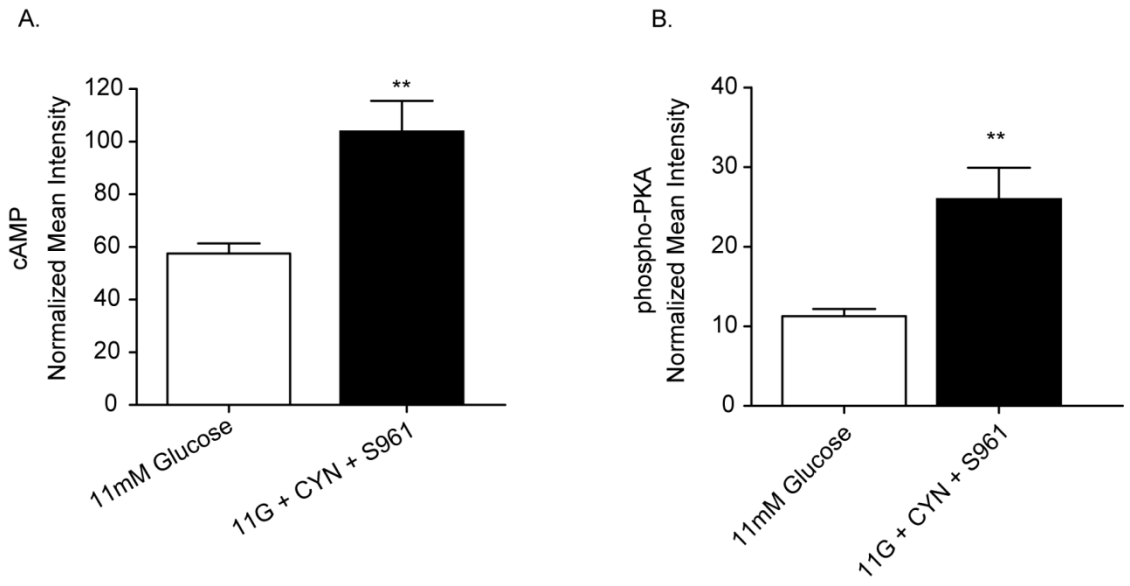

Figure 2-31: Somatostatin and insulin antagonism significantly increases cAMP and phosphorylated PKA at high glucose. (A) Normalized cAMP intensity from islet α-cells treated with 11 mM glucose (N = 13) or CYN154806 (CYN) with S961 at 11 mM glucose (N = 4). (B) Normalized phospho-PKA (N = 4) intensity from islet α-cells treated with 11 mM glucose alone (white bar) or with CYN and S961 (black bar). Error bars represent the S.E.M. and p values were determined by Student's t-test. * indicates $p < 0.05$, ** $p < 0.01$, *** $p < 0.0001$

We next wanted to determine if the effects of somatostatin and insulin on glucagon secretion are also additive, so murine islets were treated with 1 mM or 11 mM glucose in the presence and absence of somatostatin and insulin or antagonists CYN154806 and S961, as depicted in Figure 2-32. Combined somatostatin and insulin reduced glucagon secretion at 1 mM glucose 2.07 ± 0.33 fold compared with glucose alone and produced no significantly different response at 11 mM glucose compared with glucose alone. Combined CYN154806 and S961 increased glucagon secretion 2.82 ± 0.47 fold over 11 mM glucose alone and elicited no difference in secretion at 1 mM glucose, which is similar to the effect of either CYN154806 or S961 alone.

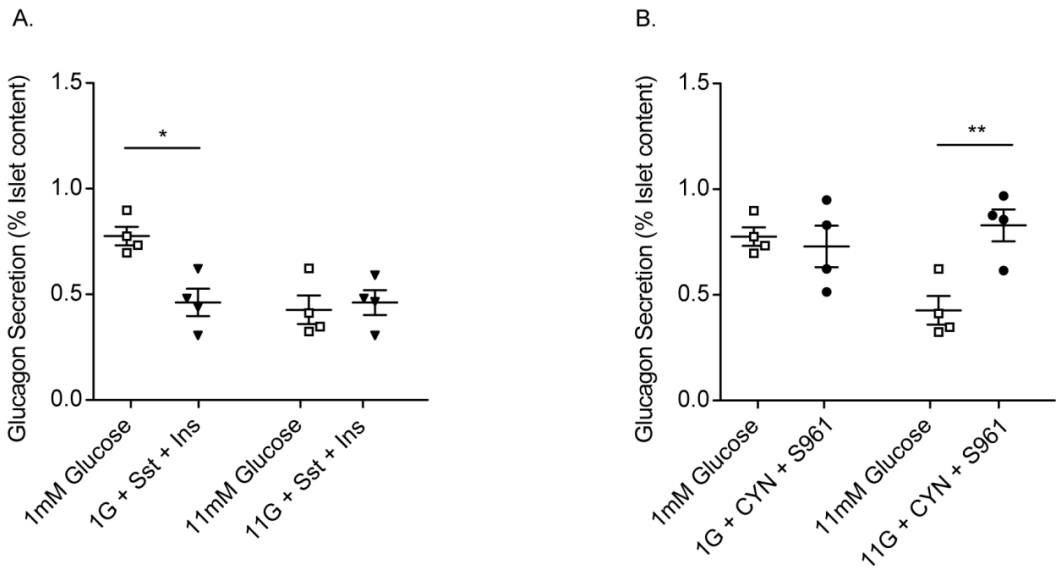

Figure 2-32: Somatostatin and insulin antagonism significantly increases glucagon secretion at high glucose. (A) Glucagon secretion from murine islets stimulated with combined Sst and Ins (black inverted triangles) or glucose alone (white squares). (B) Glucagon secretion from murine islets treated with CYN and S961 (black circles) or glucose alone (white squares). Error bars represent the S.E.M. and p values were determined by Student's t-test. * indicates $p < 0.05$, ** $p < 0.01$, *** $p < 0.0001$

Having established that somatostatin and insulin exert an additive effect on lowering cAMP levels in the α-cells, we next wanted to determine whether these regulators are interdependent, as suggested by the Pertussis toxin data shown earlier. To address this question we combined the insulin receptor antagonist S961 with exogenous somatostatin and measured glucagon secretion. In addition, we did the reciprocal experiment with the SSTR2 receptor antagonist CYN154806 in the presence of exogenous insulin. These data are displayed in Figure 2-30 below. In the first experiment, we found that at 1 mM glucose, there was not a significant difference between the glucose alone and combination treatment of S961 and somatostatin. At 11 mM glucose, S961 and somatostatin increased glucagon secretion over glucose alone by 2.40 ± 0.07 fold. Similarly, at 1 mM glucose, islets exposed to CYN154806 and insulin showed no significant difference between treated and control islets, but at 11 mM glucose, secretion was increased 2.59 ± 0.08 fold over glucose alone, shown in

Figure 2-33. From these data, we conclude that somatostatin and insulin are necessary, and neither one alone is sufficient, for the glucose-inhibition of glucagon secretion.

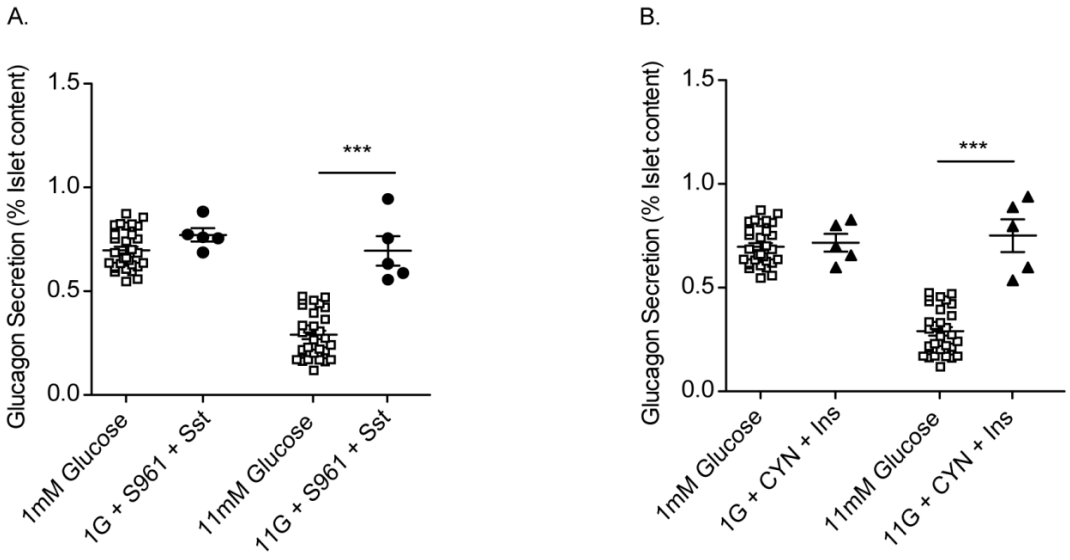

Figure 2-33: Neither somatostatin nor insulin alone is sufficient to suppress glucagon secretion in islets. (A) Glucagon secretion from murine islets treated with S961 and Sst (black circles) or glucose alone (white squares). (B) Glucagon secretion from murine islets treated with CYN and Ins (black triangles) or glucose alone (white squares). Error bars represent the S.E.M. and p values were determined by Student's t-test, *** $p < 0.0001$.

Somatostatin and insulin together are sufficient to inhibit cAMP and glucagon secretion from purified islets

Previous work demonstrated that neither somatostatin nor insulin alone inhibited glucagon secretion from sorted cells (Le Marchand and Piston 2010), which is consistent with what we observed by inhibiting these receptors in whole islets. However, the combination of both effectors was not tested in the initial screen for inhibitors in sorted α-cells. To study the effect of combined somatostatin and insulin on isolated α-cells, we FACS-sorted tdRFP-expressing α-cells from whole islets and assayed them for cAMP, phospho-PKA, and glucagon secretion at 1 mM glucose alone, or in the presence of somatostatin and insulin. From the

immunofluorescence experiments, we found that the dispersed α-cells treated with somatostatin, insulin and 1 mM glucose exhibited a significant decrease in cAMP of 92% ± 8.6 compared with glucose-alone control cells. Additionally, phospho-PKA was reduced 78% ± 11.6 compared with 1 mM glucose alone, as depicted in Figure 2-34.

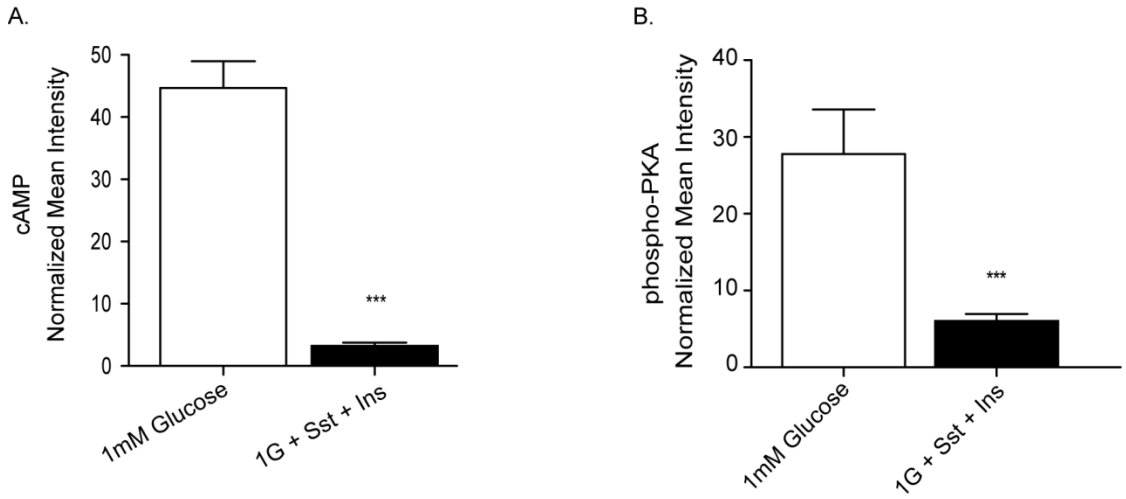

Figure 2-34: Somatostatin and insulin decrease cAMP and phosphorylated PKA from purified α-cells. (A) Normalized cAMP intensities from tdRFP-expressing α-cells purified from 5 mice and treated with either 1 mM glucose (white bar) or 1 mM glucose with Sst and Ins (black bar). (B) Normalized phospho-PKA intensities from (A). Error bars represent the S.E.M. and p values were determined by Student's t-test. * indicates $p < 0.05$, ** $p < 0.01$, *** $p < 0.0001$

Isolated α-cells treated with somatostatin and insulin exhibited a 4.61 ± 0.41 fold decrease in glucagon secretion compared with glucose alone, shown in Figure 2-35. This is consistent with our observations using the antagonists of somatostatin and insulin receptors in whole islets. The data shown here demonstrate that, in the absence of normal islet cell-cell contacts, somatostatin and insulin are sufficient to inhibit glucagon secretion.

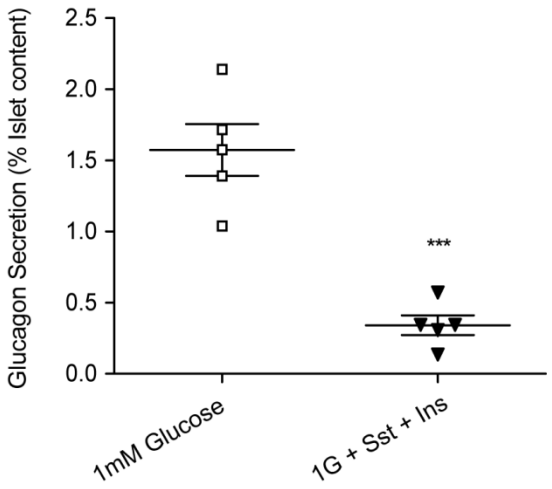

Figure 2-35: Somatostatin and insulin together are sufficient to suppress glucagon secretion in isolated α-cells. Glucagon secretion from purified α-cells treated in static incubation with 1 mM glucose (gray squares) or 1 mM glucose with Sst and Ins (black inverted triangles). Error bars represent the S.E.M. and p values were determined by Student's t-test. * indicates $p < 0.05$, ** $p < 0.01$, *** $p < 0.0001$

Summary

In this chapter, background material was described that led directly to our hypothesis that somatostatin and insulin inhibit glucagon secretion by decreasing cAMP/PKA signaling in the islet α-cells. We first examined the role of cAMP in regulating glucose inhibition of α-cell glucagon secretion, which showed that cAMP and glucagon secretion are reduced in a similar manner with increasing glucose in both human and mouse islet α-cells. This is in contrast to β-cells, where cAMP increases with increasing glucose, and is consistent with other reports showing similar difference between α- and β-cells (Gromada, Bokvist et al. 1997; Dyachok, Idevall-Hagren et al. 2008). Forced elevation of cAMP in the islet via IBMX and forskolin overcomes the natural inhibition of glucagon secretion at high glucose levels, suggesting that cAMP signaling must be decreased for glucagon suppression. Importantly, the forced cAMP changes do not affect $[Ca^{2+}]_i$ activity or oscillations in the α-cells. Together, these data support

a model where cAMP plays a central $[Ca^{2+}]_i$-independent role in regulating the inhibition of glucagon secretion.

It is difficult to inhibit all of the receptors in any given cell even when using monolayers of tissue cultured cells. In the islet, a multicellular, dense, and highly interconnected tissue, this problem is amplified. Sorting the α-cells into a pure population is the only way to completely remove any endogenous paracrine factors. The fact that sorted α-cells have dysregulated glucagon secretion argues in favor of both the paracrine and juxtracrine contacts playing critical roles in the normal suppression of glucagon.

Decreased cAMP at high glucose in islet α-cells requires activation of both somatostatin and insulin receptors. Our data show that the combination of somatostatin and insulin decreases cAMP more than either somatostatin or insulin alone at low glucose. Further, inhibiting simultaneously somatostatin and insulin receptors increases cAMP significantly more than either antagonist alone. Combined exposure to somatostatin and insulin leads to inhibition of glucagon secretion from isolated islet cells, while neither alone is sufficient (Le Marchand and Piston 2010). This requirement of combined signaling is consistent with the results from mice with genetic deletion of either somatostatin or insulin, both of which show only a partial disruption in the inhibition of glucagon secretion (Kulkarni, Bruning et al. 1999; Yue, Burdett et al. 2012). It has also been reported that neither somatostatin nor insulin alone is able to decrease glucagon secretion from a purified population of islet α-cells (Le Marchand and Piston 2010). However, we show here that the combination of these paracrine factors is sufficient to decrease in cAMP and inhibit glucagon secretion in the absence of normal islet architecture.

Somatostatin acts through a G-protein coupled receptor (SSTR) with an inhibitory $G\alpha_i$ subunit, and SSTR2 has been shown to be the functionally dominant receptor in both human and mouse α-cells (Kailey, van de Bunt et al. 2012). We determined that cAMP levels are reduced at low glucose in the presence of somatostatin, and that glucagon secretion from these islets was significantly reduced as well. Both a broad somatostatin receptor antagonist

(cyclosomatostatin) and a SSTR2-specific antagonist (CYN154806) significantly increased cAMP and glucagon secretion at high glucose, suggesting that glucagon inhibition with glucose requires somatostatin. However, there was no difference in glucagon secretion at low glucose from either human or murine islets after exposure to the SSTR2 antagonist. The comparison between the results using a broad SSTR antagonist and one specific for SSTR2 showed that inhibiting only the SSTR2 is sufficient to prevent the glucose-inhibition of glucagon secretion. Further treatment of islets with pertussis toxin to prevent the inhibitory $G\alpha_i$ subunit of the SSTR2 blocked the ability of somatostatin to inhibit glucagon or insulin secretion. We conclude from these data that somatostatin signaling plays an important role in glucose inhibition of glucagon secretion and that it does so by decreasing the production of cAMP by adenylyl cyclases via the Gαi subunit of the SSTR2.

We observed a difference in glucagon secretion at high glucose between islets treated with IBMX (phosphodiesterase inhibitor) and forskolin (activates adenylyl cyclases). This indicted that degradation of cAMP by phosphodiesterases might also be critical in glucagon suppression, which prompted us to test the role of insulin signaling in the α-cells. Insulin receptor expression is well-characterized in the α-cell, and PI3-kinase inhibition has been reported to block insulin-mediated glucagon inhibition (Chen and Ostenson 2004; Ravier and Rutter 2005). The PI3-kinase target Akt is required for glucose-inhibition of glucagon secretion and is up-regulated at high glucose (Diao, Asghar et al. 2005; Kawamori, Kurpad et al. 2009) in α-cells. We found that insulin exposure significantly decreased cAMP in islet α-cells, and that inhibiting the insulin receptor produced significant increases in both cAMP and glucagon secretion at high glucose in both human and murine islets.

To test the hypothesis that insulin inhibits glucagon secretion by activating phosphodiesterases (PDE), we treated islets with a range of cAMP analogs and selective PDE inhibitors. At high concentrations of insulin (1 μM) and high glucose levels, glucagon secretion from islets could be partially rescued by treatment with a hydrolyzable cAMP analog. However,

glucose inhibition of glucagon secretion was entirely lost in the presence of a PDE-resistant analog. We examined selective inhibitors for two of the common phosphodiesterases in islet cells, PDE3 and PDE4. A PDE4-selective inhibitor, rolipram, stimulated glucagon secretion across all glucose levels. On the other hand, a PDE3B-specific inhibitor, cilostamide, also elicited a significant increase in glucagon secretion, but strictly in a glucose-dose-dependent manner. From these data, we conclude that insulin decreases cAMP in α-cells via PI3-kinase phosphorylation of Akt and PDE3B. This is consistent with studies in other metabolic cell types, such as hepatocytes and adipocytes, that are regulated by insulin signaling through phosphodiesterase 3B to decrease cAMP and limit glycogenolysis and lipolysis (Choi, Park et al. 2006; Ahmad, Lindh et al. 2009; Degerman, Ahmad et al. 2011).

There are two primary downstream effector proteins in cAMP signaling: PKA and Epac, and both can be involved in secretory dynamics (Gromada, Bokvist et al. 1997; Dyachok, Sagetorp et al. 2006; Hatakeyama, Takahashi et al. 2007; Idevall-Hagren, Barg et al. 2010; Benninger, Head et al. 2011). To test the potential role of each of these proteins in α-cells, we measured glucagon secretion after exposure to specific activators of PKA and Epac. We found that stimulating Epac increases glucagon secretion at all glucose concentrations, whereas PKA activation elicited a secretory response only at high glucose levels. Additionally, when islets were treated with forskolin to activate adenylyl cyclases, glucagon inhibition was partially rescued at high glucose by a PKA-specific inhibitor. Thus, we conclude that stimulating PKA is sufficient to overcome glucose-inhibited glucagon secretion, and that PKA signaling must be lowered for glucose inhibition of glucagon secretion to occur.

An important feature of our work is that most experiments were performed using whole islets, so that juxtracrine and paracrine contacts were in place between the islet cells. We also measured responses from all of the α-cells (identified by glucagon immunoreactivity), which eliminates potential bias due to sampling only the minority of α-cells that are active at low glucose (Le Marchand and Piston 2012). Figure 7 schematically outlines how somatostatin and

insulin receptor activation contribute to suppressing α-cell glucagon secretion in islets with increasing glucose via decreasing cAMP, but independently of intracellular Ca^{2+} ($[Ca^{2+}]_i$). Glucagon secretion always requires $[Ca^{2+}]_i$ (De Marinis, Salehi et al. 2010), but our data support a model where $[Ca^{2+}]_i$ becomes uncoupled from secretion as glucose increases. Together, these data demonstrate a crucial role for both somatostatin and insulin in regulating glucagon inhibition, whereby a decrease in cAMP leads to glucagon suppression despite the presence of stimulatory $[Ca^{2+}]_i$ levels.

We have further shown that signaling through PKA is required for cAMP-inhibition of glucagon secretion, but the link between PKA and the exocytotic machinery remains unknown at this point. Recent literature has demonstrated the critical role of Rac-1 GTPase (Rac1), a member of the Rho family of small GTPases, in regulating the actin network to allow vesicle fusion (Konstantinova, Nikolova et al. 2007). Additionally, other studies have shown a cAMP-dependent regulation of Rac1, which would fit nicely with the studies described above (Goto, Hoshino et al. 2011). Thus, we tested the hypothesis that this was also a critical point of regulation in the α-cells. Chapter 3 will cover in detail the relevant literature that led to this hypothesis and the data we collected in addressing it.

CHAPTER 3

EXPLORING RHO-GTPASE FUNCTION IN ALPHA CELLS

Introduction

The majority of data we have collected concerning the α-cells demonstrate that glucagon secretion is suppressed downstream of any membrane depolarization and resulting Ca^{2+} influx (Le Marchand and Piston 2010; Le Marchand and Piston 2012). In an effort to determine the mechanism of inhibition at the level of vesicle fusion and exocytosis, we turned to the familiar β-cell for ideas. Recent studies have shown that a key gate keeper for vesicle fusion and exocytosis is Rac1-GTPase (Rac1), a member of the Rho family of GTPases that also includes Cdc42 and RhoA (Konstantinova, Nikolova et al. 2007). There are at least three Rac isoforms characterized in mammals with Rac1 expressed ubiquitously, Rac2 in hematopoietic cells, and Rac3 mostly expressed in the brain (Haataja, Groffen et al. 1997). The critical function of Rac1 with regard to insulin exocytosis is in transiently depolymerizing the filamentous actin, F-actin, network to allow vesicles access to the exocytotic machinery for subsequent docking and fusion with the membrane and expulsion of insulin and c-peptide (Kalwat and Thurmond 2013). Additionally, Rac1 is primarily implicated in regulating the second, sustained phase of insulin secretion, where cytoskeletal remodeling is critical for the trafficking of internal vesicle stores to the membrane (Li, Luo et al. 2004; Wang, Oh et al. 2007).

In model cell types including chromaffin and PC12 cells, F-actin has been shown to form a cortical ring just beneath the membrane that acts as a barrier to vesicle fusion (Momboisse, Ory et al. 2010). This is believed to play a critical role in limiting basal insulin secretion as well (Kalwat and Thurmond 2013). Rac1, like all small GTPases, is activated when GTP is bound

and is inactivated upon hydrolysis of the GTP to GDP and an inorganic phosphate. The cycling of nucleotides provides a switch on/off mechanism for the regulation of these proteins, whereby GTP hydrolysis is accelerated by GTPase activating proteins and exchange is catalyzed by guanine nucleotide exchange factors, schematized in Figure 3-1. Additionally, guanosine nucleotide dissociation inhibitors hold the small GTPases in their inactive state until released. These enzymes play critical roles in such cellular processes as cytoskeletal reorganization, membrane trafficking, and cell growth; and have been found to be cell type specificity in these roles (Hall 1998).

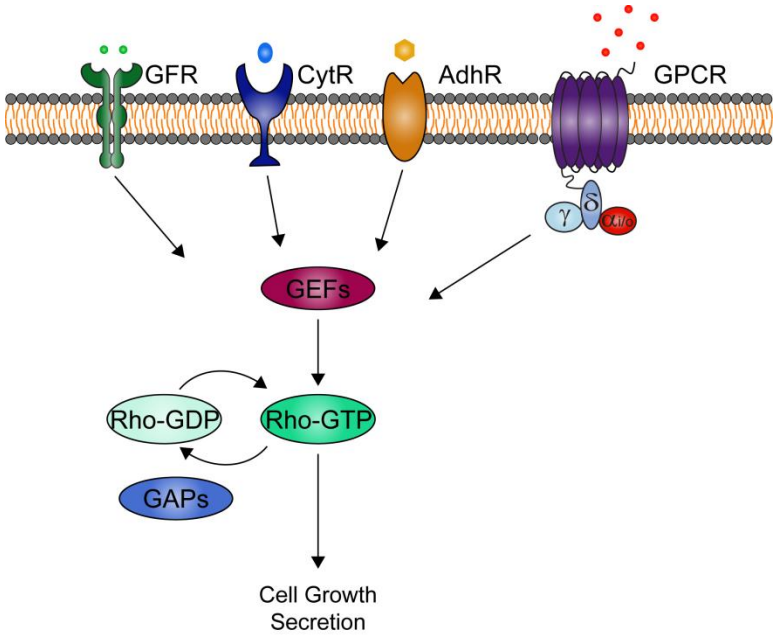

Figure 3-1. Rho-GTPase family signaling. Guanine nucleotide exchange factors (GEFs) and GTPase-activating proteins (GAPs) regulate the cycling between active (GTP-bound) and inactive (GDP-bound) small GTPases. GEF activity, modulated by a number of ligand-binding events with cellular surface receptors, regulates the activity of individual GTPases, conferring specificity. Activated GTPases are then able to interact with a number of effectors to mediate cellular responses such as growth, motility, and secretion.

The cellular signaling that leads to Rac1 activation and subsequent F-actin remodeling in the β-cells is not yet fully elucidated. However, it has been shown that Rac1 knockout mice exhibit glucose intolerance and impaired glucose-stimulated insulin secretion (Greiner, Kesavan

et al. 2009; Asahara, Shibutani et al. 2013). Clonal β-cells expressing a dominant-negative Rac1 construct showed a considerable reduction in exocytosis (Asahara, Shibutani et al. 2013). but overexpression of constitutively active Rac1 revealed no difference in secretion, suggesting that Rac1 is necessary for facilitating secretion, but is insufficient to drive or enhance secretion (Shibutani, Asahara et al. 2013). Another report demonstrated that, upon glucose metabolism, an as yet unknown signaling molecule activates the small GTPase Cdc42 (Kepner, Yoder et al. 2011) that in turn activates p21-activated kinase, PAK-1 (Kalwat, Yoder et al. 2013), which is an upstream activator of Rac1. Furthermore, β-cell cAMP signaling has been shown to lead to PAK1 activation (Nie, Sun et al. 2012; Nie, Lilley et al. 2013). A recent study in HEK293 cells demonstrated that the adrenergic receptor activation and downstream cAMP signaling could lead to Rac1 activation via complex formation with PKA. This complex was found to stabilize the PKA regulatory subunits and compartmentalize the holoenzyme (Bachmann, Riml et al. 2013). Furthermore, in endothelial cells, cAMP-dependent Rac1 activation has been shown to play important roles in barrier stabilization (Schlegel and Waschke 2009)and enhancing the peripheral actin cytoskeleton and adherens junctions (Birukova, Zagranichnaya et al. 2007).

The primary goal of this work was to elucidate the molecular mechanisms responsible for the glucose inhibition of glucagon secretion. This cAMP-dependent pathway is independent of intracellular Ca^{2+} influx and Rac1 has been shown to block insulin secretion from the β-cell when Ca^{2+} is elevated, which makes it an attractive candidate regulator for glucagon secretion from the α-cell. Since the α-cell and β-cell are closely related, we hypothesized that Rac1 might be mediating this inhibition, potentially downstream of cAMP. To address this idea, we combined hormone secretion assays, whole islet immunofluorescence, and $[Ca^{2+}]_i$ imaging with pharmacological tools. The results suggest that, contrary to our expectations, Rac1 is unlikely to be a key player in regulating the glucose-inhibition of glucagon secretion. This chapter includes the detailed results of these studies, methodology employed, and a brief summary of the significance of the findings.

Materials and Methods

Islet isolation and culture

As described in Chapter 2, Materials and Methods section.

Cell dispersion and FACS sorting

Isolated islets were cultured overnight in islet medium. They were then washed in DPBS at pH 7.4 without calcium and magnesium chloride. Accutase was used for digestion for 15 minutes at 37ºC (gentle shaking) and cells were pelleted and resuspended in secretion buffer at 11 mM glucose. One to two hours after Accutase dispersion, fluorescent cells were isolated by fluorescence-activated cell-sorting (FACS). The Vanderbilt Flow Cytometry Core facility utilized a BD FACSAria cell sorter (BD Biosciences, San Jose, CA) for purification and Dapi (0.5 µg/ml) was used for exclusion of non-viable cells. Yields were 100-800 viable alpha cells per mouse pancreas.

qPCR

Sorted alpha cells expressing tdRFP were pooled from six mice and RNA was extracted using a Qiagen RNEasy kit. SuperScript II Reverse Transcriptase (Life Technologies) was used to reverse transcribe the extracted RNA to cDNA and samples were detected using the SYBR green PCR master mix and the following protocol: 95°C for 3 min preceding 40 cycles of 95°C for 10 seconds and 70°C for 30 seconds, followed by 10 seconds at 95°C and 5 seconds at 65°C. Primers were designed for Rac1 using VectorNTI (Invitrogen).

Secretion assays

After isolation and overnight culture, islets were equilibrated for one hour in KRBH solution

containing 2.8 mM glucose at 37ºC. Islets were then placed into eppendorf tubes (15-20 islets per tube) and stimulated with differing glucose concentrations with and without 1 mM NSC23766 (Gao, Dickerson et al. 2004), a Rac1 inhibitor, at 37ºC for 45 minutes in a water bath with occasional agitation. Secretion samples were taken after centrifugation and total islet glucagon content was obtained by freezing islets overnight in 1% Triton X-100. Samples were analyzed for glucagon by radioimmuno assay in the Hormone Core. Each condition was measured in duplicate and glucagon secretion was expressed as the percentage of total hormone content over the course of the experiment. Insulin from these same samples was measured using a Mouse UltraSensitive ELISA (Alpco).

Immunofluorescence

Islets were fixed in PBS containing 2% of paraformaldehyde for 30 min and permeabilized overnight at 4°C in PBS with 0.3% Triton X-100, 5 mM sodium azide, 1% bovine serum albumin and 5% goat serum (from Jackson ImmunoResearch Laboratories, West Grove, PA). Islets were incubated in permeabilization solution supplemented with primary guinea pig anti-glucagon antibodies (1:500) and rabbit anti-phospho-Rac1 antibodies (1:100) for 24–48 h at 4°C, washed with PBS three times, incubated with secondary anti-guinea pig antibodies conjugated with Alexa Fluor 488 (1:1000) and anti-rabbit antibodies conjugated with Alexa Fluor 568 (1:250 from a stock of 2 mg/ml) for another 24–48 h, and washed three times before mounting in gelvatol for imaging. Alexa 488 and 568 were excited at 488 and 561 nm, and their emission was collected through a short (520–560 nm) and a long pass filter (>560 nm), respectively.

Results

Rac1 expression in α- and β-cells

Toward the goal of elucidating the role of Rac1-GTPase in α-cells, we first needed to verify the presence of Rac1. At the start of these experiments, there was little data available on gene expression in the α-cells. In more recent years, however, RNAseq has been utilized in dispersed islets to characterize the gamut of mRNA in relatively pure populations of glucagon-containing cells (Dorrell, Schug et al. 2011; Eizirik, Sammeth et al. 2012). We took advantage of our mouse model with tdRFP-expressing α-cells to FACS-sort them and performed quantitative RT-PCR with primers directed against the Rac1 gene. Additionally, with a mouse insulin promoter-driven GFP-expressing β-cells purified from another mouse model (Hara, Wang et al. 2003), we performed the same experiment in purified β-cells both as an experimental control (since this had been shown previously) and to determine the similarities and differences in Rac1 expression levels between cell types. We found that α- and β-cells have comparable levels of Rac1 mRNA, as shown in Figure 3-2.

In addition to the qPCR experiments for mRNA expression, we obtained an antibody raised against the GTP-bound, or active, Rac1-GTP and performed semi-quantitative immunofluorescence to determine levels of active Rac1, its localization, and to confirm protein expression in murine islets. Thus, islets were isolated, fixed, and stained for Rac1-GTP, glucagon, and/or insulin and subjected to confocal microscopy. We found similar levels of Rac1-GTP present in the α- and β-cells, which was primarily membrane-localized.

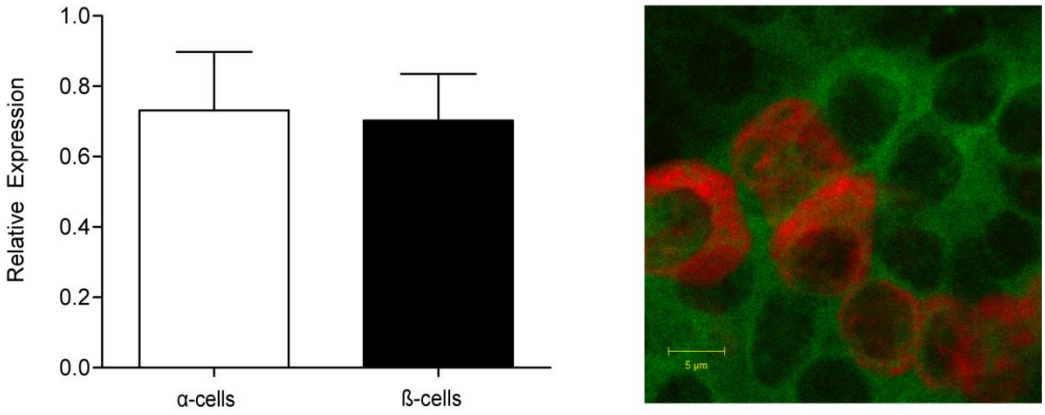

Figure 3-2. Rac1-GTPase expression in primary islet cells. QPCR was used to identify the mRNA levels in FACS-purified α-cells (white bar) and β-cells (black bar). Immunofluorescence with an anti-Rac1GTP antibody was used to detect Rac1 levels in whole islets (Rac1GTP in green, glucagon in red).

Glucose effect on Rac1-GTPase activity in α- and β-cells

Second, to identify the effect of glucose on the activation state of Rac1, we used semi-quantitative immunofluorescence to identify glucagon and active Rac1-GTP in isolated islets after stimulation with 1 mM or 11 mM glucose. In these experiments, for simplification of the staining procedure, we considered the Rac1-GTP positive cells that did not co-stain for glucagon to be β-cells, as they make up the majority of islet cells. In the β-cells, we expected to see increased Rac1 activation at high glucose compared with low glucose, and indeed this was what was measured (Figure 3-3), consistent with known Rac1 function in insulin secretion. Assuming similar function in the α-cell, we expected to see decreased activation at elevated glucose levels, where glucagon exocytosis is suppressed, but instead, the α-cells also showed increased activity at high glucose. This suggests that Rac1 has a different function in the α-cell that is not related to remodeling the F-actin for secretion. Thus, it does not appear that Rac1 is responsible for mediating glucose-dependent glucagon suppression. Due to the difficulty in delivering engineered protein constructs to primary islet tissue and lack of functional α-cell lines, we were unable to take advantage of the dominant negative and constitutively active forms of

Rac1. Thus, to measure the effect of Rac1 modulation on hormone secretion, we turned to a pharmacological inhibitor that we also tested for its impact on Rac1 activity, via immunofluorescence.

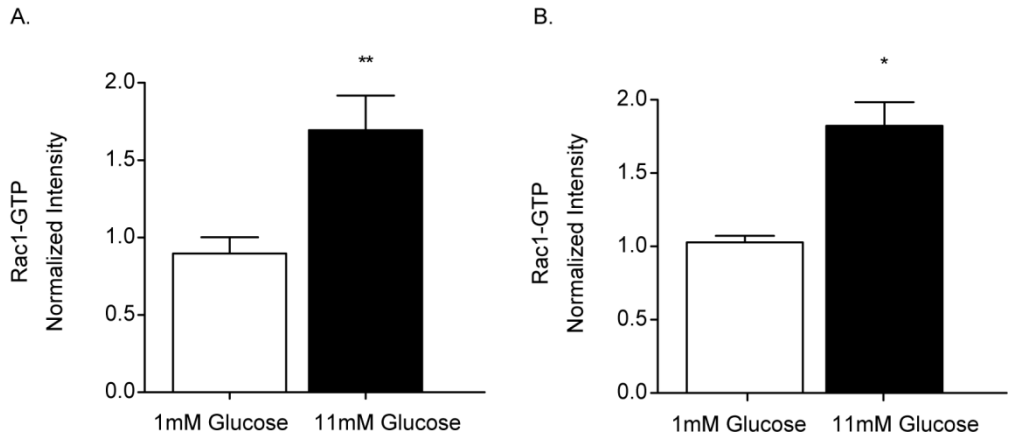

Figure 3-3. Rac1 activity increases with glucose in both α- and β-cells. (A) Rac1GTP mean intensity from islets treated with 1 mM or 11 mM glucose in the α-cells and (B) the β-cells (N = 4-6 islets from 8 mice in (A) and 4 mice in (B). p values were determined by Student's t-test. * indicates $p < 0.05$, ** $p < 0.01$, *** $p < 0.0001$.

Effect of Rac1 inhibition on Rac1-GTPase activity in islet cells

The specific Rac1 inhibitor NSC23766 (Gao, Dickerson et al. 2004) prevents the exchange of the guanidine nucleotide required for activation, without affecting the other Rho family members Cdc42 or RhoA, and prevents its downstream effects. This drug has been characterized in the β-cells and was found to prevent the Rac1-dependent modulation of the actin cytoskeleton required for exocytosis (Veluthakal, Madathilparambil et al. 2009). We utilized a concentration of 1 mM NSC23766, which is well above the EC50 of ~50 μM, in an attempt to overcome any diffusion issues that might arise from treating whole islets. We expected to see a decrease in Rac1-GTP in the islet β-cells and α-cells after treatment with the Rac1 inhibitor as a control for the antibody used to detect Rac1-GTP and the ability of the drug

to reduce global levels of active Rac1 in the islets. We found that Rac1-GTP levels were reduced across glucose levels in both islet cell types after treatment with the specific inhibitor, as shown in Figure 3-4.

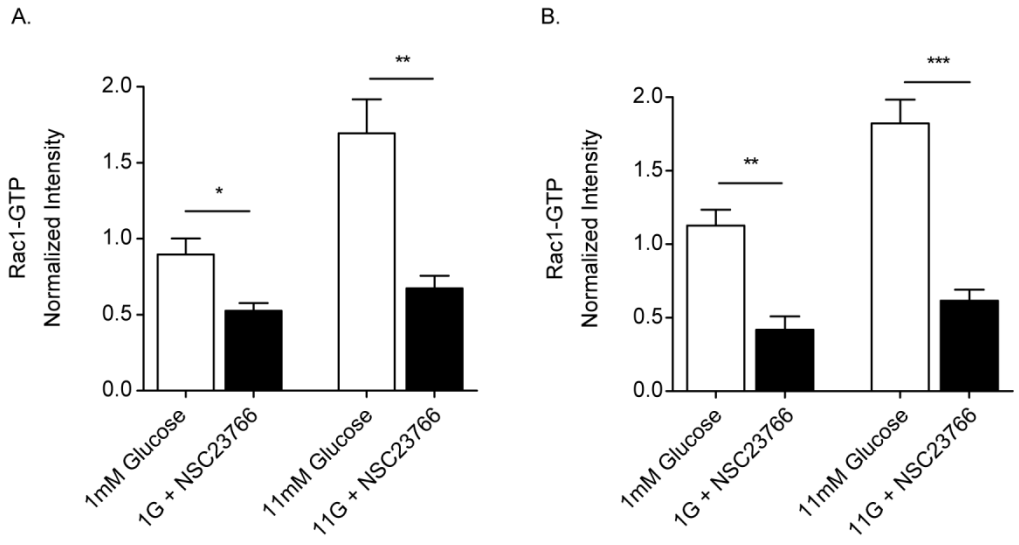

Figure 3-4. A Rac1-GTPase inhibitor blocks Rac1-GTP immunofluorescence. (A) Normalized mean intensity of Rac1-GTP in islet α-cells treated with 1 mM and 11 mM glucose in the absence and presence of NSC23766. (B) Rac1-GTP mean intensity from β-cells in the same islets as in (A). N = 4-6 islets from 6 mice, p values were determined by Student's t-test. * indicates $p < 0.05$, ** $p < 0.01$, *** $p < 0.0001$.

Effect of Rac1 inhibition on glucagon and insulin secretion

Finally, the Rac1 inhibitor was utilized to test the dependence of insulin and glucagon secretion on the activity of Rac1. Since this drug has been used before to study β-cell exocytosis, we expected a decrease in insulin secretion upon treatment with the Rac1 inhibitor. By contrast, in the α-cell, based on the experiments done above looking at the glucose dependence of Rac1, we expected to see no effect on glucagon secretion since it does not appear that Rac1 was responsible for glucagon suppression. Interestingly, we found that glucagon secretion was potentiated at low glucose and stimulated at high glucose, as shown in

Figure 3-5, when Rac1 activation is prevented. This data is consistent with the Rac1 activation data described above and further demonstrates that Rac1 is unlikely to perform the same modulation of exocytosis in both α- and β-cells.

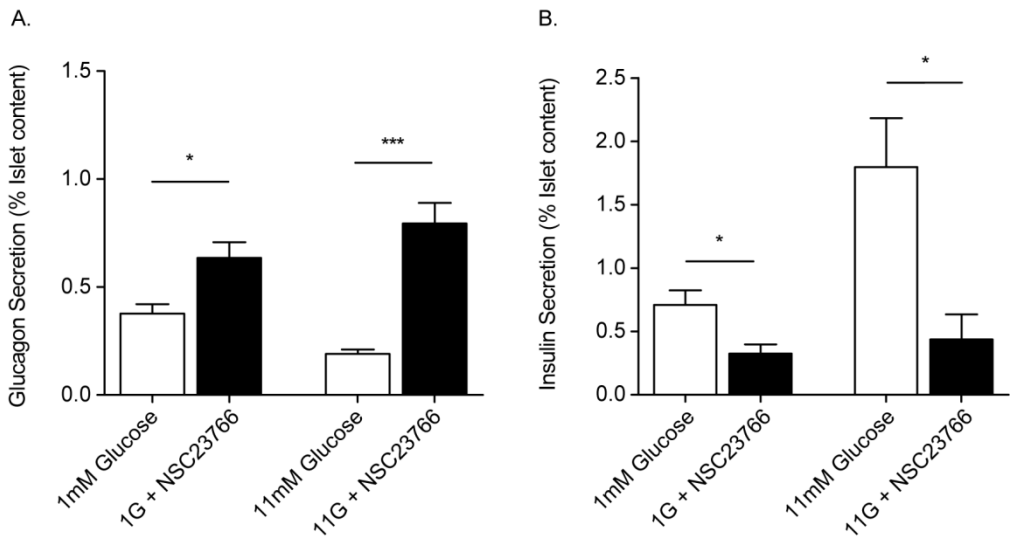

Figure 3-5. Hormone secretion from islets treated with a Rac1-GTPase inhibitor. (A) Glucagon secretion from islet α-cells treated with 1 mM and 11 mM glucose in the absence and presence of NSC23766. (B) Insulin secretion from β-cells in the same islets as in (A). N = 4-6 mice, p values were determined by Student's t-test. * indicates $p < 0.05$, ** $p < 0.01$, *** $p < 0.0001$.

Summary

Toward the goal of elucidating the role of Rac1 in regulating glucagon secretion from pancreatic α-cells, we first confirmed its expression in the islets using quantitative RT-PCR on cDNA from sorted β- and α-cells. Immunofluorescence was used to identify the cellular localization of active Rac1 (Rac1-GTP) in isolated islets, as shown in Figure 3-2. Similar expression profiles were observed in both cell types and localization was largely at the membrane, as expected for the active form of the enzyme. To identify the effect of glucose on the activation state of Rac1, semi-quantitative immunofluorescence was used to identify

glucagon and Rac1-GTP in isolated islets after treatment with low (1 mM) or high (11 mM) glucose levels. In the β-cell, Rac1 activation was increased at high glucose, compared with low glucose, consistent with known Rac1 function with regard to insulin secretion. In the α-cell, we also observed an increase in Rac1 activation at high glucose, in contrast to what we expected. This suggests that Rac1 has a different function in the α-cell and that Rac1 activation is not a gatekeeper for exocytosis of glucagon containing vesicles.

We also utilized an inhibitor that specifically prevents Rac1 activation. Upon staining the islets after treatment with low or high glucose in the absence and presence of the inhibitor, we found the mean intensity was reduced in both α- and β-cells, which provided confirmation of both the inhibitor and the antibody used to identify active Rac1. We treated islets in a similar fashion and measured insulin and glucagon secretion at low and high glucose with and without the Rac1 inhibitor. Consistent with previous reports, we found that inhibiting Rac1 drastically reduced insulin secretion from the islets compared with glucose-only controls. However, glucagon secretion was potentiated at low glucose and stimulated at high glucose levels.

We conclude from this study that Rac1 activity in the α-cells is not glucose dependent and that Rac1 is not a critical player in regulating glucagon secretion. As the function of Rac1, like many small GTPases, is cell-type specific and varies significantly from cell to cell, this is not a particularly surprising finding. However, it does leave open another line of questioning in determining the precise molecular regulators of glucagon suppression from the α-cells. The other two small GTPases in the Rho family, Cdc42 and Rho-GTPase, are the next most likely candidates for cortical F-actin regulation and future directions may include testing their function in the α-cells using a similar paradigm as described here. Additionally, the recent development of novel tools including tissue specific knockout mouse models (Gu, Filippi et al. 2003), photoactivatable GTPases (Wu, Frey et al. 2009), and specific pharmacological agents (Gao, Dickerson et al. 2004) should drive increased understanding about the molecular regulation and roles of F-actin in insulin secretion.

CHAPTER 4

QUANTITATIVE FLUORESCENCE IMAGING OF CELLULAR FUNCTIONS

(Adapted from Elliott & Gao, et al. JCS, 2012; Elliott, et al. in preparation, 2014; Grabowska, et Mol Endo, 2014)

Introduction

The complexity of islet physiology, particularly with regard to molecular events, requires the pursuit of novel and creative methodologies for studying these processes in living cells. In addition to metabolic regulation by glucose, there are many external factors that modulate cellular function by manipulating intracellular signaling. While an increasing number of fluorescent reporters are available for the study of such signaling pathways, the overlapping emission spectra of commonly used fluorophores, especially for the fluorescent proteins, limit the number of reporter molecules that can be used in any given experiment. Thus, a limiting factor in studying molecular events in islet tissue is our inability to detect simultaneously multiple biosensors. One solution to this problem is spectral imaging, which potentially allows background-free live-cell imaging with two or more fluorescent markers.

The goal of the work described here was to exploit hyperspectral imaging to measure simultaneously the temporal and spatial dynamics of multiple fluorescent biosensors that report on signaling pathways in live cells. We validated this approach in the context of β-cell biology, which is described in Part 1. As part of this work, we developed a novel snapshot spectral imaging system for widefield microscopy and also utilized state-of-the-art confocal spectral imaging. We utilized the confocal spectral imaging technique to study transcription factor protein-protein interactions, described in Part 2.

Spectral and hyperspectral imaging

Spectral imaging techniques combine imaging with spectroscopy and are increasingly used in biological experiments for detecting fluorescence from two or more reporter molecules. While well-matched dichroic/filter combinations are available for segregating different fluorescent signals, the emission spectra of most fluorescent proteins (FPs) are 50-150 nm wide with long red-edge tails. Thus, one FP's signal may bleed-through into another's emission channel making distinction difficult (Piston and Kremers 2007). Utilizing spectral imaging removes the problem of crosstalk and increases the signal to noise because the full spectra can be collected since a narrow bandpass is not required. This provides a particular advantage as the ongoing development of fluorescent proteins, organic fluorophores, and other optical highlighters greatly expands the toolkit for interrogating cellular dynamics (Pinaud, Michalet et al. 2006; Lavis and Raines 2008; Rizzo, Davidson et al. 2009).

An important technique used in building fluorescent biosensors is Förster resonance energy transfer (FRET), which is the phenomenon of non-radiative transfer of photon energy absorbed by a donor fluorophore to a nearby (<10 nm) acceptor fluorophore. Upon transfer of energy to the acceptor, the emitted photon will reflect the emission spectrum of the acceptor. When the donor and acceptor are further away than ~10 nm, transfer will not occur so the emission spectrum will reflect only the donor. This technique is often used to create genetically encoded biosensors composed of donor and acceptor fluorescent proteins conjugated to either end of an environmentally sensitive peptide (Rizzo, Springer et al. 2006).

Since FRET is a distance-limited phenomenon, it is also useful for studying protein-protein interactions, whereby each protein of interest is tagged with a fluorescent protein (FP-FRET). This is also used to indicate the proximity of proteins of interest to identify if a direct interaction is possible. However, there are significant challenges with conducting quantitative FRET experiments with the primary limiting factor being crosstalk, or bleed-through, between the two FPs (Piston and Kremers 2007). Spectral imaging techniques can be used to resolve

the overlapping spectra and obviate the need for complicated correction procedures or photobleaching experiments to account for the crosstalk. Thus, the FP-FRET experiments conducted in the course of this dissertation were all performed using a novel hyperspectral-imaging device, the Image Mapping Spectrometer (Part I), or spectral imaging with confocal microscopy and two-photon excitation (Part II).

Part 1

Introduction

Hyperspectral imaging has a number of applications including medical imaging, environmental chemical detection, geographical information, and others (Graham, de Pater et al. 1995; Ferris, Lawhead et al. 2001; Kandpal, Lee et al. 2013). In the snapshot class of hyperspectral imagers, there are several approaches to achieve a 3D spatial-spectral datacube (x, y, λ). These include image slicers, lenslet arrays or fiber field splitting, and image mapping spectrometers, all of which have a unique method of redistributing the spatial information in an object to collect simultaneously spectral and spatial information onto one or more detectors (Matsuoka, Kosai et al. 2002; Gao, Kester et al. 2009; Gao, Kester et al. 2010). The ability of such devices to collect the whole spectrum per pixel allows for the use of multiple probes in a single experiment. While the increasing number of available biosensors makes this methodology attractive for studying multiple molecular processes simultaneously, the spectral windows of available fluorescent proteins limit its ultimate usefulness. Additionally, high quality data is necessary for measuring the small changes often associated with FP-FRET sensors (Piston and Kremers 2007).

Most multispectral imaging systems that are available for studying multiple biosensors use scanning, either in the spatial domain, e.g. hyperspectral confocal microscope [9] or in the spectral domain, e.g., liquid-crystal tunable filter or AOTF [10]. As mentioned above, the

confocal method requires increased illumination to achieve a high enough SNR across the spectrum, which may result in photodamage. Additionally, these methods rely on sequential image acquisition so are limited in temporal resolution, which is another critical factor in measuring cellular activity with fluorescent biosensors. A solution that can overcome these problems is a recently developed snapshot device, the Image Mapping Spectrometer (IMS), which acquires full spectral information simultaneously from every pixel in the field of view and is coupled to a widefield microscope such that all of the photons in the focal volume are collected (Elliott, Gao et al. 2012). The tradeoff with the widefield configuration is the lack of optical sectioning afforded by a pinhole in the confocal configuration. This makes thick specimens challenging to collect and interpret data from, due to the out-of-focus light and sample scattering. In the experiments conducted here, monolayers of tissue culture cells were used to facilitate data collection and analysis.

Briefly, the IMS maps adjacent pixels from the object to create space between them in the image, and then uses a grating to spread wavelength content from each pixel into this space. Direct image re-mapping provides the final 3D (x, y, λ) data cube (Gao, Kester et al. 2009; Kester, Bedard et al. 2011; Bedard, Hagen et al. 2012). The IMS has a unique geometry that allows rapid collection of high-resolution spectral data in a single snapshot. This methodology is based on the image mapping principle, which maps a sample's 3D datacube (x, y, λ) onto a 2D detector array for parallel measurement. The operating principle is displayed in Figure 4-2 and the primary constituents are described in detail below.

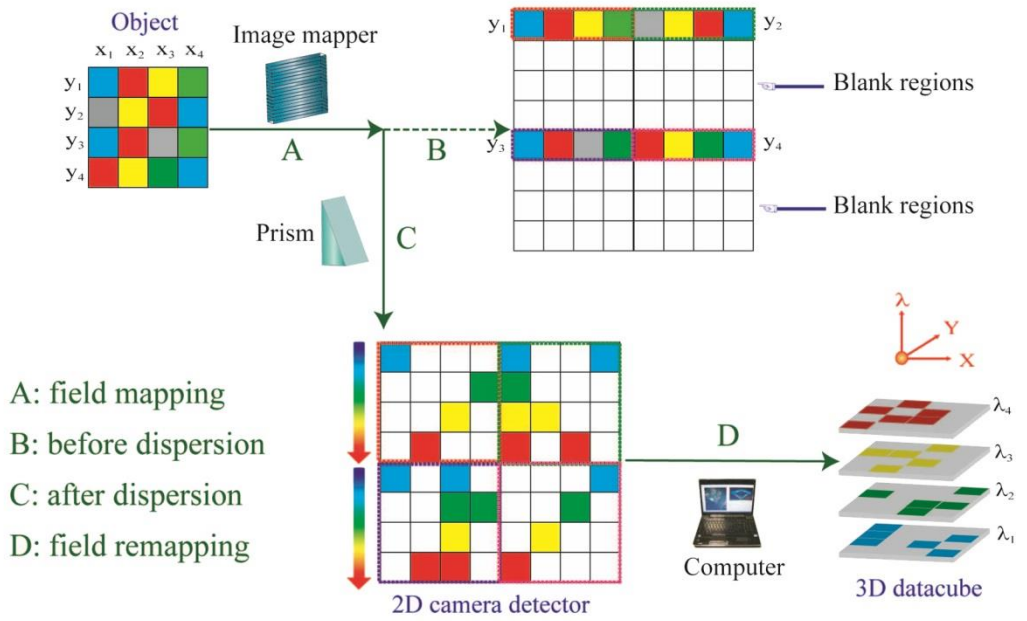

Figure 4-2: Operating principle and system configuration of the IMS. In the IMS, the object's different image zones are mapped and dispersed onto different locations of a 2D camera detector (the object's rows y1, y2, y3 and y4 are mapped onto the second quadrant, first quadrant, third quadrant, and fourth quadrant of the camera respectively in this simple example). The grey pixel in the original object represents a spatial sampling point that has all colors. An x, y, λ datacube is reconstructed by remapping camera pixels encoded with the same color back to the corresponding spectral layer. The full-resolution datacube is acquired by the IMS via a single snapshot.

The IMS system consists of four major optical components, including:

a. Image relay. The image relay has two functions: to transfer the intermediate image from the microscope image port to the image mapper; and to force the light rays to be telecentric at the image side. The telecentricity at the image side is the requirement for correct guidance of light rays reflected from the image mapper. The image relay optics include a Zeiss (Oberkochen, Germany) 2.5×/0.075 Plan-Neofluar objective and Zeiss 130 mm tube lenses (F.L. = 165 mm, Edmund optics, Barrington, NJ, P/N: NT58-452). The distance between the objective back pupil aperture and the tube lens is set to be 165 mm, equal to the focal length of the objective, so that the chief rays are parallel to the optical axis at the image side.

b. Image mapper. The image mapper is a custom fabricated component, which consists of 350 strip mirror facets (70 μm wide, 25 mm long) on a 25 mm × 25 mm high purity Kobe aluminum substrate. Each mirror facet has a 2D tilt angle (αx, αy) (αx = 0.075, 0.045, 0.015, -0.015, -0.045, -0.075 rad.; αy = 0.045, 0.015, -0.015, -0.045 rad.) to reflect light into different sub-pupils. The image mapper was fabricated by the ruling approach on a 4-axis ultra-precision lathe (Moore Nanotechnology Systems, Swanzey, NH, 250UPL).

c. Collecting lenses. We use an Olympus (Center Valley, PA) 1× objective (P/N: MVPLAPO, F.L. = 90 mm, N.A. = 0.189) to collect light reflected from the image mapper. A 6 × 4 sub-pupil array is formed at the back focal plane of the collecting lenses.

d. Prism array and re-imaging lens array. The role of the prisms and re-imaging lenses is to disperse the sub-pupils and re-image them onto the CCD detector. The prisms are constructed as a 6×1 array of double-Amici prisms fabricated by Tower Optical, Inc (Boynton Beach, FL). Each double-Amici prism consists of two identical Amici prisms separated by a pupil mask (Dia. = 3 mm). The designed spectral range is from 450 nm to 650 nm. The re-imaging lens array is composed of 6 × 4 achromatic doublets (Edmund optics, Barrington, NJ, P/N: 45-408, Dia. = 5 mm, F.L. = 20 mm). The field of view of each re-imaging lens on the CCD detector is of size 5.55 mm ×5.55 mm. When the PSF on the image mapper matches the mirror facet width, the PSF on the CCD detector is about 16.8 μm in diameter, and is sampled by ~ 2 camera pixels (pixel size: 7.4 μm × 7.4 μm).

IMS calibration and corrections

There are several calibration procedures that have been developed for the IMS to account for mechanical and chromatic aberrations in the components. The protocols developed for calibrating and standardizing the IMS after fabrication are reported here (Bedard, Hagen et al. 2012). Since the IMS devices that were available to us over the course of this project were

fabricated before rigorous optimization of the procedures, there were a number of imperfections to correct for either pre- or post-data collection. We utilized a three-step calibration procedure, the first of which was accounted for before arrival in our laboratory and is described in detail here (Bedard, Hagen et al. 2012). A flat-field correction was performed before beginning experiments to account for intensity variations across the raw image. Using a halogen lamp and an empty microscope stage with a neutral density filter in place, a datacube (flat-field image) was recorded and subsequent datacubes acquired by the IMS are divided by the flat-field image to normalize the response of each voxel in the datacube. A new flat-field control image was collected for each set of IMS experiments to account for any changes in alignment, and an example is shown in Figure 4-3. A number of mechanical issues can be identified from such an image and reflect small imperfections in the image mapper.

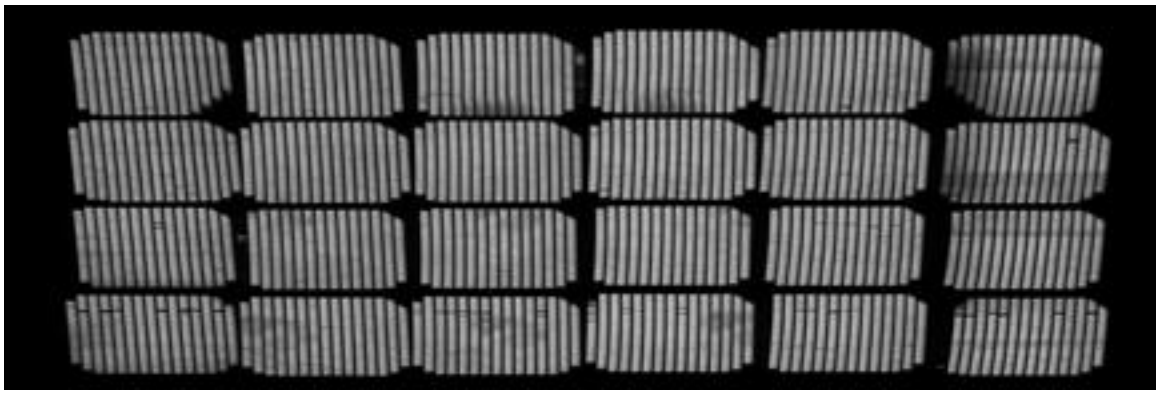

Figure 4-3: Sample flat-field calibration image from the IMS.

The next calibration step consisted of collecting the halogen lamp spectrum with a point spectrometer and multiplying this correction factor by each of the spectral images within the datacube to provide spectral sensitivity standardization. This procedure was done once for each of the metal and plastic versions of the IMS that we used for experiments. Additionally, the IMS alignment and focus was achieved after setup using a USAF resolution target. All of

the calibration procedures were performed with the 40x oil immersion objective that we utilized for experiments to account for the specific optics and aberrations on the objective lens.

Spectral data cube processing and analysis

The 3D datacubes are read out from the detector as tiff files and custom programs have been created in MatLab to handle the remapping and three or four-color unmixing processes. A lookup table that relates the image voxels to exact locations on the detector for the X and Y image planes is generated in the first calibration step and was provided with the IMS. These lookup tables are required for the remapping algorithm. Briefly, the MatLab program reads in a raw tiff file, multiplies it by the correction factor for spectral sensitivity, divides by the flat-field correction image, and remaps this corrected raw data into a useable datacube. The algorithm responsible for the remapping is a bicubic interpolation of the raw detector data and is described in detail here (Bedard, Hagen et al. 2012). This program outputs a folder of 70 xy tiff files, one for each wavelength bin, for each time point tiff.

The lambda series are then read into the unmixing program, which executes a linear unmixing algorithm. Linear unmixing is a commonly used method for extracting multiple spectra from an image. It is based upon the principle that each pixel in an image represents a complex spectrum of intensities from more than one fluorescent species. This mixture of signals can be deconvolved into the proportion of each individual fluorophore based on their reference spectra (Zimmermann 2005), which we collected from cells transfected with the individual fluorescent proteins used in the experiments. Additionally, an untransfected control was imaged to provide a reference for the autofluorescence spectrum. This unmixing program outputs a single tiff for each reference spectrum that has all of the remapped spatial information and can be analyzed using standard image processing software. Here, ImageJ was utilized for the image processing, often with macros written to increase the efficiency of processing multiple files. After

background correction, intensities were measured as the average over each cell, defined by a ROI selection. The cellular intensities were then averaged across the FOV and for FRET pairs the ratio of acceptor to donor was calculated. Finally, data were normalized to the average of the first several frames in each experiment to facilitate interpretation of changes over the timecourse due to perturbations.

Hyperspectral image mapping spectrometry for live-cell imaging

To demonstrate the IMS advantages for imaging dynamic cellular processes, we assayed multiple fluorescent biosensors of pancreatic β-cell signaling molecules. While our current interest lies in the glucagon-secreting α-cell, as evidenced by previous chapters, the IMS configuration with a widefield microscope does not have optical sectioning capability and thus, whole islet imaging required for studying the α-cells was outside of the scope of this work. The β-cells, by contrast, can be studied in monolayers of cultured cells that reasonably mimic some of the islet β-cell behaviors, so this was the model we worked with for characterizing the IMS system for live-cell imaging. As mentioned in previous chapters, the roles of $[Ca^{2+}]_i$ and cAMP signaling in regulating glucose-stimulated insulin secretion from pancreatic β-cells have long been known (Landa, Harbeck et al. 2005; Holz, Heart et al. 2008). These signaling pathways are the targets of numerous physiological regulators and several pharmaceuticals that combat the symptoms of diabetes. However, it has been challenging to study temporal relationships between these signaling molecules due to the spectral overlap of most $[Ca^{2+}]_i$ and cAMP biosensors (Landa, Harbeck et al. 2005).

Throughout the following studies, we utilized an optimized fluorescent protein (FP)-based FRET biosensor for cAMP called ^{T}-Epac-^{VV}, which contains an monomeric Turquoise donor and tandem circularly permuted Venus-mVenus (Venus-Venus) acceptor (Klarenbeek, Goedhart et al. 2011). To image $[Ca^{2+}]_i$, we used a GCaMP family (Wang, Shui et al. 2008;

Tian, Hires et al. 2009) biosensor with a circularly permuted GFP fluorophore, called GCaMP5G (Akerboom, Chen et al. 2012). While the emission spectra of the three FPs (Turquoise, Venus-Venus, and cpGFP) overlap significantly, the IMS can simultaneously measure changes in their intensity and distinguish between their spectra over time. The resulting 4D dataset (x, y, λ, t) permits detailed examination of the temporal dynamics and relationships between different signaling molecules. However, biosensors like ^{T}-Epac-^{VV} based on FP-FRET depend on measurements of small changes in FRET and thus require high signal-to-noise data (Piston and Kremers 2007; Lin 2010). Using the IMS, we can resolve the effects of modulating these signaling molecules simultaneously to determine the effects of various perturbations.

We also monitored Caspase-3 activity with a cleavable biosensor composed of either an ECFP/EYFP FRET pair (Scat3.1) (Nagai and Miyawaki 2004) or a newly prepared sensor (GRScat) with the recently published green/red FRET pair mClover and mRuby2 (Lam, St-Pierre et al. 2012). Combinations of these biosensors allowed us to monitor pairs of molecular processes simultaneously and we were able to use linear unmixing with either three or four fluorophores. Combining the cAMP FRET biosensor and the new GRScat Caspase-3-cleavable sensor, we utilized a dual FRET approach with the IMS to study the relationship between cAMP and Caspase-3-mediated apoptosis in pancreatic β-cells, for which the molecular mechanism is not well understood but is known to play an important role in the pathology of type 2 diabetes. In the following studies, we have used the IMS approach to interrogate the normal relationship between $[Ca^{2+}]_i$ and cAMP in β-cells that have been stimulated with glucose, and we have characterized this relationship under oxidative stress conditions along with the onset of caspase-3 activation that leads to apoptosis.

Materials and Methods

Cellular sample preparation

HeLa, MIN6, or βTC3 tissue culture cells were transiently transfected with plasmid DNA encoding one or more of the fluorescent protein-tagged proteins in the Table below. Transfection was accomplished using Lipofectamine2000 (Invitrogen, Carlsbad, CA) transfection reagent according to the manufacturer's instructions. Cells were seeded onto No. 1 coverglass bottomed dishes (MatTek, Ashland, MA) and cultured as previously described for microscopy studies. 24 hours after transfection, samples were fixed with 4% paraformaldehyde, washed in DPBS, and mounted on microscope slides with gelvatol. For live-cell experiments, imaging was accomplished in extracellular-like buffer 24-48 hours after transfection.

The results for this chapter are organized into sections by imaging modality, with the first being a technical comparison of the hyperspectral IMS and the spectral detection mode of the laser-scanning microscope (LSM) 710 (Zeiss). The data collected with the IMS in β-cells is then presented and summarized, and this chapter ends with a collaborative project using spectral FP-FRET with the confocal method to study transcription factor interactions.

Results

Quantitative comparison of the IMS and LSM710

We have compared quantitatively the detection efficiencies of the IMS system and the Zeiss LSM710 confocal microscope that we commonly use for spectral imaging. While the two systems have comparable detection efficiencies, the IMS offers advantages in acquisition speed that increase as larger image sizes are used due to the snapshot format. To compare quantitatively the detection efficiency (defined as the ratio of photons detected over photons excited, or $D=N_d/N_e$) of two systems, we measured their relative excitation intensities and

fluorescent photon detection. We imaged the same sample volume on both systems and measured the collected fluorescent photons under matched excitation conditions, which were determined by matching the photobleaching rate in the two systems. The procedure was as follows: we matched the total image acquisition time, the image size and the pixel size, then we measured the photobleaching rates for such settings, and their value was used to scale the different excitation intensities. The imaging settings for the experiment on the IMS were: integration time 500 ms, pixel size 0.7 µm, image size 348 * 348 pixel, excitation filter 436/20, dichroic T455LP, emission filter HQ460LP, 40x/1.3 oil objective. The imaging settings for the experiments on the LSM710 (Zeiss, Oberkochen, Germany) were: excitation laser 458 nm, power 5% of 100 mW, scan time 531 ms, dwell time 3.76 µs, pixel size 0.68 µm, pinhole diameter 609 µm corresponding to an optical section of 15.5 µm, image size 348 * 348 pixel, Zeiss Fluar 40x/1.3 oil objective.

We designed two independent sets of experiments to calculate the relative detection efficiency of the two systems, D_{IMS}/D_{710}. First, we compared the excitation power acting on the sample using microdroplets with a 10 µM aqueous solution of fluorescein (F-1300 from Molecular Probes, Carlsbad, CA) dispersed in a hydrophobic medium to create a layer of fluorescent droplets with a thickness less than 3 µm (Kremers and Piston, 2010). The use of microdroplets removes the need to consider lateral diffusion in the sample, and the relatively thin sample thickness is also critical for the comparison. The LSM710 is a confocal system, which only collects photons from a section of the sample, while the IMS is coupled to a widefield microscope (Nikon TE 300 inverted microscope, Melville, NY) and therefore receives photons from the whole sample volume. In the confocal configuration, using a thin sample allows the pinhole size to be set so that all the photons coming from the sample volume are collected.

The measured photobleaching rates were used to estimate the ratio between the excitation intensities delivered into the sample by the two systems, which is an estimate of the number of incoming photons. For the power levels that are used in fluorescence microscopy,

the relationship between excitation intensity and photobleaching rate is generally accepted to be a linear one: $k = aI$. Under this assumption with matched excitation power P, imaged area A, and imaging time on the two systems, the intensities and photobleaching rates are related by: $I_{710}/I_{IMS} = k_{710}/k_{IMS} = n_{pixel}$.

For the second set of experiments we used a thin film of fluorescein solution to measure the number of photons collected by the two systems. Again, the sample being thinner than the optical section selected on the LSM710 allowed for a direct comparison between the widefield and confocal systems. The number of emitted fluorescence photons is now only proportional to the number of excited photons. Moreover in these conditions there is no background to be subtracted from the signal and the only source of noise is the shot noise that follows Poisson's distribution. The number of detected photons (i.e. photo-electrons) N_d equals $\bar{x}^2/\sigma^2$, where $\bar{x}^2$ is the mean of the grey level distribution and σ is the standard deviation of the same distribution. For the LSM710 the number of detected photons in a single spectral bin centered at 519 nm, with a spectral width of 9.7 nm, was $N_{d710} = 78$. For the IMS the number of detected photons in an 8 nm spectral bin centered at 519 nm was $N_{dIMS} = 1465$. Thus, assuming linear photobleaching, the ratio of $D_{IMS}/D_{710} = (N_{dIMS}/ N_{d710})\cdot(I_{710}/I_{IMS})\cdot(A_{IMS}/A_{710}) = (N_{dIMS}/ N_{d710})\cdot(k_{710}/k_{IMS})\cdot(A_{IMS}/A_{710}) = 8.4$

This large difference in collection efficiency is surprising considering the improvements introduced to confocal microscopy over the last 25 years. However, these comparisons are based on equal amounts of photobleaching, which is an appropriate comparison for practical imaging but may not accurately reflect actual collection efficiency. It has been shown that the photobleaching rate in laser scanning confocal microscopy is supra-linear (Patterson and Piston, 2000). Assuming this supra-linear dependence $k^* = aI^{1.2}$, we would need to introduce a correction factor in the relation linking intensities and rates: $I_{710}/I_{IMS} \approx (k^*_{710}/k_{IMS})/(n_{pixel})^{0.2}$. For an image of 348*348 pixels, this correction is ~10, which would bring the overall detection efficiencies of the two systems to nearly the same level.

Further optimization of the IMS system, including the use of a high quantum efficiency camera, will lead to higher collection efficiency in the IMS than is possible with a laser scanning system. It should be noted that if image collection rates are not an issue, any hyperspectral imaging approach could be utilized, including confocal spectral imaging such as we have used with the LSM710. In fact, the main advantages of widefield microscopy over laser scanning confocal imaging are the higher signal collection and resultant increased data acquisition rates. Further, the superior temporal resolution given by the IMS system becomes greater as larger frame sizes are captured.

Spectral unmixing of triply-labeled HeLa cells

Our first goal with in using the IMS for cell biology was to test its spectral resolution with regard to known overlapping fluorophores. The commonly used fluorescent proteins CFP, GFP, and YFP have considerable overlap in their emission spectra, requiring post-collection unmixing to separate the signals (Kremers 2011). To demonstrate the efficacy of the IMS system for this purpose, we expressed proteins with known localizations fused to ECFP, EGFP, or SYFP (Rizzo, Springer et al. 2006) (em 480 nm, 509 nm, and 528 nm respectively) in HeLa cells and fixed them for IMS imaging. Since linear unmixing algorithms rely on reference spectra to calculate components, we first acquired these from singly labeled control cells. The resulting base emission spectra were determined independently for all three fluorophores using the IMS and the shapes and emission profiles were found to be accurate compared with conventional methods for measuring spectra. However, spatially distinct fluorophores are still a limited test as the overlapping spectra will only occur is a small percentage of pixels in the image. A more robust test, and closer to the ideal experiments, would be to use spatially and spectrally overlapping fluorophores, as many cellular processes occur in the cytosol and are not compartmentalized.

Thus, triply labeled cells expressing ECFP in the mitochondria, EGFP on the on the plasma membrane, and SYFP in the nucleus were imaged by the IMS with an integration time of 0.5 seconds. The spectral component images were determined by implementing a linear spectral unmixing algorithm (Zimmermann 2005) on the measured datacubes. To provide a reference image for comparison, we used a color camera to capture an image of the same field of view. In this color image, all three components appear as shades of green and cannot be discriminated. In contrast, spectral unmixing reveals the three components clearly and identifies their sub-cellular localization. Since each channel represents the spectral emission profile for each fluorophore, crosstalk from the other two fluorophores is minimized. These data are presented in Figure 4-4.

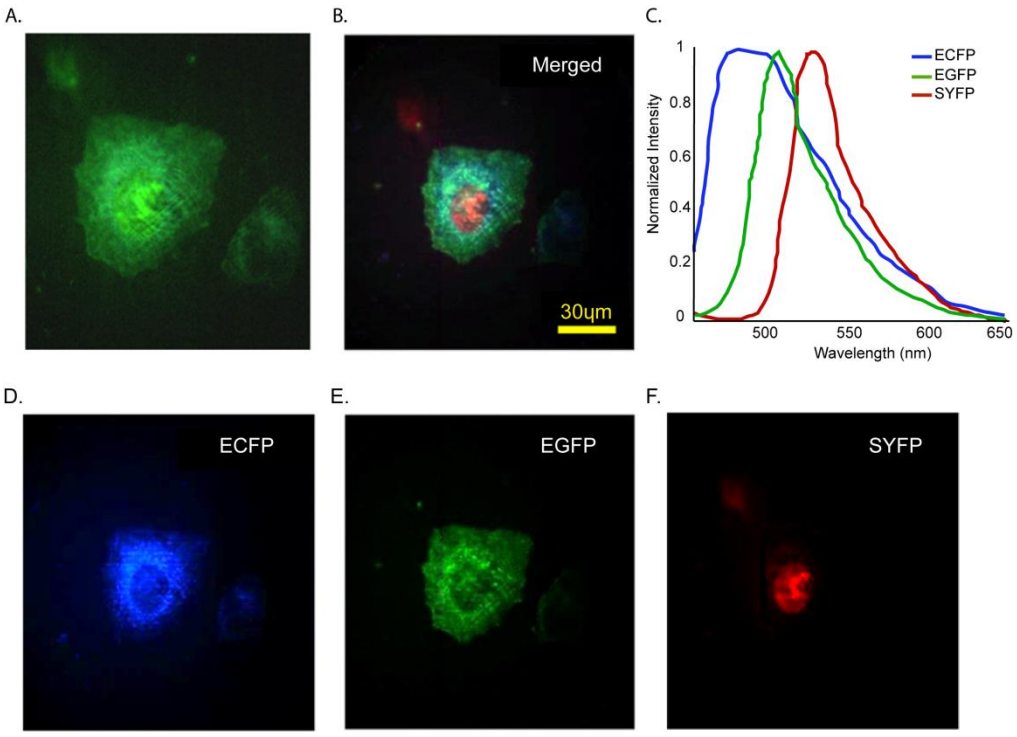

Figure 4-4: Linear unmixing of spatially separated overlapping fluorophores with the IMS. (A) The baseline reference image was captured by a color camera (Infinity 2-1C) directly at a microscope's side image port. (B) A merged image of D, E, and F. (C) The unmixed component spectra. (D-F) The spectral component images were acquired by implementing a linear unmixing algorithm on the IMS measured datacube (captured with 0.5 s integration time). D-F were pseudo-color rendered to indicate FPs' sub-cellular localizations.

Real-time hyperspectral imaging of $[Ca^{2+}]_i$ and cAMP oscillations

Having successfully demonstrated in fixed tissue that the IMS was capable of providing high quality spectral and spatial data for transfected cells, we next turned to a live-cell system to test its capabilities in measuring dynamic processes. Since we coupled the IMS to a widefield microscope, we did not have the optical sectioning that is conferred by a pinhole in a confocal configuration. Thus, studying the thick, dense multicellular islets was not possible, so instead we used MIN6 tissue culture β-cells, which form a monolayer convenient for widefield imaging and are functionally similar to islet pancreatic β-cells. The MIN6 cells exhibit similar intracellular calcium ($[Ca^{2+}]_i$) pulses with a period of 30–80 s and a duration of 1–4 s that underlie pulsatile insulin secretion from these cells (Holz, Heart et al. 2008). These pulses of $[Ca^{2+}]_i$ arise due to $[Ca^{2+}]_i$ flux across the plasma membrane through voltage-gated $[Ca^{2+}]_i$ channels (VGCCs) that open after membrane depolarization caused by the closure of ATP-sensitive K^+ channels. Subsequent opening of $[Ca^{2+}]_i$-dependent K^+ channels then repolarizes the membrane and closes the VGCCs. The observed pulses are a measure of the repeated opening and closing of these ion channels.

To demonstrate the ability of the IMS to monitor the temporal dynamics of $[Ca^{2+}]_i$ activity *in vivo*, MIN6 cells were transfected with GCaMP5G (ex. 495 nm, em. 519 nm). GCaMP5G is made of a circularly permuted GFP moiety and a portion of the $[Ca^{2+}]_i$ binding protein calmodulin (Baird, Zacharias et al. 1999; Nagai, Sawano et al. 2001). In the unbound state, the fluorescent signal from the GFP is quenched. Then, upon binding $[Ca^{2+}]_i$, the protein changes conformation, activates the chromophore, and produces fluorescence with peak emission of 519 nm. Changes in GCaMP5G fluorescence show an increase in intensity upon stimulation with 20 mM glucose and 20 mM TEA and pulses in $[Ca^{2+}]_i$ at the expected frequency of 1–2 per min in 20 mM glucose, as displayed in Figure 4-5. Thus, the IMS system provides the sub-second resolution needed to quantify these pulses and study calcium signaling in a time-resolved manner with different perturbations.

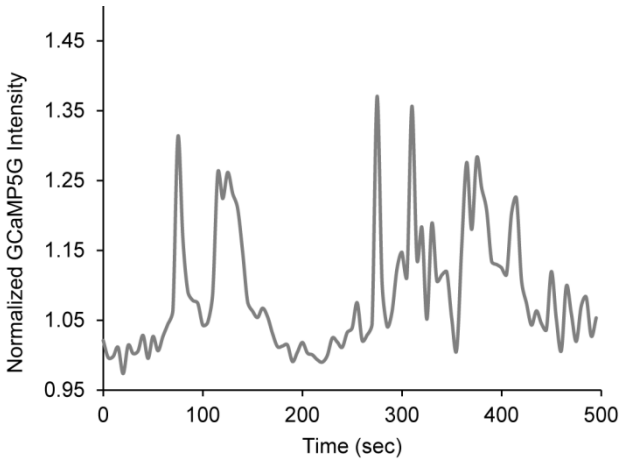

Figure 4-5: $[Ca^{2+}]_i$ oscillations with GCaMP5G in MIN6 β-cells. Singly-transfected $[Ca^{2+}]_i$ intensity collected 5 minutes after stimulation with 20 mM glucose and 20 mM TEA with a 0.5 s integration time every 2 minutes.

We next sought to measure an FP-FRET biosensor in live cells to demonstrate that the spectral resolution provided by the IMS is sufficient to unmix donor and acceptor spectra in a dynamic setting. Thus, MIN6 cells were transfected with the FRET-based cAMP sensor ^{T}-Epac-^{VV}, a fusion protein containing Turquoise (Goedhart, van Weeren et al. 2010) and tandem Venus-Venus connected by a portion of the cAMP binding protein Epac1 (de Rooij, Zwartkruis et al. 1998). Importantly, since this biosensor is based on intramolecular FRET, the stoichiometry of the donor and acceptor fluorophores is one to one, which allows for data analysis of the direct ratio of donor to acceptor fluorescence. In cells, donor Turquoise and acceptor Venus-Venus are linked and a strong FRET signal is observed in the absence of cAMP. Upon production of cAMP by adenylyl cyclases, the sensor binds cAMP and undergoes a conformational change resulting in a loss of FRET. As FRET is eliminated with the change in fluorophore conformation, there is an increase in donor Turquoise fluorescence and decrease in acceptor Venus-Venus intensity, which is typically expressed as the ratio of Venus-Venus/Turquoise (called the FRET ratio throughout this document).

In our first experiment, transiently transfected MIN6 cells were exposed to 20 mM glucose and 20 mM TEA 24 hours after transfection to stimulate cAMP signaling and were monitored for changes in FRET with continuous collection at 2 fps. As expected, glucose and TEA stimulated an increase in cAMP activity, and led to sustainable cAMP oscillations, which are shown in Figure 4-6. As with the $[Ca^{2+}]_i$ oscillations, these occur at the expected frequency of 1-2 per minute. Importantly, the oscillations are also observed in the unmixed Turquoise and Venus-Venus spectral components of ^{T}-Epac-^{VV}, verifying that the cAMP oscillations we observe in the ratio are not the result of an unmixing artifact or background noise.

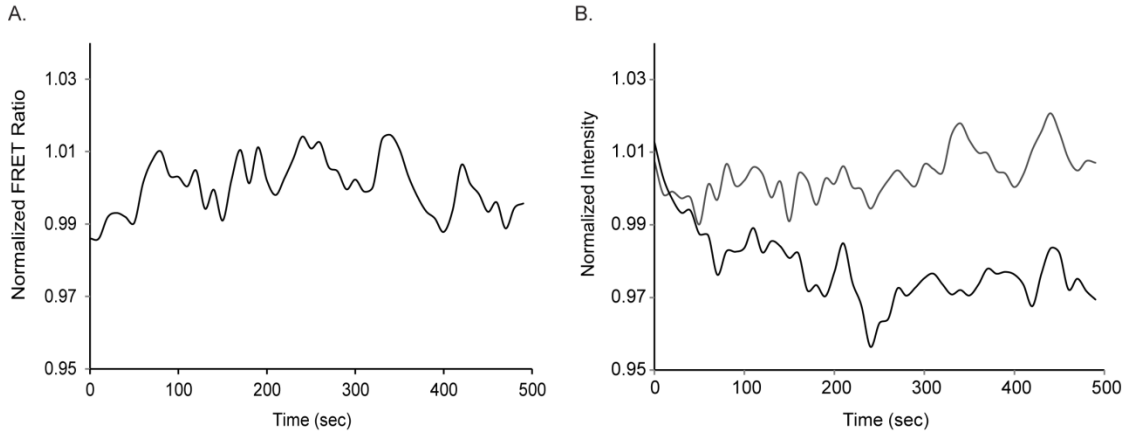

Figure 4-6: cAMP oscillations in β-cells. (A) The ^{T}-Epac-^{VV} FRET ratio over time 5 minutes after stimulation with 20 mM glucose and 20 mM TEA collected with a 0.5 s integration time every 2 minutes. (B) Time-resolved components of (A) with Turquoise in blue and Venus-Venus in yellow.

Simultaneous imaging of $[Ca^{2+}]_i$ and cAMP oscillations in MIN6 cells

A major advantage of hyperspectral imaging is its ability to correlate multiple signals. To demonstrate this ability with multiple live-cell dynamic processes we transfected MIN6 cells with both GCaMP5G and ^{T}-Epac-^{VV} biosensors. This allows the measurement of both $[Ca^{2+}]_i$ and cAMP activation after glucose stimulation in the MIN6 cells. Figure 4-7 shows that the two

biosensors can be simultaneously measured and spectrally unmixed to indicate the expected dynamics as compared to singly transfected controls that were displayed in Figures 5-5 and 5-6.

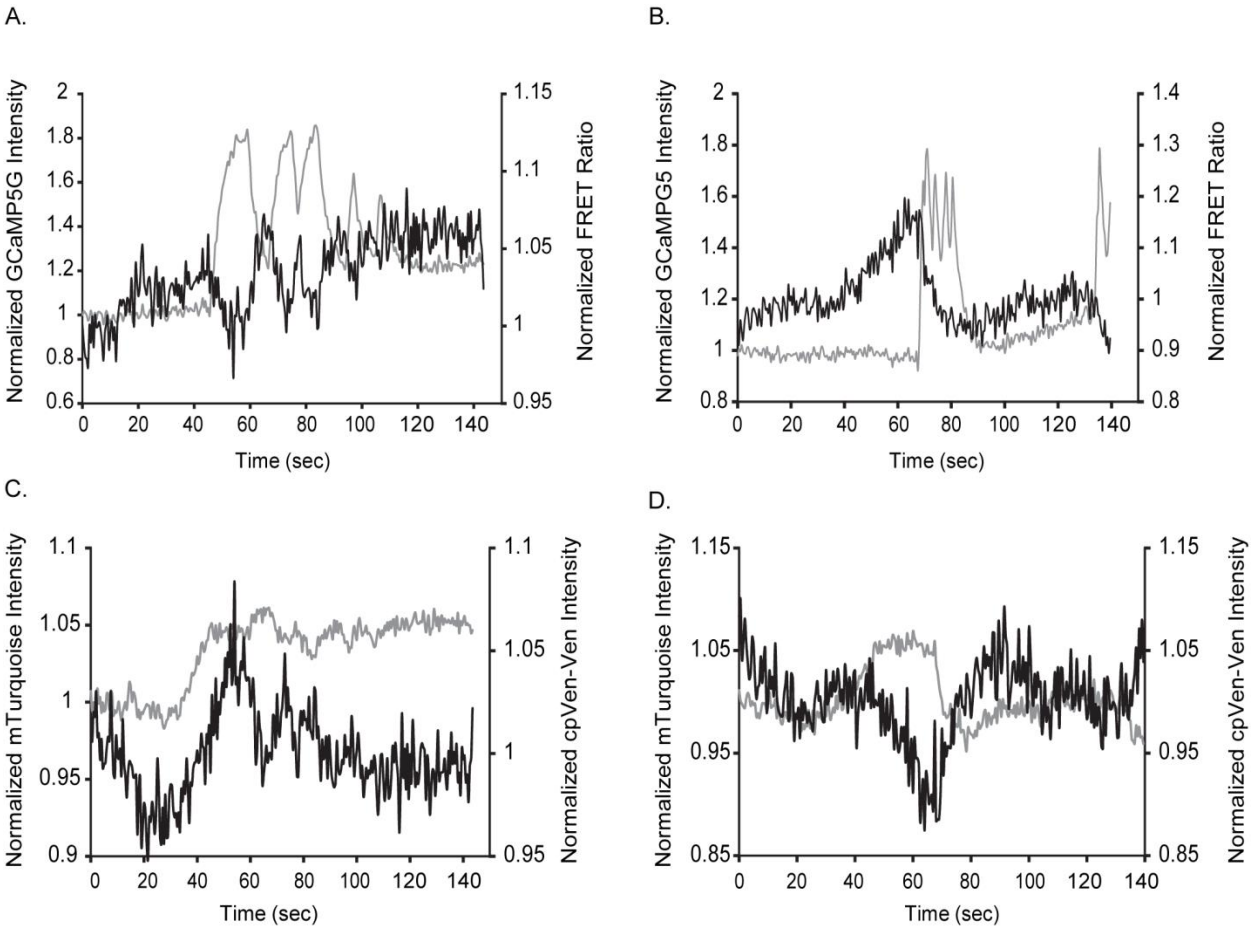

Figure 4-7: Simultaneous imaging $[Ca^{2+}]_i$ and cAMP oscillations at 2 fps. (A) $[Ca^{2+}]$i (gray) and cAMP (black) oscillations after 5 minutes of stimulation with 20 mM glucose and 20 mM TEA stimulation collected at 2 fps. (B) [Ca2+] and cAMP oscillations from a cell in a different FOV stimulated and collected as in (A). (C, D) Time resolved components of ^{T}-Epac-^{VV} (Turquoise in gray, Venus-Venus in black) from cells A and B respectively. Venus traces are corrected to account for the observed photobleaching (see Methods).

Looking at the unmixed data, two representative cells imaged at 2 fps show that $[Ca^{2+}]_i$ and cAMP oscillations occur with a similar frequency after stimulation by glucose and TEA. Due to data acquisition restrictions in the IMS computer's memory, we were restricted to collecting

data at 2 fps, which severely limited the number of oscillation periods in each collection record, and thus prohibited a detailed analysis of the temporal relationship between $[Ca^{2+}]_i$ and cAMP oscillations. At this imaging rate, we also collected data from co-transfected cells after stimulating with either KCl to maximize the Ca^{2+} signal, or IBMX and forskolin to maximize cAMP, as displayed in Figure 4-8. These experiments demonstrated the dynamic range of both sensors and the ability of the unmixing algorithm to distinguish between signals, since we are able to selectively change the dynamics of one biosensor or the other based on known stimulatory substances.

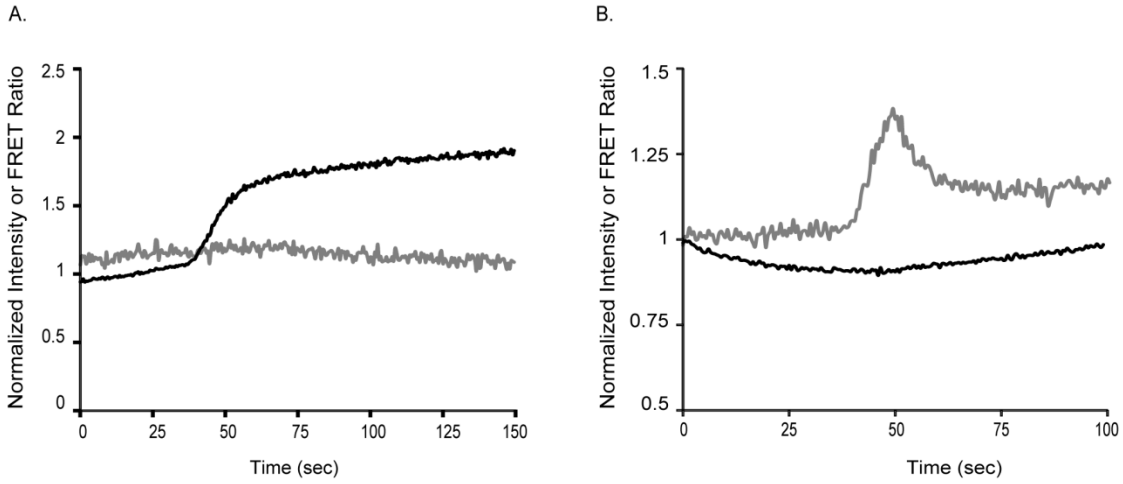

Figure 4-8: Functional biosensor isolation by selective stimulation. (A) Timecourse of T-Epac-VV in black and GCaMP5G in gray after treatment with 20 mM KCl. (B) As in (A) after treatment with 100 µM IBMX and 50 µM forskolin.

To overcome the data collection limitation imposed by the hardware, we performed experiments with the same 0.5 second integration time, but a frame rate of once every 2 seconds. This protocol allowed us to image for a longer period (400 seconds) and obtain more oscillations per single stimulus. The GCaMP5G and ^{T}-Epac-^{VV} traces over this time period for glucose and TEA treatment show anti-correlative oscillations, as displayed in Figure 4-9.

Additionally, the component traces from the cAMP sensor demonstrate that these oscillations are not an artifact of unmixing or averaging.

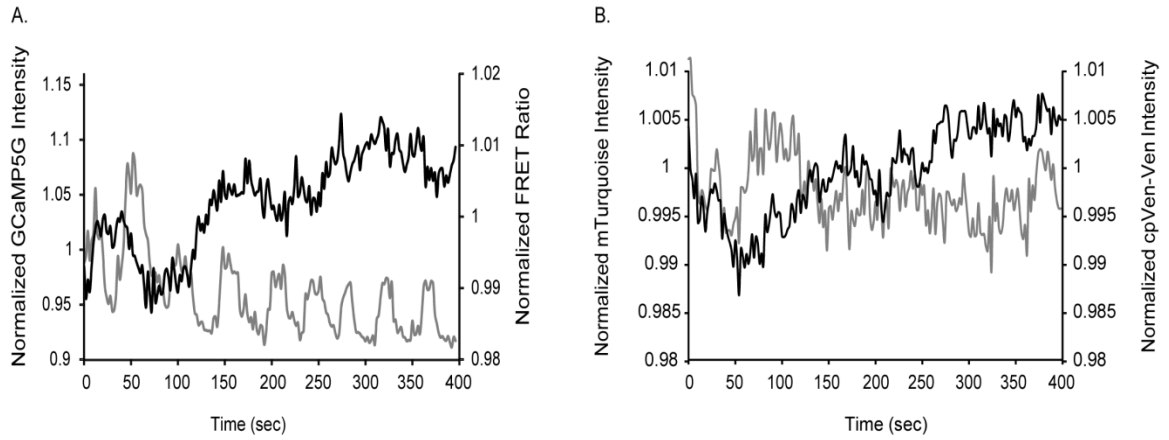

Figure 4-9: Simultaneous $[Ca^{2+}]_i$ and cAMP oscillations in stimulated β-cells. (A) $[Ca^{2+}]_i$ (gray) and cAMP (black) activity average in 5 cells after stimulation with 20 mM glucose and 20 mM TEA collected with a 0.5 s integration time. (B) Average components of ^{T}-Epac-^{VV} (Turquoise in gray, Venus-Venus in black) cAMP sensor from (A).

We also plotted the time variant GCaMP5G against the ^{T}-Epac-^{VV} and confirm a negative correlation with a Pearson coefficient of -0.5720 (n = 5 cells). One other cell exhibited similar negative correlation of its smaller-amplitude peaks, but also showed a single large-amplitude peak with a strong positive correlation. For the average traces shown in Figure 4-9, data from this cell were not included since we could not confirm whether the single peak was an artifact or a unique biological event. Additionally, a cross-correlation analysis provided the same negative correlation coefficient of -0.5720 for the GCaMP5G and ^{T}-Epac-^{VV} signals, as shown in Figure 4-10. This analysis also demonstrated that the GCaMP5G signal rise precedes the ^{T}-Epac-^{VV} decrease. Together, these data show that $[Ca^{2+}]_i$ and cAMP signals are anti-correlated in pancreatic β-cells, and $[Ca^{2+}]_i$ oscillations lead those of cAMP by 2.5 seconds in response to glucose and TEA. Because this difference in rise time is comparable to previously used imaging rates, the relative rise times of these two signals have not been assessed. The

observed anti-correlation confirms the predictions of computational models (Holz, Heart et al. 2008), and the superior time resolution of the IMS system represents a significant potential for further detailed analysis of the interplay between the $[Ca^{2+}]_i$ and cAMP under various treatments.

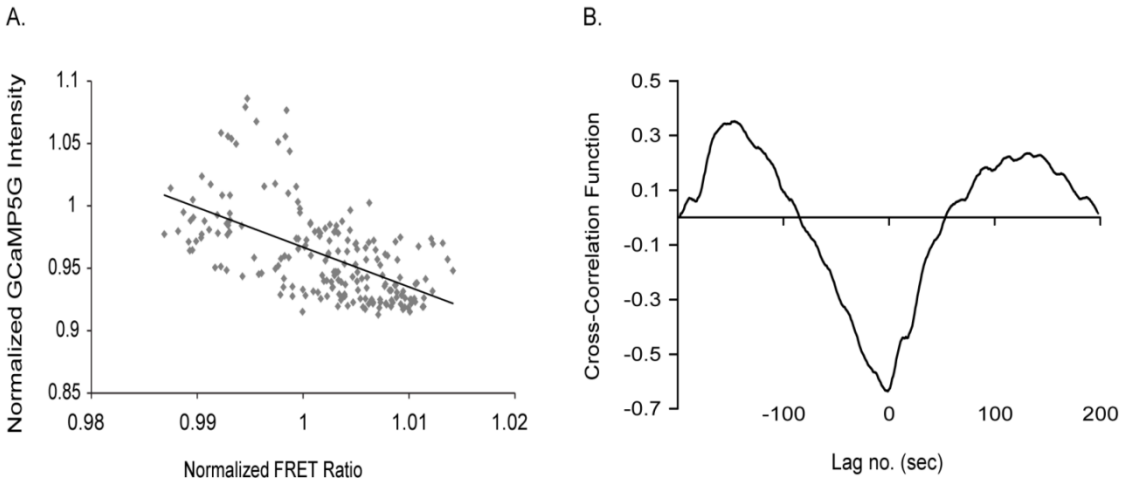

Figure 4-10: Correlating $[Ca^{2+}]_i$ and cAMP oscillations. (A) Correlation plot of average $[Ca^{2+}]_i$ and cAMP traces from Figure 4-5, r = -0.5720. (B) Cross-correlation plot of data in (A).

Real-time hyperspectral imaging apoptosis in β-cells

A major goal in cell biology is to correlate multiple live-cell dynamic processes in real-time, which we demonstrated is possible using the IMS to study the relationship between $[Ca^{2+}]_i$ and cAMP signaling. These two signaling pathways are ubiquitous in nearly all cells and have particular relevance to islet physiology because the islet cells are bombarded with extracellular factors that utilize these second messengers to drive various functions. One of the functions that both pathways have been implicated in is that of mitochondria-mediated apoptosis. This is a critical point, as dysregulated β-cell apoptosis contributes to the development of type 1 and type 2 diabetes, and limits the ability of islet transplantation as a therapeutic for patients with type 1 diabetes (Mathis, Vence et al. 2001; Butler, Janson et al. 2003; Butler, Janson et al.

2003).

Recent reports have demonstrated a strong temporal correlation between $[Ca^{2+}]_i$ elevation and morphological changes, as well as Caspase-3 activity (Lee, Lu et al. 2010). Since Ca^{2+} is known to be critical for β-cell function and is dysregulated in both type 1 and type 2 diabetes, a better molecular understanding of this relationship would be beneficial. Furthermore, Ca^{2+} channels are commonly affected by drugs that treat diabetes, such as the sulfonylureas, which act directly on K^+ channels to increase membrane depolarization, Ca^{2+} channel activation, and Ca^{2+} influx (Shiota, Rocheleau et al. 2005). Notably, this particular class of drugs has also been shown to affect the cAMP pathway via Epac2 (Zhang, Katoh et al. 2009). However, too much $[Ca^{2+}]_i$ activity can lead to inappropriate mitochondrial membrane depolarization, cytochrome c release, Caspase-3 and -9 activation, and ultimately apoptosis (Boehning, Patterson et al. 2003).

The generation of reactive oxygen species (ROS) is another route by which β-cell apoptosis is stimulated in the diabetic state, which has been correlated with both glucotoxicity and lipotoxicity (Luciani, Gwiazda et al. 2009; Syeda, Mohammed et al. 2013). The molecular mechanisms underlying ROS generation and subsequent apoptosis are unclear. However, both $[Ca^{2+}]_i$ (Boehning, Patterson et al. 2003) and cAMP (Li, Li et al. 2012) have been shown to play roles this process, though their relative contributions have yet to be clarified. Having established that we can measure $[Ca^{2+}]_i$ and cAMP simultaneously in response to several stimuli, we sought to determine the relationship between $[Ca^{2+}]_i$, cAMP signaling and apoptosis via caspase-3 activation. To accomplish this, we utilized the IMS to detect the dynamics of GCaMP5G for $[Ca^{2+}]_i$ or the cell-permeant dye Fluo4; ^{T}-Epac-^{VV} cAMP FRET sensor; and two Caspase-3 cleavable FRET biosensors with different FPs, Scat3.1 with ECFP/EYFP, and GRScat with mClover/mRuby2, in pairwise combinations in pancreatic β-cells lines.

In healthy cells, the donor and acceptor of the Caspase-3 cleavable sensors remain linked and FRET is observed until Caspase-3 is activated, whereupon the active protease

cleaves the donor from acceptor resulting in a loss of FRET. Thus, as cleavage occurs and FRET is eliminated, donor fluorescence increases, and the acceptor intensity decreases. An important advantage of the IMS system and the green/red FRET pair is that using a single excitation source, the acceptor mRuby2 in the GRScat is not stimulated directly. Thus, the mRuby2 fluorescence is only observed when the cells are healthy and as the Caspase-3 increases, the FRET ratio decreases until mRuby2 is no longer detectable.

To induce apoptosis, we treated the transiently transfected cells with a high (30 mM) concentration of H_2O_2, a common model for oxidative stress. βTC3 cells were exposed to H_2O_2 24 hours after transfection to induce apoptosis and were subsequently monitored for changes in FRET (frame integration time: 0.5 s, frame interval time: 2 min). By 50 min post-H_2O_2-treatment, a significant reduction in FRET was observed and continued until the cell died, as demonstrated by morphological changes characteristic of dying cells (~90 min post-H_2O_2-treatment). An advantage of the IMS in this experiment is the high-throughput nature, which allows for extended time-lapse imaging (~2.5 hours in this case) with the low excitation intensities needed to minimize photobleaching and photodamage. The IMS system also allows us to observe morphological changes in the cells as apoptosis occurs. In this case, the cells shrink and bleb over time reflecting the gradual loss of membrane architecture (Hacker 2000). Snapshots of the cells in one field before and 90 min after oxidative challenge with H_2O_2 show apoptotic cell shrinking and a 85.7% decrease in the Caspase-3 sensor FRET ratio, shown in Figure 4-11.

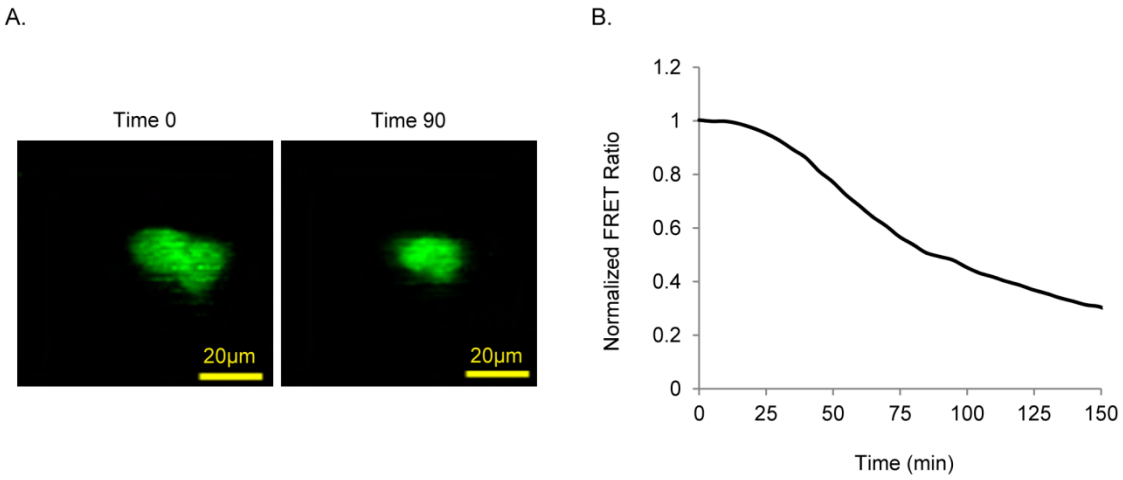

Figure 4-11: Apoptotic dynamics and morphology in βTC3 cells. (A) Snapshots at the onset of imaging and 90 minutes after H_2O_2 treatment where cell shrinkage becomes noticeable. (B) Timecourse of FRET loss as Caspase-3 is activated by oxidative stress.

Next, to study the relationship between $[Ca^{2+}]_i$ and caspase-3 activation, we labeled the βTC3 cells expressing SCAT3.1 with the Ca^{2+} indicator dye Fluo4. Using multiple biosensors allows us to measure changes in $[Ca^{2+}]_i$ and caspase-3 activation as a result of oxidative challenge to βTC3 cells induced by H_2O_2. Upon oxidative stress, our data indicate negligible Ca^{2+} pulses, despite the high glucose levels used in these experiments. Interestingly, 150 min after the addition of H_2O_2, we observed a ~ 3.6 % increase of Fluo4 fluorescence in the first 50 min followed by a ~ 5.4 % decrease over the remainder of the experiment, consistent with previous reports that show a calcium-mediated apoptosis signal *in vivo* (Zhang, Zhang et al. 2000). Simultaneously, we observed the characteristic decrease in the FRET ratio that indicates activation of Caspase-3 and cleavage of the biosensor, as shown in Figure 4-12. The average change in FRET observed was 62% for three co-transfected cells in the field of view in 150 minutes. Plotting the time variant for caspase-3 activation and $[Ca^{2+}]_I$, we observe a Pearson correlation coefficient of 0.095, indicating very little correlation between oxidative stress induced activation of caspase-3 and the changes in $[Ca^{2+}]_i$.

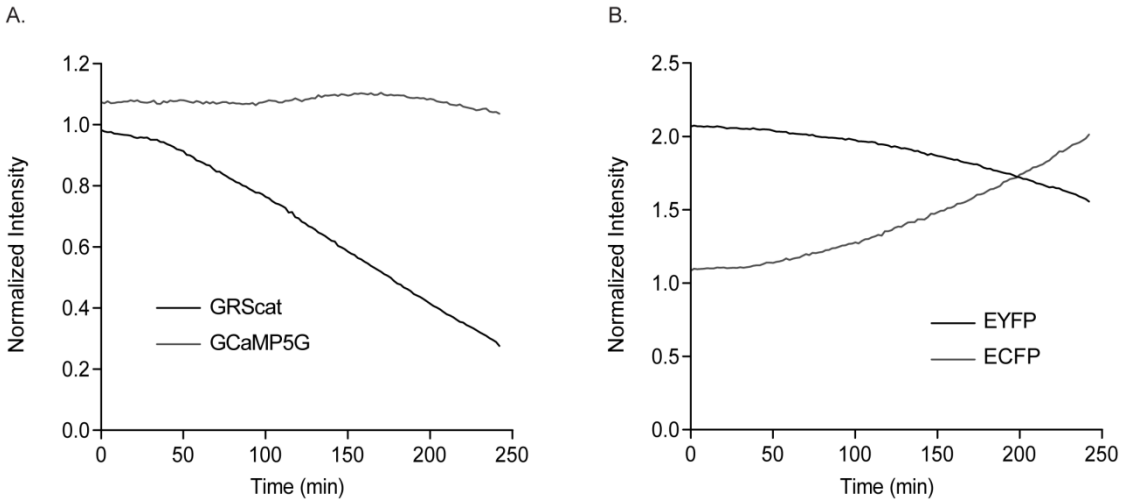

Figure 4-12: Caspase-3 and $[Ca^{2+}]_i$ dynamics upon oxidative challenge. (A) Timecourse of FRET loss (orange) and $[Ca^{2+}]_i$ (green) as Caspase-3 is activated by oxidative stress. (B) Time-resolved components of the T-Epac-VV cAMP sensor from (A).

Hyperspectral Dual-FRET for screening cAMP dynamics and apoptosis in β-cells

Since we had demonstrated the ability to unmix the cyan, green, and yellow FPs, the experiments performed above using a green $[Ca^{2+}]_i$ indicator and cyan/yellow FRET pair were not technically challenging for the IMS. However, the question of correlating cAMP with caspase-3 activation could not be done with just three colors, as there isn't a unimolecular FP-based sensor for either molecule. Additionally, the majority of FRET-based biosensors are composed of a cyan fluorescent protein variant donor and a yellow fluorescent protein variant acceptor and the ^{T}-Epac-^{VV} FRET-based cAMP biosensor and the caspase-3 cleavable FRET sensors we utilized previously both fall into this category.

While there are a few green/red FRET pairs, dual-FRET is rarely attempted due to the overlapping emission spectra of all four fluorophores and challenges in configuring a single excitation with a snapshot modality, required for simultaneous imaging. Since the IMS is ideally suited for this experiment in terms of excitation and data collection, we designed a green/red caspase-3 cleavable biosensor (easier to prepare) to be used with the traditional cyan/yellow

cAMP sensor to measure simultaneously caspase-3 activation and cAMP activity in the MIN6 β-cells. This biosensor is composed of the two best and brightest FPs in this part of the spectrum, mClover and mRuby2, which were recently characterized as a very strong FRET pair (Lam, St-Pierre et al. 2012). To test the unmixing capability of the IMS with both biosensors, we transiently transfected cells with single fluorophores to collect reference spectra or both FRET sensors. The unmixed components from one cell in a single field of view are shown in Figure 4-13. These are raw data so that the relative differences in intensities for the individual FPs can be appreciated. Ultimately, the readouts from these experiments are the ratios of acceptor/donor as with the FRET sensors utilized described in the above studies.

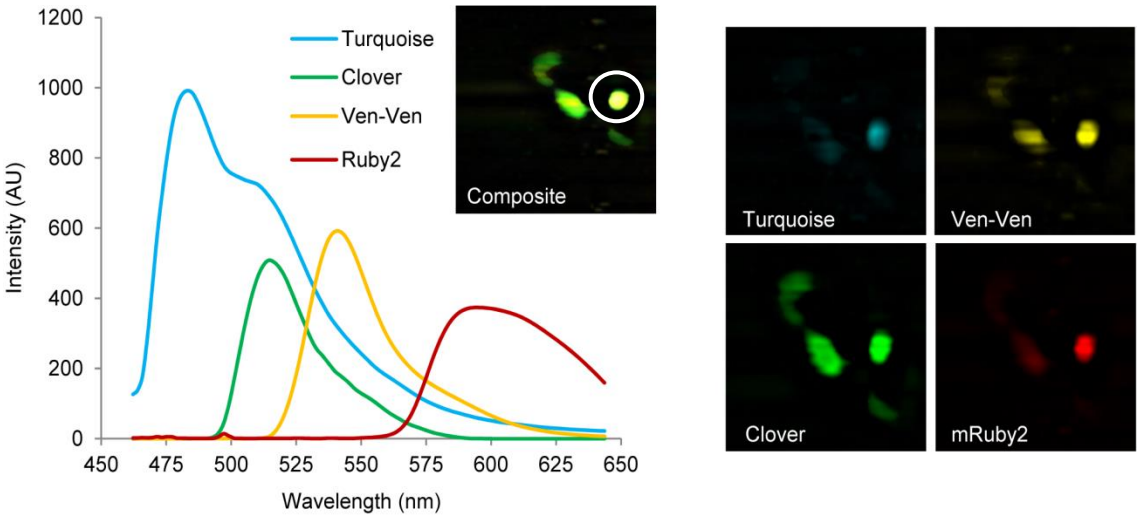

Figure 4-13: Unmixed component spectra of a single cell expressing ^{T}-Epac-^{VV} and GRScat. Raw intensities for the unmixed components of the FRET sensors from the circled cell are shown (left) with the RGB images of the same FOV (right).

We next needed to ensure that we could isolate the individual biosensor functions to confirm that the spectra are being correctly unmixed and interpreted. Thus, we treated co-transfected MIN6 cells with either IBMX/forskolin, which we have shown stimulates the ^{T}-Epac-

^{VV} cAMP sensor (Figure 4-8), but should not activate caspase-3. Indeed, IBMX/forskolin treatment elicited a 1.14 ± 0.03 increase in the T-Epac-VV FRET ratio in 30 minutes with no significant change in the GRScat FRET ratio even out to 60 minutes. Additionally, the fungal toxin staurosporine (STS), which has been shown to directly and quickly activate caspase-3 (Rizzo and Piston 2005), was used to isolate the GRScat sensor. We observed a 1.88 ± 0.4 fold decrease in the GRScat FRET ratio, indicating a significant activation of caspase-3 in 30 minutes following STS treatment with no significant change in cAMP as indicated by the FRET ratio of the ^{T}-Epac-^{VV} sensor over a 60 minute timecourse. These data are displayed in Figure 4-14.

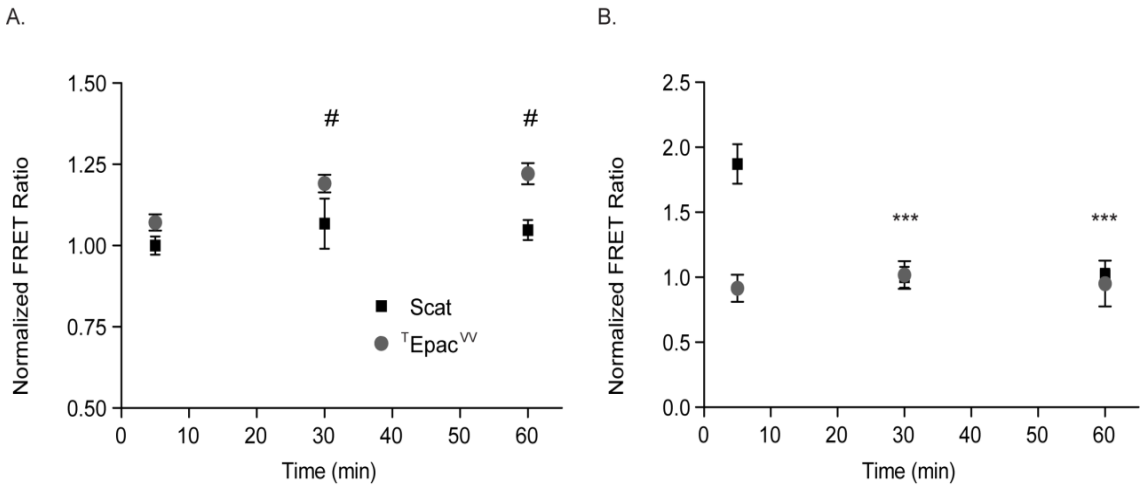

Figure 4-14: Dual-FRET biosensor isolation by selective stimulation. Timecourse of caspase-3 activation (orange) and cAMP (blue) after stimulation with (A) IBMX/forskolin or (B) STS. p values were determined by one way ANOVA. *** indicates $p < 0.0001$ compared to caspase-3 time 0. # indicates $p < 0.05$ compared to cAMP time 0.

To address the relationship between the dynamics of the two sensors, the same experimental paradigm of H_2O_2-induced apoptosis was used. It should be noted here that two different IMSs were used for these experiments and while the calibration procedures are the same, the hardware is different, which likely accounts for some of the statistical variance in our

findings. We are still processing and analyzing the data from these experiments so the statistics, as reported here, are preliminary.

Oxidative stress was induced after culturing the cells for 36-72 hours post-transfection with high glucose (11 mM). Then, on the day of experiments, the cells were incubated for several hours with a supra-physiological (20 mM) glucose concentration to simulate glucotoxicity, or a sub-stimulatory 5 mM glucose level prior to the addition of H_2O_2. Since we characterized the slow time to onset of caspase-3 activation in previous experiments, we pre-treated cells with H_2O_2 for 15 minutes before commencing imaging to improve the efficiency of the experimental setup. In long-term imaging experiments, we find that the cells pre-treated with 20 mM glucose displayed a significant increase in cAMP and caspase-3 activity by 45 minutes after treatment with H_2O_2 (30 minutes after start of imaging), as indicated by the loss of FRET from both biosensors. The cells that were pretreated with low glucose exhibited no significant difference in caspase-3 or cAMP for the same duration of oxidative stress, as displayed in Figure 4-15. These data demonstrate a strong correlation, as determined by a Pearson correlation (0.999). By contrast, the Pearson coefficient for caspase-3 and cAMP FRET is 0.142 at 5 mM glucose, suggesting that the relationship between cellular apoptosis and cAMP elevation is glucose-dependent under conditions of oxidative damage.

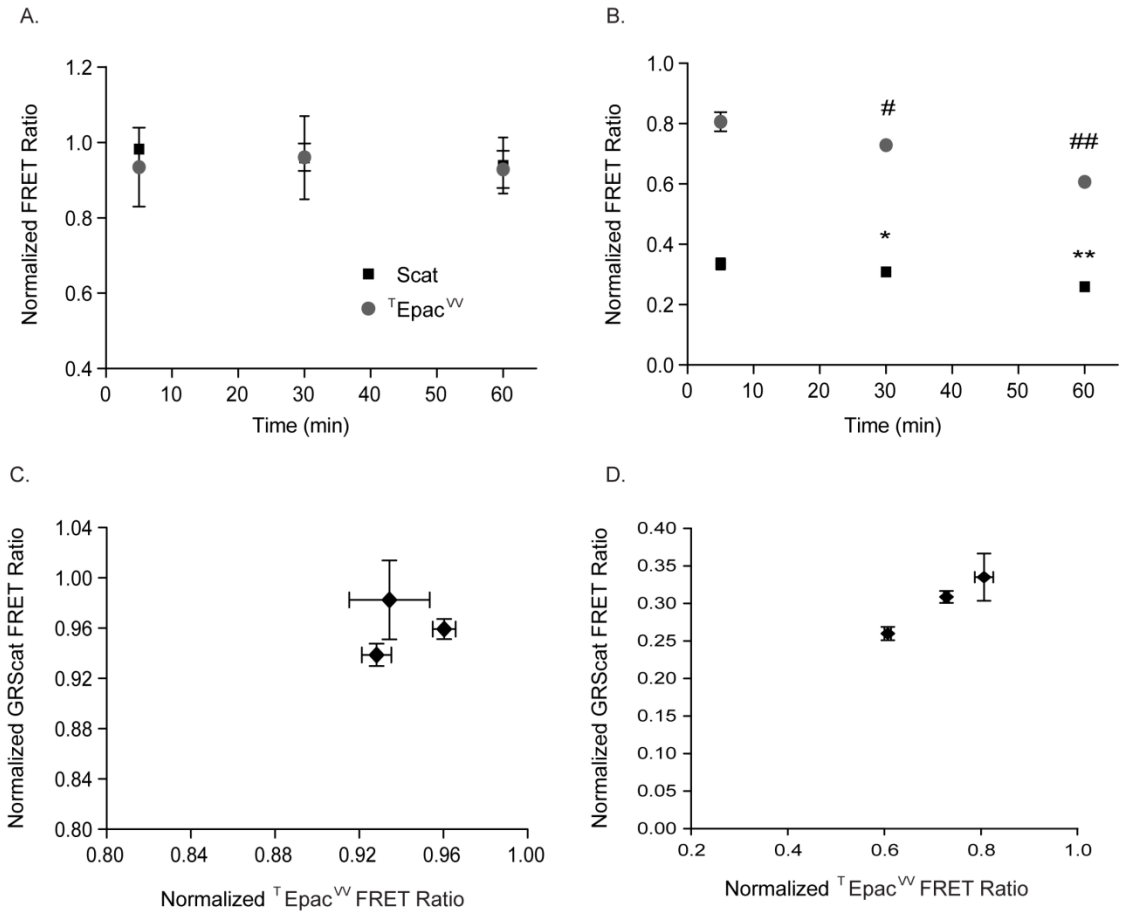

Figure 4-15: Role of glucose in caspase-3 activation and cAMP generation under acute oxidative stress. (A) Co-transfected cells were treated with 5 mM glucose prior to the addition of H2O2. (B) As in (A) but with 20 mM glucose pre-treatment. These data represent averages from cells in 3 different dishes, with each dish having N=4-10 cells. (C) Correlation plot of data in (A). (D) Correlation plot of data in (B). p values were determined by one way ANOVA. * indicates *** $p < 0.0001$ compared to caspase-3 time 0. # indicates $p < 0.05$ compared to cAMP time 0.

Additionally, the baseline FRET ratio for caspase-3 after 15 minute pre-treatment with H_2O_2 and 20 mM glucose was significantly lower than the ratio at the same time point in cells pretreated with 5 mM glucose and H_2O_2. Together, these data suggest that a high glucose environment is highly toxic to β-cells under oxidative stress and the elevation of cAMP with glucose does not appear to have an intrinsic protective effect. However, since these data were collected in β-cell lines, the possibility of cAMP modulators secreted from neighboring islet cells

under the same stress conditions is not addressed. Ideally, these experiments would be repeated in whole islets to observe whether or not the islet context is important for the cellular response to oxidative damage.

Finally, we wanted to repeat the oxidative stress induction paradigm in cells co-transfected with the ^{T}-Epac-^{VV} biosensor and the GCaMP5G $[Ca^{2+}]_i$ sensor to characterize the changes in the relationship between these two signaling molecules under the oxidative conditions that led to apoptosis in the earlier experiments. Having established that within 30 minutes of imaging with a 15 minute incubation period with H_2O_2, caspase-3 activity is significant, we chose to more closely look at the cAMP and Ca^{2+} dynamics leading up to this change. To address this, cells were imaged over ~15 minutes at two different frame rates – 1 frame every 2 minutes, or 1 frame every 5 seconds in an effort to characterize any faster events that may occur. Looking at the slower imaging data, we observe similar anti-correlation in oscillations that was noted in our early experiments with high glucose and TEA, as shown in Figure 4-16.

Interestingly, whereas glucose produced anti-correlated oscillations in $[Ca^{2+}]_i$ and cAMP with Ca^{2+} spikes having a larger amplitude (Figure 4-5), pretreatment with H_2O_2 significantly increased the amplitude of cAMP spikes and reduced the correlation coefficient to -0.106, a significant decrease. The low amplitude $[Ca^{2+}]_i$ oscillations are consistent with our previous data suggesting a blunted response to glucose in Ca^{2+} pulses during oxidative challenge. These data suggest that oxidative stress may decouple Ca^{2+} signaling from glucose and induce changes the crosstalk between these critical signaling pathways ahead of caspase-3 activation. Additionally, it highlights the importance of fast frame rates in multimodal imaging, as the relationship between $[Ca^{2+}]_i$ and cAMP is less obvious with intermittent imaging and may have important implications for studying the molecular processes leading up to mitochondria-mediated apoptosis in β-cells during glucotoxic conditions like chronic hyperglycemia.

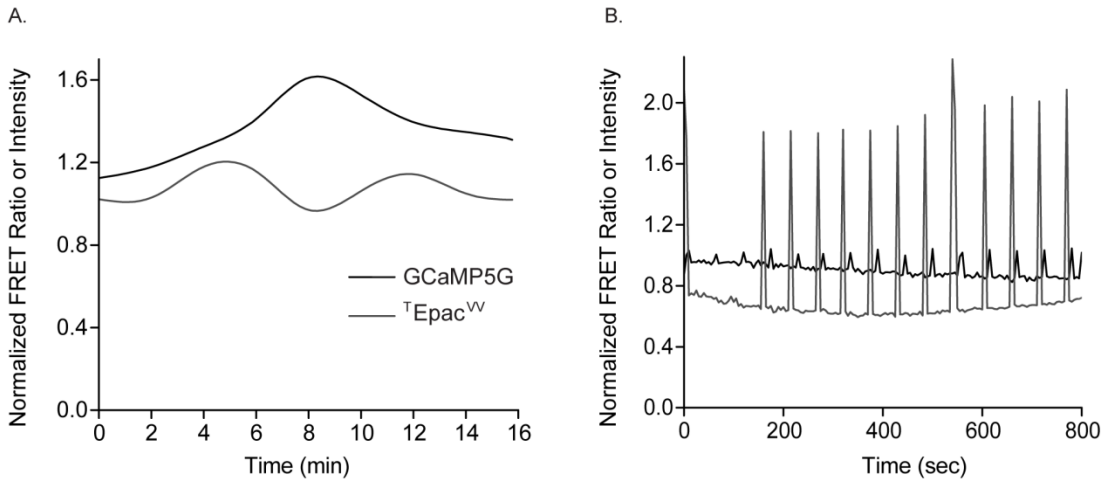

Figure 4-16: Effect of H_2O_2 on $[Ca^{2+}]_i$ and cAMP activity in β-cells at high glucose. (A) $[Ca^{2+}]_i$ (black) and cAMP (gray) activity average in 3 dishes after pre-incubation with H_2O_2 and stimulation with 20 mM glucose, collected one frame every 2 minutes with a 0.5 s integration time. (B) As in (A) but collected once every 5 seconds with a 0.5 s integration time.

Summary

We utilized time-resolved image mapping spectrometry for real-time hyperspectral imaging of pancreatic β-cell dynamics, and successfully monitored $[Ca^{2+}]_i$ and cAMP activity during glucose stimulation (Elliott, Gao et al. 2012). The interplay between these two dynamic signaling pathways has been difficult to determine due to the spatially and spectrally overlapping sensors available to study them in living cells. This is a common hurdle as the overlapping emission spectra of many biosensors prevent the real-time study of signaling dynamics from multiple pathways. A previous study assaying the relationship of $[Ca^{2+}]_i$ and cAMP in live cells using spinning disc confocal microscopy suffered from the inability to collect data with a single hardware configuration (Landa, Harbeck et al. 2005). While the fluorophores used in that study (Fura2 for $[Ca^{2+}]_i$ and Epac1-camps) are spectrally separated with excitation and emission, they are both ratiometric, with Fura2 requiring dual-excitation and Epac1-camps reported as a ratio of emissions. Thus, at least three images were acquired at each time point

(two for Fura2 and one for Epac1) with needed configuration switching between each one, leading to a total acquisition time of a couple of seconds. Our results demonstrate the ability of the IMS approach to address the collection of two biosensors in a snapshot format that is truly simultaneous. This is particularly critical for biological questions that probe temporal relationships and have spectrally overlapping biosensors.

Many questions remain about stimulus-secretion coupling in pancreatic β-cells, especially regarding the role of intracellular second messengers in maintaining proper cell health and function. Significant progress in elucidating these roles in β-cell function will be possible with the simultaneous monitoring provided by the IMS system. Since the 4-D (*x, y, λ, t*) datacube is captured in a single snapshot, there is no compromise between system throughput and image acquisition rate. Thus, high dynamic range images are captured in real-time imaging experiments, and provide reliable measurements of spectrally overlapped biosensors. While in this study we utilized FRET and cpGFP-based sensors, there are many spatially and spectrally overlapping sensors available for studying dynamic processes. The IMS approach allows simultaneous measurement in real cells of these dynamics, and thus can assist in identifying relationships between multiple cellular processes as well as individual molecular events.

Among the remaining questions in β-cell function is the role of $[Ca^{2+}]_i$ and cAMP signaling during oxidative stress. Since the β-cells do not express high levels of scavenging enzymes for reactive oxygen species, oxidative damage is particularly deleterious and has been hypothesized to be a sizeable contributor to β-cell dysfunction and death during glucotoxicity and diabetes (Robertson, Harmon et al. 2003; Donath, Ehses et al. 2005). Additionally, mitochondria mediated apoptosis, which proceeds from DNA damage initiating Bax and Bak activation to the caspase cascade, which consists of a series of enzyme cleavages culminating in formation of an apoptosome and death. In addition to these molecular markers of apoptosis, there are morphological changes including cytosolic shrinking, chromatin condensation, and membrane blebbing that characterize this process (van de Schepop, de Jong et al. 1996).

In many cell types, oxidative stress has been show to contribute to apoptotic cell death, but the molecular mechanism is less well understood. It has been shown that treatment of β-cells with hydrogen peroxide to induce oxidative damage increases apoptosis. However, pre-incubation with forskolin, a cAMP activator, protected against cell death. These experiments were conducted using traditional biochemistry, which provides only a single snapshot (via Western blot) of a dynamic process [3]. We utilized our microscope-coupled IMS system to study oxidative-stress induced caspase-3 activation in the presence of H_2O_2. Using a green/red caspase-3 cleavable FRET sensor simultaneously with either a unimolecular $[Ca^{2+}]_I$ biosensor (three colors) or a cyan/yellow FRET biosensor in a dual-FRET configuration, we successfully monitored the $[Ca^{2+}]_i$ and caspase-3 activities during cellular apoptosis. The results presented here demonstrate the ability of the IMS approach to address complex biological questions with high sensitivity, spectral resolution, and temporal resolution.

The acquisition rate of our current IMS system is up to 7.2 fps, which is limited by the CCD camera data transfer rate. If acquisition speed was not a limiting issue, these experiments could be done on any spectral imaging device, including the Zeiss LSM710, which provides a spectral resolution to 3.2 nm. However, upon performing the experiments on the LSM710 (data not shown), we found that for spectral resolution comparable to the IMS, the acquisition speeds of >10 sec was insufficient for drawing conclusions about the temporal relationships between the cAMP and $[Ca^{2+}]_i$ signaling pathways. Subtle changes in either cAMP or $[Ca^{2+}]_i$ with pharmacological modulation require high temporal resolution to identify changes in oscillation frequency, rise time, and the effect these changes have on the relationship between pathways in both healthy and stressed cellular conditions.

Part 2

Introduction

Prostate cancer is the second leading cause of death in men in the U.S. and roughly 200,000 men were diagnosed in 2010. The role of hormones, including testosterone and estrogen, in the development of cancer within these healthy tissues is well recognized. Androgen receptor (AR) signaling has important roles in the development and maintenance of the male reproductive system and underlies the pathology of androgen-dependent prostate cancer. There are two primary courses of treatment for prostate cancer: castration and anti-androgen therapies. Both of these measures nearly always lead to castrate-resistant prostate cancer (CRPCa), which is a lethal condition. Current research in the development of novel treatments is focused on identifying small molecules that limits AR translocation to the nucleus, which prevents the dysregulated transcription of genes that underlies CRPCa.

However, the AR requires other transcription factors that work in combination to drive tissue-specific gene expression in the prostate (Gierer 1974; Matusik, Jin et al. 2008). The Forkhead box A 1 (FOXA1) gene has been previously identified as an AR interacting protein (Gao, Zhang et al. 2003; Gao, Ishii et al. 2005), and was shown to be essential for the expression of AR regulated, prostate specific genes (see review (DeGraff, Yu et al. 2008)). FOXA1 increases transcription factor accessibility to the DNA by displacing linker histones from nucleosomes so that the chromatin can unfold (Cirillo, Lin et al. 2002).

Since the identity of additional FOXA1 binding partners required for prostate-specific expression remains unknown, we set out to identify new FOXA1 binding partners important for this process. Briefly, NFIx was one of sixteen proteins identified by tandem affinity purification and mass spectrometry to interact with FOXA1. The NFI family of TF contains four genes (NFIA, NFIB, NFIC, NFIX), encoding proteins which bind to the consensus DNA sequence

TTGGCN5GCCAA (Murtagh, Martin et al. 2003). Further, NFI family members can form either homodimers or heterodimers with each other. FOXA1 was previously identified to interact with a member of the NFI transcription factor family (Norquay, Yang et al. 2006). While the identity of the NFI family member(s) capable of interacting with FOXA1 was not determined, this observation still has important implications for tissue-specific gene expression. Knockout studies of individual NFI genes in mice revealed a variety of phenotypes, including corpus callosum agenesis (NFIA) (Wong, Schulze et al. 2007), lung hypoplasia (NFIB) (Grunder, Ebel et al. 2002), tooth defects (NFIC) (Steele-Perkins, Butz et al. 2003), and neurological and skeletal defects (NFIX) (Driller, Pagenstecher et al. 2007; Campbell, Piper et al. 2008). Thus, each NFI family member has non-redundant roles during development.

In the following work, we set out to identify if NFIx interacts with FOXA1, and determine the role of this transcription factor in complex formation with AR using Förster resonance energy transfer (FRET). FRET is a phenomenon useful for studying protein-protein interactions, which is facilitated by tagging the proteins of interest with fluorescent proteins (FP-FRET) as reporters (Piston and Kremers 2007). Since FRET occurs only when the FPs are within 10 nm, it is commonly used to indicate the proximity of proteins of interest. Here, we developed FRET constructs for FOXA1, NFIx, and the AR to determine if these proteins are in close enough proximity to suggest complex formation. These data would support a number of other studies and provide a useful screening system for other AR coregulators and interacting proteins both in healthy and diseased tissues.

Materials and Methods

FRET construct development

The AR construct was created by amplifying the gene encoding AR with the following primers (Forward – AAAGCTAGCGCCACCATGGAAGTGCAGTTAGGGC; Reverse –

AAAACCGGTCCACGCGTCTGGGTGTGGAAA) and sequential digestion/ligation of the product and mCerulean3-C1 vector using NheI and AgeI restriction enzymes. NFIX was created similarly with primers (Forward – AAAAGATCTATGTATAGCCCGTACTGCCTCACC; Reverse – AAAGGTACCTTCAGAAAGTTGCCGTCCC) for the NFIX gene and an mVenus-C1 vector was used with NheI and AgeI restriction enzymes. The FOXA1 construct was created with amplifying primers (Forward – AAAGCTAGCGCCACCATGTTAGGAACTGTGAAG; Reverse – AAAACCGGTCCGGAAGTGTTTAGGACGGG) for FOXA1 and an mVenus-C1 vector using BglII and KpnI restriction enzymes. Sequences of resultant constructs were verified using the Vanderbilt Genome Sciences Sanger DNA Sequencing laboratory. To summarize the constructs, they include a 3'-mCerulean3-AR, 3'-mCerulean3-NFIx, 3'-mVenus-FOXA1, 3'-mVenus-NFIx.

Cellular sample preparation for FRET studies

HeLa cells were transiently transfected with plasmid DNA encoding mCerulean3-tagged AR, mVenus-tagged NFIX and/or mVenus-tagged FOXA1; FRET8 (a dimer of ECFP and EYFP), or mCerulean3 and mVenus were used as controls. Transfection was accomplished using Lipofectamine2000 (Invitrogen, Carlsbad, CA) transfection reagent according to the manufacturer's instructions. Cells were seeded onto No. 1 coverglass bottomed dishes (MatTek, Ashland, MA) and cultured in DMEM medium (Invitrogen/Gibco, Carlsbad, CA) supplemented with 10% fetal bovine serum (Invitrogen/Gibco, Carlsbad, CA), 100 units/ml penicillin (Mediatech, Manassas, VA), and 100 µg/ml streptomycin (Mediatech, Manassas, VA), at 37ºC under 5% humidified CO2. 24 hours after transfection, samples were fixed with 4% paraformaldehyde, washed in DPBS (Invitrogen/Gibco, Carlsbad, CA), and mounted with gelvatol. For samples containing the androgen receptor plasmid, 24 hours after transfection cells were incubated overnight with media containing charcoal-stripped serum and then treated

with dihydrotestosterone (DHT - Sigma. St. Louis, MO) for 4 hours prior to fixing as above.

Fluorescence microscopy

FRET imaging was performed using a Zeiss LSM780 confocal microscope with excitation provided by a Coherent chameleon two-photon laser at 800 nm with emission collected in spectral mode from 465-692 nm with 8.7 nm spectral resolution. Additionally, images were collected with an argon laser at 514 nm to confirm cells expressing the mVenus-tagged constructs. Data were analyzed using ImageJ and Graphpad Prism software. FRET ratios were expressed as mVenus/mCerulean3 after linear unmixing and normalized to the vehicle treated AR + FOXA1 control ratios. 70-100 cells per dish were quantified for mean intensity and the experiments were repeated in three cellular preparations. P values are the result of ANOVA compared to NFIX + AR.

Results

Construction of FRET pairs with FOXA1, NFIx, and AR

To test the hypothesis that FOXA1, NFIx and AR interact to form a complex, we used FP-FRET to interrogate the possibility of protein-protein interactions between them. Constructs of FP tagged AR, FOXA1 and NFIx were engineered using mVenus (mVen) and mCerulean3 (mCer3) as the acceptor and donor FPs, respectively. This FP-FRET pair has been well characterized and is robust for quantifying protein-protein interactions (Rizzo, Springer et al. 2006). To confirm that tagging the AR did not impair its function, we serum-starved transiently transfected cells to remove the nuclear AR and then treated them with the androgen dihydrotestosterone (DHT), which induces nuclear translocation of the AR. In parallel, we used the same procedure without the DHT, as a vehicle control to demonstrate a primarily cytosolic pool of tagged AR-

mCer3. As shown in Figure 4-17, DHT treatment did cause nuclear localization of the AR-mCer3 whereas the vehicle control did not, confirming the translocation function of the tagged AR.

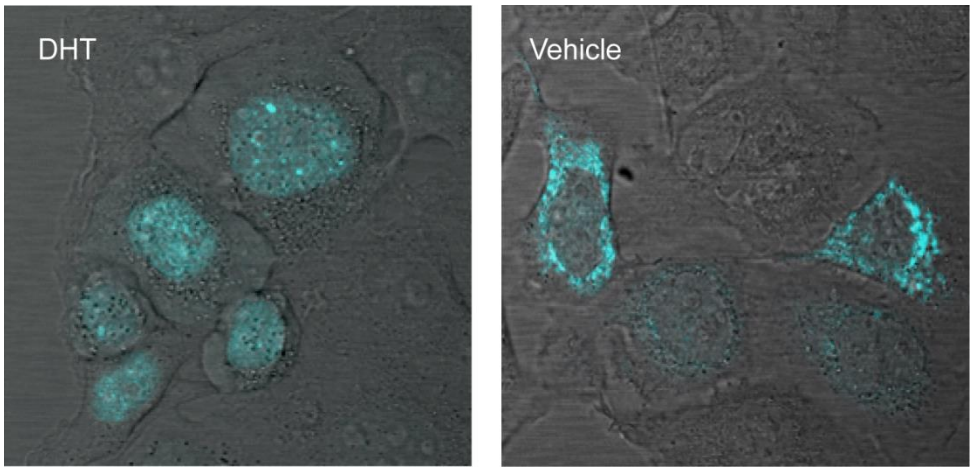

Figure 4-17: Localization of AR-mCer3 with and without androgen stimulation. Confocal microscopy images of transfected AR-mCer3 after serum starvation and treatment with DHT (left) or without DHT (right).

The FOXA1 and NFIx transcription factors were tagged with mVen as the acceptor constructs, which gave inducible control over the FRET due to DHT translocation of the donor. FOXA1 and NFIx are primarily expressed in the nucleus and also show appropriate localization, with little to no cytosolic background expression, as shown in Figure 4-18.

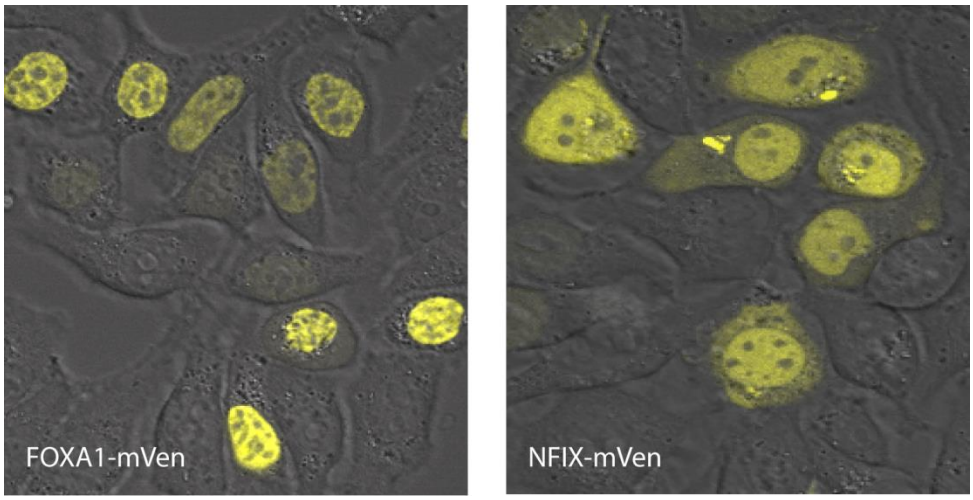

Figure 4-18: Localization of FOXA1-mVen and NFIx-mVen. Confocal microscopy images of transfected plasmids for FOXA1-mVen (left) or NFIx-mVen (right).

NFIX interacts with FOXA1 and AR only in the presence of FOXA1

In addition to the FRET constructs we prepared, each experiment was done in parallel with co-transfected mCer3 and mVen, as well as a tandem dimer of this pair, as negative and positive controls, respectively. These controls also set our baselines for maximal (1.05 ± 0.07) and minimal (0.06 ± 0.01) normalized FRET ratios for the microscope settings that were used. The next test for functionality of the FRET pairs was to look at the AR-mCer3 with DHT treatment and FOXA1-mVen, since that interaction is well characterized by several methods. Consistent with our previous reports of AR and FOXA1 interaction (Gao, Zhang et al. 2003; Gao, Ishii et al. 2005), the FRET ratio for AR-mCer3 and FOXA1-mVen was 0.93 ± 0.052 compared to vehicle controls in HeLa cells.

Our next experiment was to identify if the AR-mCer3 and NFIx-mVen FRET pairs would be close enough to interact directly. We have previously shown that these transcription factors bind the probasin promoter adjacent to each other and immunoprecipitation studies suggest an interaction. The AR-mCer3 and NFIx-mVen FRET ratio of 0.23 ± 0.021 was significantly lower,

suggesting that these two proteins are further away from each other than the AR and FOXA1. These data are presented in Figure 4-19 below along with the negative and positive controls.

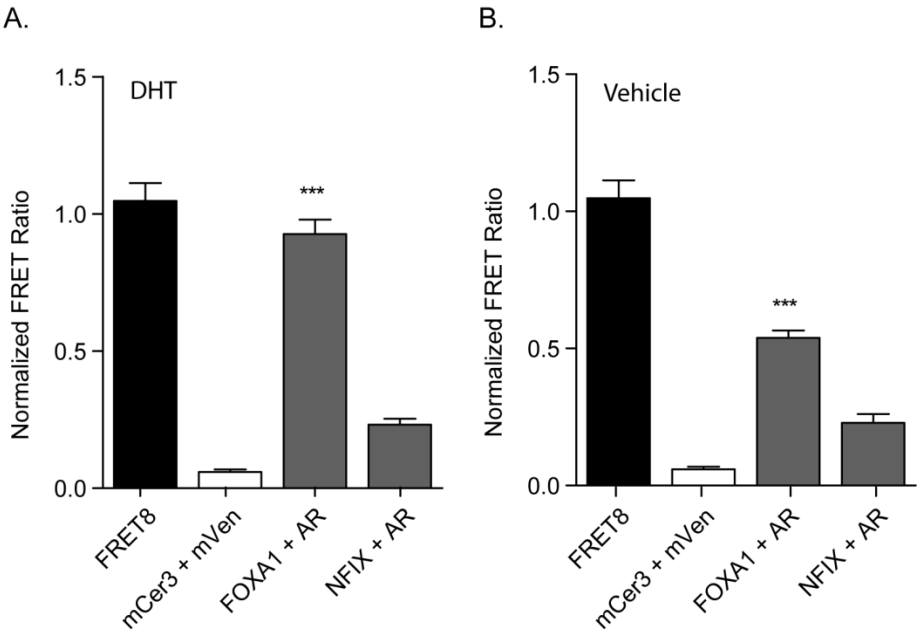

Figure 4-19: AR with FOXA1, but not AR with NFIx, exhibits a high FRET ratio. (A-B) Quantification of FRET ratios for three independent transfections treated with DHT (A) or left untreated (B). Error bars represent the S.E.M. and p values were determined by ANOVA, ** indicates $p < 0.001$ compared with NFIX + AR.

The results of the previous two experiments demonstrate that the AR and NFIx may require another factor to form a complex. Since the AR and NFI proteins are known to form dimers, it is significant that with two potential donors and acceptors on the same promoter region, the FRET ratio was so low. This also supports the possibility of another protein either preventing their interaction or facilitating it. We hypothesized that this factor would be the FOXA1 that we already knew to interact with the AR. To test this idea, we first sought determine whether NFIX and FOXA1 are close enough to interact directly, having already shown that they both localize predominantly to the nucleus. Thus, we created another donor construct, by tagging FOXA1 with mCer3. Upon co-transfection, these proteins exhibited

nuclear localization and a FRET ratio of 0.59 ± 0.026, which was significantly higher than the negative control but not as strong a pairing as the AR and FOXA1. Importantly, when we performed this experiment with NFIx-mCer3 as the donor and FOXA1-mVen as the acceptor, the FRET ratio was comparable to the negative control, as shown in Figure 4-20. This demonstrates that the folding and orientation of the proteins with FP tags is critical for FRET to occur.

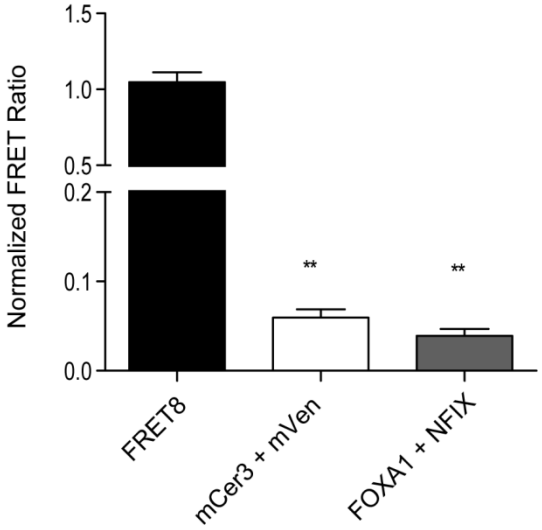

Figure 4-20. NFIx and FOXA1 FRET is dependent on tagged terminus. Normalized FRET ratios for positive (FRET8) and negative (mCer3 + mVen) controls and FoxA1 + NFIX. Error bars represent the S.E.M. and p values were determined by Student's T-test, ** indicates $p < 0.01$ compared with FRET8.

Finally, to test the idea that over-expressing FOXA1 could bridge the interaction between NFIX and AR, we co-transfected cells with AR-mCer3 and NFIX-mVen as before, along with untagged FOXA1. After treatment with DHT, the FRET ratio of AR-mCer3 and NFIX-mVen was increased to 0.53 ± 0.058, a level intermediate between the FOXA1/AR and NFIX/AR pairs, as depicted in Figure 4-21.

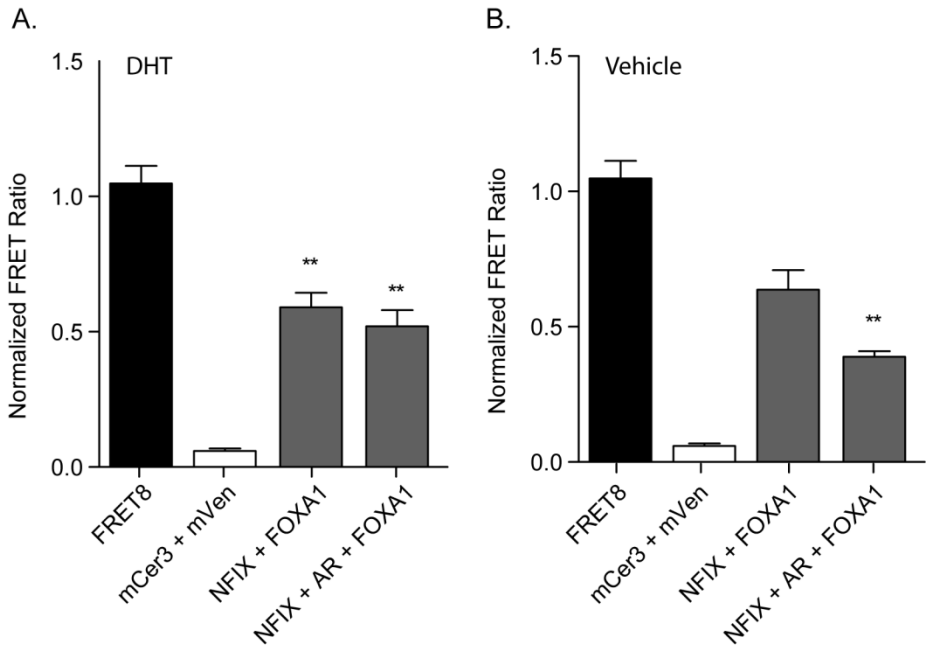

Figure 4-21: FOXA1 increases the FRET ratio of AR and NFIx. (A-B) Quantification of FRET ratios for three independent transfections treated with DHT (A) or left untreated (B). Error bars represent the S.E.M. and p values were determined by ANOVA, ** indicates $p < 0.01$ compared with NFIX + AR.

Summary

Several AR coregulators have been identified that both control and fine tune AR activity, and previous work reported that FOXA1 interacts with AR to control multiple prostate specific genes (Gao, Zhang et al. 2003) and that FOXA1 expression is restricted to prostatic epithelium (Mirosevich, Gao et al. 2006). Also, rescuing prostate tissue from FOXA1 knockout mice exhibit an arrested organ development phenotype, demonstrating a global role for FOXA1 to regulate organ development (Gao, Ishii et al. 2005). Much like FOXA proteins, NFI proteins are well known for their ability to regulate the activity of endocrine responsive cis elements, such as the murine mammary tumor virus (MMTV) and the PEPCK promoter (Li, Margueron et al. 2010; Archer, Lefebvre et al. 1992; Aoyagi and Archer 2008). Furthermore, NFI activity is required to regulate expression of mammary gland specific differentiation markers, including whey acidic protein (WAP) and α-lactalbumin, among others (Murtagh, Martin et al. 2003) as well as

estrogen and androgen regulated genes (Carroll, Liu et al. 2005; Wang, Li et al. 2007; Lupien, Eeckhoute et al. 2008). The frequent occurrence of NFI sites adjacent of AR and FOXA1 sites in multiple genes (Jia, Berman et al. 2008; Sharma, Massie et al. 2013) suggest that the NFI family is a central TF for androgen-regulated genes.

FP-FRET was used to test the prediction that AR/FOXA1/NFIX are in close contact, which supports a potential direct interaction and formation of a stable complex. The high FRET ratios shown by AR and FOXA1 were dependent on pre-treatment of the cells with DHT to drive AR into the nucleus. While AR and NFIX did not exhibit a significant FRET ratio compared to negative controls, the additional transfection of an untagged FOXA1 significantly increased this ratio. Additionally, the strong FRET ratio of FOXA1 and NFIX supports the hypothesis that FOXA1 mediates the formation of a complex with AR and NFIX.

It is also consistent with extensive data showing that these two proteins do interact and are frequently associated with each other on AR target genes in the prostate (Gao, Zhang et al. 2003; Jia, Berman et al. 2008; Lupien, Eeckhoute et al. 2008; Sharma, Massie et al. 2013) and in breast (Carroll, Meyer et al. 2006; Eeckhoute, Carroll et al. 2006; Ross-Innes, Stark et al. 2012). We anticipate that this paradigm of NFI being involved in the AR/FOXA1 complex will extend to ER/FOXA1 complexes. Finally, the recent *in vivo* ChIP-Seq report on castrate resistant prostate cancer patient samples shows both a progression of the AR to new target genes but also it demonstrates that that many common sites still involve the AR/FOXA1/NFI motifs. Taken together, these data show that different NFI isoforms will play an important role in AR action in different cell types, and during tumor development and progression. In summary, specific NFIx interacts with FOXA1, binds to androgen responsive elements and facilitates AR-mediated gene transcription, implicating this complex as a potent controller of androgen responsive, prostate-specific gene expression.

CHAPTER 5

CONCLUSIONS AND FUTURE DIRECTIONS

Concluding remarks

The goals of the work described above were to identify the paracrine mechanisms involved in suppressing glucagon secretion and develop a spectral imaging technique for monitoring multiple dynamic molecular processes in live cells. These projects are unified by the importance of second messenger signaling and crosstalk in islet hormone regulation. The fact that intracellular signaling mechanisms differ between α- and β-cells has profound implications for the etiology of metabolic disease and highlights the importance of developing sophisticated tools to tease apart the highly complex environment that constitutes the pancreatic islets.

There are significant challenges to multi-label imaging, as islet biology is complex and there are many molecular events whose roles in islet function remain unclear. Thus, monitoring simultaneously multiple events will help shed light on the interactions between these molecules and may provide insight as to their normal and disease-state functions. Additionally, the development of robust biosensors for critical molecules such as cAMP, $[Ca^{2+}]_I$ will also provide a significant advantage in characterizing these events. Cell type-specific genetic labeling is another important tool in identifying a given cell type within the islet and comparing it with the other neighboring cells. We have taken advantage of this technology in the use of a mouse with tdRFP-labeled α-cells in the work described here (Soriano 1999; Luche, Weber et al. 2007). Eventually, the confluence of these tools and unanswered questions may lead to the generation of robust working models for islet regulation that provide predictive power in evaluating novel therapeutics.

Toward the first goal of identifying the paracrine mechanisms responsible for glucose-inhibited glucagon secretion, data was presented demonstrating that somatostatin and insulin converge on the α-cell to decrease the production of cAMP and increase its degradation, by means of their respective receptors, and this behavior is, at least in part, responsible for glucose-inhibited glucagon secretion. Previous experiments in our laboratory had demonstrated a decoupling of $[Ca^{2+}]_I$ and glucagon secretion at inhibitory glucose concentrations (Le Marchand and Piston 2012), which invalidated the prevailing models that rely upon decreasing global Ca^{2+} activity for glucagon inhibition (Xu, Kumar et al. 2006; MacDonald, De Marinis et al. 2007; Tuduri, Filiputti et al. 2008; Zhang, Ramracheya et al. 2013). In pursuit of the molecular mechanism that does regulate glucagon suppression; we considered intracellular signaling molecules other than Ca^{2+} that might be a key player in this regulation. Of the other prevalent signaling messengers, cAMP is known to be differentially regulated between α- and β-cells and this made it a likely candidate for mediating glucose inhibition of glucagon secretion (Mauriege, Klein Kranenbarg et al. 1996; Gromada, Bokvist et al. 1997; Tian, Sandler et al. 2011).

We first tested this hypothesis by maximizing cAMP production and inhibiting its degradation and measuring the effect on glucagon secretion at low and high glucose levels. We found that stimulating cAMP is sufficient to overcome glucagon inhibition at high glucose. We showed that cAMP levels are lower at high glucose in both human and mouse isolated islets. Importantly, this modulation of cAMP and glucagon secretion was not accompanied by a detectable change in $[Ca^{2+}]_I$ activity, suggesting a Ca^{2+}-independent mechanism. Furthermore, cAMP and insulin secretion were both increased by high glucose levels in β-cells of the same islets, which supports previous reports and validates our experimental approach. As an additional control, epinephrine, which is known to selectively stimulate glucagon secretion, increased cAMP in the islet α-cells with no detectable effect on β-cell cAMP levels.

To identify the signal(s) responsible for mediating this decrease in cAMP, we first tested the most obvious candidate – somatostatin, which is long known to be a potent inhibitor of

glucagon secretion (Strowski, Parmar et al. 2000; Cejvan, Coy et al. 2003). We found that antagonizing the somatostatin receptor type 2, SSTR2, caused a loss of glucagon inhibition and increased cAMP levels at high glucose, suggesting that this receptor mediates the observed suppression with glucose alone. Furthermore, somatostatin decreased cAMP levels and glucagon secretion at low glucose in the islets. The fact that SSTR2 is a GPCR raised the possibility that the Gαi and/or the Gβγ dimer were responsible for the observed decrease. To test the hypothesis that the Gαi subunit, known to inhibit adenylyl cyclases, was a critical mediator, we treated islets with the pertussis toxin (PTX) to prevent Gαi signaling (Cawthorn and Chan 1991) and found that somatostatin was incapable of decreasing glucagon secretion after PTX pretreatment. These data demonstrate that somatostatin inhibits cAMP production via SSTR2 Gαi, which leads to a reduction in glucagon secretion.

An early observation in experiments manipulating cAMP levels with IBMX and forskolin was that the phosphodiesterase (PDE) inhibitor IBMX led to an increase in glucagon secretion that surpassed adenylyl cyclase activator forskolin alone. This led to the idea that the PDEs may play a key role in decreasing cAMP leading to inhibition of glucagon secretion. To identify the possible signaling pathways regulating the PDE activity, we turned to the literature and found that in other metabolic tissues such as liver and adipose cells (Beebe, Redmon et al. 1985; Choi, Park et al. 2006; Ahmad, Lindh et al. 2009), insulin signaling decreases cAMP by activating Akt and PDE3B downstream of insulin receptor (IR) activation.

Previous reports in the α-cells confirmed the expression of these insulin-signaling constituents (Kawamori and Kulkarni 2009; Heimann, Jones et al. 2010; Dorrell, Schug et al. 2011; Eizirik, Sammeth et al. 2012) so we pursued this line of enquiry experimentally. We found that phospho-Akt was increased by insulin, consistent with previous findings. Additionally, IR antagonism led to a significant glucose-dependent increase in cAMP and glucagon secretion in human and mouse islets at high glucose. Exogenous insulin applied to islets at low glucose decreased cAMP and glucagon secretion and treatment of islets with the PDE inhibitor IBMX

prevented insulin from driving this decrease in secretion. Furthermore, micromolar levels of exogenous insulin were able to counter islet glucagon stimulation by a hydrolyzable cAMP analog, but did not affect the increased secretion in islets stimulated with a PDE-resistant cAMP analog. Selective inhibition of PDE3B relieved glucagon suppression in a glucose-dependent manner, whereas inhibiting PDE4 stimulated glucagon secretion across glucose levels. Taken together, these data support the hypothesis that insulin, via IR activation of Akt and PDE3B, decreases cAMP and glucagon secretion in islet α-cells.

Downstream of cAMP signaling, we showed that PKA and not Epac, must be inhibited for glucagon suppression. Selectively activating PKA showed a glucose-dependent increase in glucagon secretion at high glucose in both human and mouse islets, while Epac stimulation resulted in a significant increase in secretion at both low and high glucose concentrations. Furthermore, the specific inhibition of PKA rescued glucagon suppression at high glucose levels, even in the presence of forskolin, which stimulates adenylyl cyclases to produce cAMP. By contrast, antagonizing Epac did not significantly impact glucagon secretion at high glucose. Finally, we measured phospho-PKA in the α-cells at low and high glucose and found that it is lower at high glucose levels, just as the cAMP is, suggesting a glucose-dependent decrease in phosphorylation, presumably due to the decrease in cAMP, which is the primary activator.

Importantly, previous work in the laboratory demonstrated that neither insulin nor somatostatin alone was sufficient to inhibit glucagon secretion from a purified population of α-cells (Le Marchand and Piston 2012). Based on the above data in whole islets, we hypothesized that the combination of insulin and somatostatin would suppress cAMP and glucagon secretion at low glucose, which is exactly what we observed in purified α-cells. Additionally, exogenous insulin or somatostatin in whole islets was insufficient to inhibit glucagon secretion in the presence of either receptor antagonist. Furthermore, the combination of both SSTR2 and IR antagonists significantly increased cAMP and glucagon secretion compared to treatment with just one antagonist. These data, together, confirm that neither

insulin nor somatostatin alone is sufficient to decrease cAMP and glucagon secretion and demonstrate that the convergence of these pathways is required. A schematic diagram of the primary findings in this study is presented in Figure 5-1.

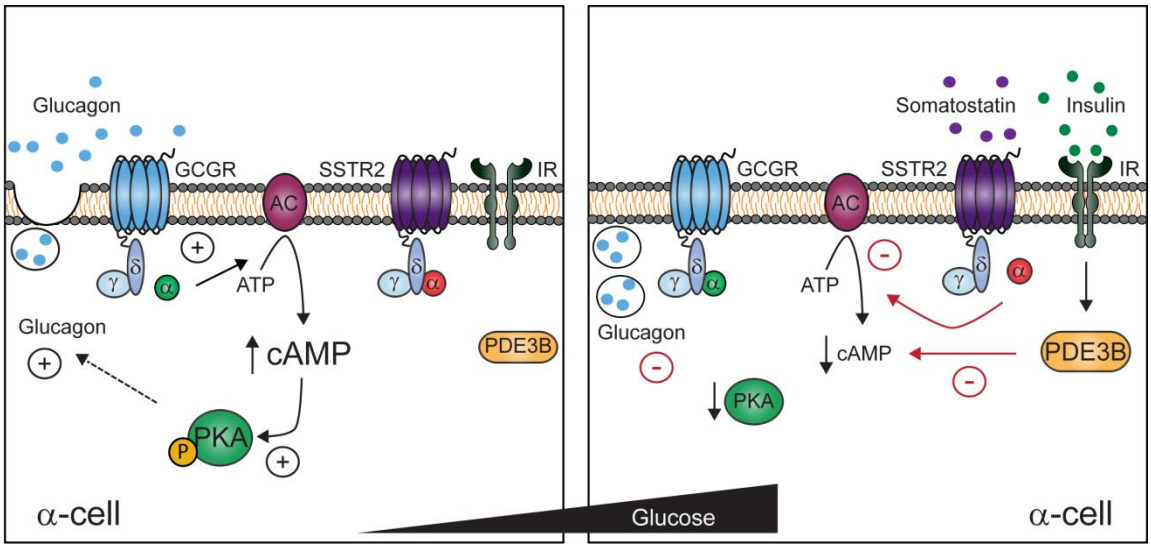

Figure 5-1: Glucagon inhibition via insulin and somatostatin's effects on cAMP/PKA in α-cells at high glucose. Illustration of the stimulatory effect of cAMP via PKA on glucagon secretion from the pancreatic α-cell (left); and the inhibitory roles of insulin and somatostatin in lowering cAMP/PKA signaling at high glucose (right).

Having established the paracrine regulation of glucagon inhibition from the membrane through PKA, we next wanted to identify molecular target(s) being suppressed at the exocytotic level. A wealth of literature exists on the role of Rho-GTPases in remodeling, by depolymerization, the dense network of cortical F-actin in β-cells to allow vesicle fusion with the membrane (Li, Luo et al. 2004; Konstantinova, Nikolova et al. 2007; Veluthakal, Madathilparambil et al. 2009; Asahara, Shibutani et al. 2013; Kalwat, Yoder et al. 2013). The primary enzyme involved in permitting vesicle fusion was identified as Rac1-GTPase in the β-cells. Considering the many similarities between the α- and β-cells, as well as our own data showing that Rac1 is expressed in the α-cells, we expected active Rac1 (GTP-bound) to be

decreased with high glucose. However, we observed the opposite; Rac1-GTP, like $[Ca^{2+}]_I$, increased with increased glucose levels, suggesting that the role it plays in α-cell physiology is distinct from that in β-cells. Additionally, we treated islets with a Rac1 inhibitor (Gao, Dickerson et al. 2004), which locks Rac1 in the GDP-bound inactive state, and observed an increase in glucagon secretion across glucose levels. The roles of the Rho-GTPases, which include Rac1, Rho, and Cdc42, are numerous and vary by cell type (Heasman and Ridley 2008; Schlegel and Waschke 2009; Momboisse, Ory et al. 2010; Baier, Ndoh et al. 2014). However, in most endocrine cells, one or more of these small regulatory proteins is involved in the distal steps of exocytosis. Thus, it is likely that the gate-keeper function in α-cell vesicle fusion is performed by another member of this family, but this question remains unanswered.

While the studies presented in this work primarily rely on static incubations for assaying glucagon secretion, they do help explain some of the dynamics observed in doing perifusion experiments in whole islets. The dynamics of glucagon regulation by glucose concentration have several important features. Firstly, as blood glucose increases to about ~3 mM glucose, there is a reasonably sharp drop in glucagon secretion, which is maximally inhibited at 6-7 mM. While the concentrations here vary in the literature, they are consistent with our model of somatostatin secretion decreasing glucagon secretion followed by insulin secretion driving full inhibition. However, a key point is that maximally inhibited α-cell exocytosis still retains ~40% of peak secretory activity (Le Marchand and Piston 2010). Our data suggest that the equilibrium of cAMP production and degradation is a significant regulatory point in regulated glucagon exocytosis. At high glucose levels, a plethora of signaling molecules is bombarding the islet, many of which are directing the activation of GPCRs and downstream cAMP activity in both the α-cells directly, and in neighboring cells that secrete paracrine factors to modulate α-cell function.

It is tantalizing to speculate then, that in the presence of conflicting stimulatory and inhibitory signals, cAMP is maintained such a level that glucagon secretion cannot be

decreased below the observed maximum. Furthermore, while we have shown that insulin and somatostatin decrease cAMP levels, there are a variety of cAMP generating adenylyl cyclases (AC) expressed in the islets with Gαi-inhibited AC1, Ca^{2+}/calmodulin-inhibited AC6, and Gβγ-stimulated AC2 being enriched in the α-cells (Bramswig, Everett et al. 2013). This highlights the complexity in cAMP regulation in the α-cells and suggests the possibility that even in the presence of both insulin and somatostatin, there are alternative mechanisms for countering stimulating cAMP generation. The fact that different adenylyl cyclases are enriched in β-cells vs α-cells also supports the hypothesis the regulation of cAMP generation and signaling is fundamentally different between the cell types. The same studies demonstrate differences in the enrichment of phosphodiesterases expressed in α- versus β-cells (Bramswig, Everett et al. 2013). Finally, perifusion experiments show that while there is a sharp drop in secretion with increasing glucose levels, as the glucose levels decrease again, the resulting rise in glucagon secretion is quite slow (Le Marchand and Piston 2012). This observation also fits nicely with our data; as the significant decrease in cAMP levels and active PKA would be expected to take longer to regenerate upon a relief of inhibiting signals.

Collectively, we presented data supporting a previously uncharacterized mechanism underlying the glucose inhibition of glucagon secretion from α-cells. We found that somatostatin and insulin in decrease cAMP/PKA signaling to inhibit glucagon secretion independently of global changes in $[Ca^{2+}]_{i,}$ which provides new insight into a controversial problem in islet biology (Gromada, Franklin et al. 2007). Importantly, this mechanism is conserved in human and mouse islets. The model we developed from these data is supported in the literature by reports from three decades ago showing a glucose-dependent cAMP regulation (Jarrousse and Rosselin 1975) and recent studies measuring dynamic differences in cAMP regulation between α- and β-cells (Tian, Sandler et al. 2011). Furthermore, clinical studies in diabetic patients have demonstrated that the combination of insulin and somatostatin has a much higher efficacy for lowering blood glucose in response to high glycemic load than either hormone alone (Gerich,

Lorenzi et al. 1974).

This model of cAMP modulation of glucagon secretion is in sharp contrast to the current theories about the mechanism of glucagon inhibition, which assume that a decrease in $[Ca^{2+}]_i$ is the driving factor (Salehi, Vieira et al. 2006; Vieira, Salehi et al. 2007; Zhang, Ramracheya et al. 2013). A major limitation in models based on ion channel modulation of $[Ca^{2+}]_i$ is the sampling bias imposed on the islets by using a single-cell patch clamping methodology to measure conductance and voltage changes. In these experiments, α-cells are identified in these studies by a characteristic Na^+ channel current (MacDonald, De Marinis et al. 2007), but studies with Na^+ channel blockers have demonstrated that α-cells do not require this current to secrete glucagon (Le Marchand and Piston 2012). The Na+ channels have been shown to be important in glucagon secretion in other studies, so their role is debated. However, there is an increasing appreciation in the field for the heterogeneous nature of islet α-cells (Gromada, Bokvist et al. 1997; Gopel, Kanno et al. 2000; MacDonald, De Marinis et al. 2007), which may explain the different reports. Whereas β-cells generally have identical behavior across an islet, the relatively dispersed α-cells appear to have functional populations, which create another hurdle for single-cell studies. Finally, in spite of increasingly complicated experiments and explanations for the Ca^{2+}-dependent models of glucagon inhibition, looking across whole islets, the average $[Ca^{2+}]_i$ response increases with glucose and purified populations of α-cells behave very much like β-cells in the absence of juxtacrine and paracrine regulators present in the whole-islet context. Thus, a one-size-fits-all explanation of α-cell behaviors is unlikely to prove sufficient.

As evidenced by the complex signaling networks described above, the ability to simultaneously monitor multiple molecular events is necessary for a complete understanding of islet cell function and regulation. While the number of fluorescent biosensors for individual molecules is growing, there are a relatively limited number of fluorescent proteins (FPs) with distinct spectral signatures to utilize as reporters. Furthermore, data collection and analysis of

multiple biosensors requires high spectral, spatial, and temporal resolution. Traditional laser scanning confocal spectral imaging techniques, which provide high spectral and spatial resolution, sacrifice frame rates in scanning the image. Toward the goal of developing a methodology that permits rapid multi-label imaging, we utilized a hyperspectral imaging system (Gao, Kester et al. 2010; Bedard, Hagen et al. 2012) called an image mapping spectrometer (IMS) coupled to a widefield microscope to study the dynamics of $[Ca^{2+}]_I$, cAMP, and caspase-3 activation in cultured β-cells.

The IMS has a unique geometry and optical components that allow for the simultaneous collection of spectral and spatial information per pixel in an image in a single snapshot. This system overcomes many of the limitations in traditional spectral imaging by avoiding a scanning modality, collecting all of the photons in the focal volume, and utilizing a single excitation source. Using the IMS, we measured changes in $[Ca^{2+}]_i$ and cAMP in β-cells in response to stimulation with high glucose and TEA, which decreases the action potential firing frequency allowing measurement of $[Ca^{2+}]_i$ oscillations during each spike. We found oscillations in these two signaling molecules to be anti-correlated, which was predicted by mathematical models but not previously measured simultaneously. Additionally, by using frame rates up to 4 fps and cross-correlation analysis, we were able to show that $[Ca^{2+}]_I$ leads cAMP in response to glucose and TEA by 2.5 seconds. These data were collected with a FRET-based biosensor for cAMP consisting of a mTurquoise donor and tandem cpVenus-Venus acceptor (Klarenbeek, Goedhart et al. 2011), and a circularly-permuted GFP-based biosensor for $[Ca^{2+}]_I$ called GCaMP5G (Akerboom, Chen et al. 2012).

Having established that the IMS was useful for studying multiple signaling events with three overlapping FPs, we next sought to test the system with a dual-FRET experimental design, which requires spectral unmixing of four FPs. For these experiments, we used the same cAMP FRET biosensor as above, along with a caspase-3 cleavable biosensor consisting of either a mClover donor and mRuby2 acceptor, or an ECFP donor and EYFP acceptor. This

biosensor allowed us to study the correlations between cAMP signaling during oxidative stress that lead to caspase-3 activation and apoptosis. Our findings show a strong correlation between the onset of caspase-3 activation, and cAMP activity, but no correlation with $[Ca^{2+}]_i$. We next utilized the same oxidative challenge paradigm to identify any changes in the anti-correlated oscillations in $[Ca^{2+}]_i$ and cAMP that we observed with glucose and TEA. Oxidative stress was found to cause a loss of correlation between the oscillations, greatly increased the amplitude of cAMP oscillations, and reduced the amplitude of $[Ca^{2+}]_i$ oscillations compared to glucose and TEA stimulation. While many experiments remain to elucidate the significance of these findings, these data demonstrate the capabilities of the IMS for multi-label fluorescence imaging for cellular dynamics.

Continuing studies

Paracrine regulation of glucagon secretion

Role of cAMP signaling and modulation in regulating glucagon secretion

We have shown that insulin and somatostatin increase the degradation and decrease the production of cAMP, respectively, which drives the inhibition of glucagon secretion with increasing glucose levels. However, many questions still remain about the normal and pathophysiological regulation of glucagon secretion from islet α-cells. For example, since Rac1-GTPase did not have the expected gate-keeper role in remodeling F-actin ahead of glucagon vesicle fusion, the signaling events downstream of PKA and proximal to membrane fusion and exocytosis remain to be elucidated. The first experiment here would be to interrogate the effect of glucose on the remaining Rho-GTPase family members, Cdc42 and Rho, which could be done with immunofluorescence as described in Chapter 2. Pharmacological intervention with specific inhibitors of these enzymes should show a measurable decrease in glucagon secretion

if one or both are involved in exocytosis. Additionally, identifying the proteins involved in the exocytotic machinery and their regulation with respect to glucose, cAMP, and PKA in the α-cells remains to be done for a more complete understanding of glucagon suppression.

As mentioned above, the glucagon secretion studies performed in this body of work were static incubation-based assays. However, since the dynamics are likely to be a critical part of the physiological regulation of glucagon, perifusion assays should be done, particularly on purified α-cells, to determine whether the order of somatostatin and insulin onset is an important parameter in their inhibition of glucagon. It would also be interesting to test the addition of insulin to isolated α-cells, followed by somatostatin, again to determine if there is significance in the kinetics or order that these paracrine factors are introduced to the cells.

Role of $[Ca^{2+}]_i$ in α-cell function at high glucose

It has been established by our group and others that glucagon inhibition does not depend on a decrease in $[Ca^{2+}]_i$, and in fact, it has been shown to increase in the α-cells with increasing glucose. This decoupling along with the observed increase suggests that $[Ca^{2+}]_i$ has a role in the function α-cells even at high glucose. An important remaining question is the nature of that function. A GCaMP3 Ca^{2+} biosensor, which is an earlier generation of the GCaMP5G that we utilized in Chapter 4 has been integrated into a floxed transgenic mouse line (Zariwala, Borghuis et al. 2012). When crossed with the Glucagon-Cre mouse, the resulting line will facilitate an in-depth analysis of $[Ca^{2+}]_i$ in the α-cells, including a much-needed characterization of the different populations of α-cell behaviors. The improved dynamic range of the GCaMP5G sensor is also likely to be integrated into a transgenic mouse model that could be used for this type of study.

Another interesting question is the role of metabolism regulating glucagon secretion. The generation of cAMP is an ATP-dependent process, so changes in the cytosolic ATP levels

may be another potent regulator of cAMP signaling. There is a ratiometric fluorescent biosensor for measuring the ATP/ADP ratio, called Perceval (Berg, Hung et al. 2009) that would be useful for such a line of enquiry. It contains a circularly permuted mVenus FP, and so could be used with islets from the tdRFP-expressing α-cells to study cell-type specific metabolic regulation. In addition to having a potential role in cAMP regulation, the cytosolic ATP/ADP ratio is a key player in modulating the ATP-sensitive K^+ channel (K_{ATP}), which has been hypothesized to be a critical factor in regulating glucagon secretion (Gopel, Kanno et al. 2000; Cheng-Xue, Gomez-Ruiz et al. 2013; Zhang, Ramracheya et al. 2013). A significant limitation in working with primary islet tissue throughout the course of this study was the delivery of such genetically-encoded biosensors to the cultured islets. However, packaging the biosensors into viral vectors for transfection will greatly improve their usability in isolated islets and is an ongoing project.

Glucose regulation of δ-cells and somatostatin secretion

The roles of somatostatin and insulin in inhibiting glucagon exocytosis have been described in this work and there has been a lot of research characterizing the β-cells and glucose-stimulated insulin secretion. However, many questions remain about the δ-cells and the role of glucose and α- and β-cells in regulating somatostatin secretion. The identification of δ-cells in the islet has been a significant barrier to answering these questions, but the availability of a somatostatin-promoter driven Cre mouse line and the tdRFP mouse line that we currently use has facilitated the genetic labeling of the δ-cells for interrogation by imaging. Additionally, it will be important to characterize the roles of the insulin, glucagon, and somatostatin receptors in regulating δ-cell function during normal and pathological states.

Having identified the primary somatostatin receptor subtype responsible for regulating glucagon exocytosis as SSTR2, along with others (Strowski, Parmar et al. 2000; Kailey, van de Bunt et al. 2012; Yue, Burdett et al. 2012), we have obtained a knockout mouse for this gene.

The first set of experiments to do with these knockout mice will include determining cAMP levels as well as glucagon and insulin secretion at low and high glucose. While we expect the resulting data to match our results using the pharmacological inhibitor, the long term deletion of this gene may stimulate compensatory mechanisms including the up-regulation of other receptor subtypes. Isolated islets from these mice do show a two-fold increase in glucagon secretion compared with wild type mice, supporting a critical role for these receptors in modulating glucagon exocytosis (Strowski, Parmar et al. 2000). These mice may also be useful for studying other paracrine intra-islet regulators that may affect glucagon secretion indirectly by modulating the δ-cells and somatostatin secretion.

Regulation of cAMP signaling during diabetes

One of the significant remaining questions about the regulated decrease in cAMP to lower glucagon secretion is whether or not this mechanism is significantly impaired during metabolic disease. We have begun to address this question by obtaining isolated islets from a human donor with type 1 diabetes, type 2 diabetes, or severe obesity (BMI > 45). We subjected these islets to a static incubation with low (1 mM) or high glucose (11 mM) and measured the cAMP levels and glucagon secretion. Though we have only had the tissue to perform this experiment once, the preliminary data are presented in Figures 5-2 and 5-3 along with a normal human control (N = 6). The obese human islets exhibited glucagon secretion and cAMP levels slightly lower than the normal control islets at low glucose. However, at high glucose, glucagon secretion was increased over 6 fold compared to controls and cAMP levels were flat and similar to the high glucose levels of the normal control, rather than reduced only at high glucose.

The type 1 diabetic islets were found to have increased glucagon secretion at both low and high glucose, a complete loss of inhibition. As with the obese samples, cAMP levels at low glucose were slightly lower. However, at high glucose, cAMP levels were quite high, reflecting a

total loss of inhibition observed at high glucose in normal controls. Interestingly, with respect to the secretion profile from this sample, the type 1 diabetic islets were similar to what we have observed in purified α-cells. Unfortunately, there were not enough islets from the type 2 diabetic human donor to perform both the glucagon secretion assay and measure cAMP levels, so we chose to measure cAMP, as glucagon secretion is being assessed in parallel by a collaborating lab. We found that the cAMP levels in islets from the type 2 diabetic donor were considerably lower at low glucose compared to the normal control as well as the obese and type 1 islets, but were comparable at high glucose. These experiments must be repeated before drawing any conclusions, but at first glance they seem to support our hypothesis that impaired cAMP signaling is a critical part of the glucagon dysregulation observed in metabolic diseases.

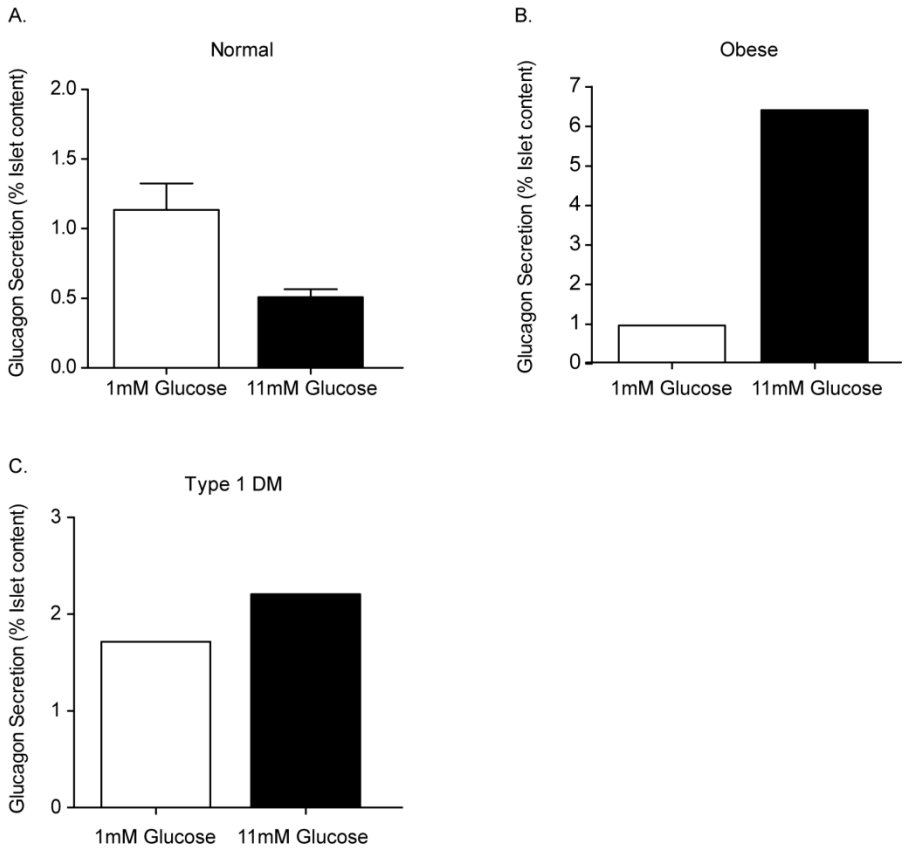

Figure 5-2: Glucagon secretion from normal, diabetic, and obese human islets. Glucagon secretion from islets statically incubated with low (1 mM) or high (11 mM) glucose from the islets of 5 human donors (A), 1 obese (B), and 1 type 1 diabetic human donor (C).

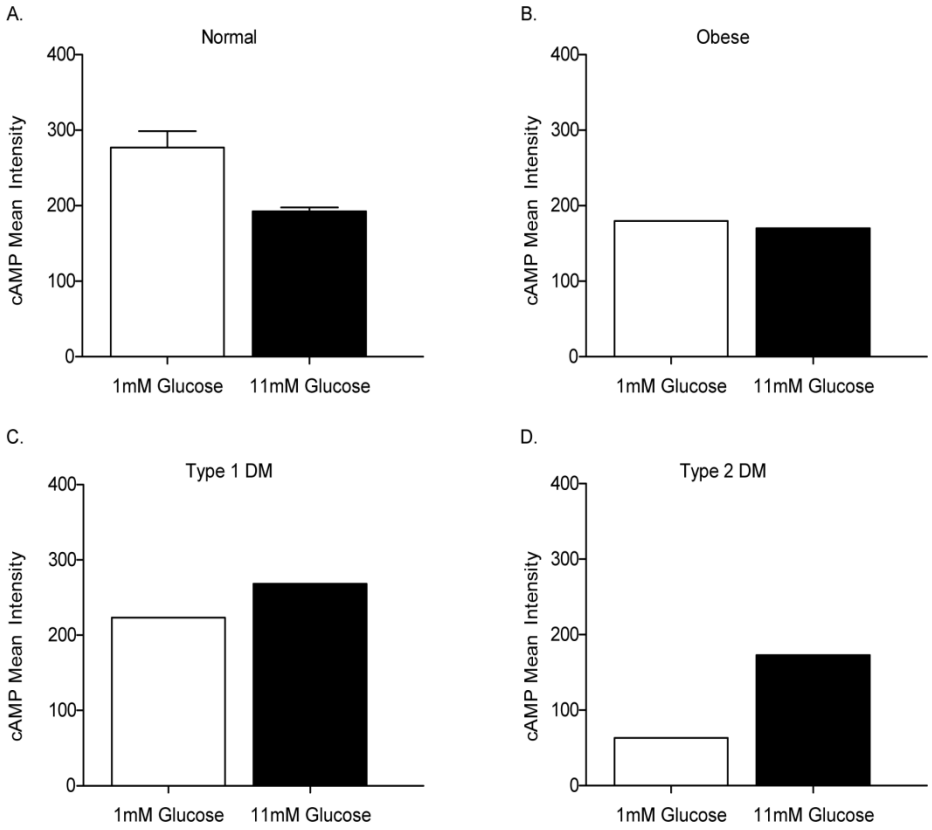

Figure 5-3: Relative cAMP levels from normal, diabetic, and obese human islets. Quantification of mean intensity normalized to pre-immune controls from the immunofluorescence images. (A) Normalized mean intensity from 4-6 islets from 5 human donors stimulated with low or high glucose before fixing and staining for glucagon and cAMP. (B-D) Islets treated as in (A) from a single obese (B), type 1 diabetic (C), or type 2 diabetic (D) human donor.

Optical sectioning and optimizing analysis of hyperspectral live-cell imaging

The IMS system provides a significant improvement in the temporal collection of data from simultaneous measurement of $[Ca^{2+}]_i$ and cAMP, and is a powerful tool for multidimensional analysis of signaling pathways. The device used in the experiments described here would be improved by the use of a scientific CMOS (sCMOS) detector arrays, which can provide image acquisition rates up to 100 fps while maintaining low readout noise (< 3 e^{-1}). Such a rapid imaging system would not only improve the ability to study transient relationships between signaling molecules, but would also be useful for very rapid biological processes like

action potentials in cardiac or neural tissue.

An important consideration for utilizing the IMS with islet samples is the need for effective optical sectioning due to the thickness of this tissue (up to ~100 μm). The widefield configuration utilized in our studies was effective for cultured cell monolayers. However, in the dense, multicellular islets, this system would suffer from spatial –spectral crosstalk due to light scattering from out-of-focus layers, which reduces the resolution and decreases compromises the ability to unmix the component spectra. There are a number of technologies available for addressing this problem, including the laser scanning confocal configuration, structured illumination microscopy (Gustafsson 2000), and light sheet microscopy (Keller, Schmidt et al. 2010; Truong, Supatto et al. 2011).

A depth-resolved IMS with structured illumination (SI) capability has been described, which implements epi-illumination with a Ronchi ruling grid in the optical path at a conjugate plane to the sample plane (Gao, Bedard et al. 2011). This system has the advantage of being easy to implement with a standard inverted microscope and collects 4D (x, y, z, λ) datacubes with significantly increased contrast provided by the SI configuration. The implementation of such an SI system with a sCMOS detector would provide robust improvements to the current capabilities of the IMS. However, since out-of-focus light still contributes to the shot noise under SI, very bright samples with a dominating signal from the out-of-focus may be better served by a light sheet approach, also called selective plane illumination microscopy (SPIM).

SPIM is a technique that uses a detector arm to collect fluorescence at a right angle to the illumination axis, which is excited by a thin laser beam from a single plane of the specimen (Keller, Schmidt et al. 2010). There are several advantages to this technique, including rapid data collection, high signal-to-noise, and low laser power, which limits the fluorophore photobleaching and sample phototoxicity. Additionally, the hardware arrangement lends itself to the addition of the compact IMS on the detector arm. Recently, the addition of a second detector arm and an inverted configuration was shown to provide isotropic resolution (x, y and z)

by imaging the sample with two perpendicular light sheets. This technique, called dual-view inverted SPIM (diSPIM) alternates the illumination and detection between two perpendicular objectives and is capable of collecting up to 200 images/second with a resolution of 330 nm (Wu, Wawrzusin et al. 2013). Considering the thickness of pancreatic islets and desire to study rapid molecular events in the whole volume, the diSPIM configuration would be convenient.

Spectral detection has not yet been integrated with the SPIM techniques and the snapshot modality of the IMS would be advantageous for maintaining the rapid imaging speeds necessary for many live-cell applications. Furthermore, two-photon excitation coupled with SPIM has been shown to provide twice the depth of a single photon and ten times the speed of a two-photon coupled point scanning system (Truong, Supatto et al. 2011). While it is expected that a single-photon excitation will be sufficient for most islet applications, detecting low signal events may benefit from the higher signal rate provided by the two-photon excitation light sheet.

Finally, with regard to the analysis of data collected using the IMS, we have considered alternative methods to our current linear unmixing protocol, which requires collecting reference spectra that adds experimental time. An emerging methodology called spectral phasor analysis can unmix multiple spectra in an image without the need for reference spectra (Fereidouni, Bader et al. 2012). We have begun using the ImageJ plugin for this technique to deconvolve data collected with the IMS. Briefly, the Fourier transform is taken for each pixel in an image, after which the real and imaginary components of the first harmonic are plotted as X and Y coordinates in a spectral phasor plot, shown in Figure 5-4 for data collected with the IMS from a three-color experiment. The phasor of the spectrum for the linear combination of the three components falls within a triangle with vertices of the discrete Fourier transform. The fractional contribution from each component is calculated geometrically from the area of the triangle defined by each phasor's position in the plot divided by the area of a reference triangle (Fereidouni, Bader et al. 2012).

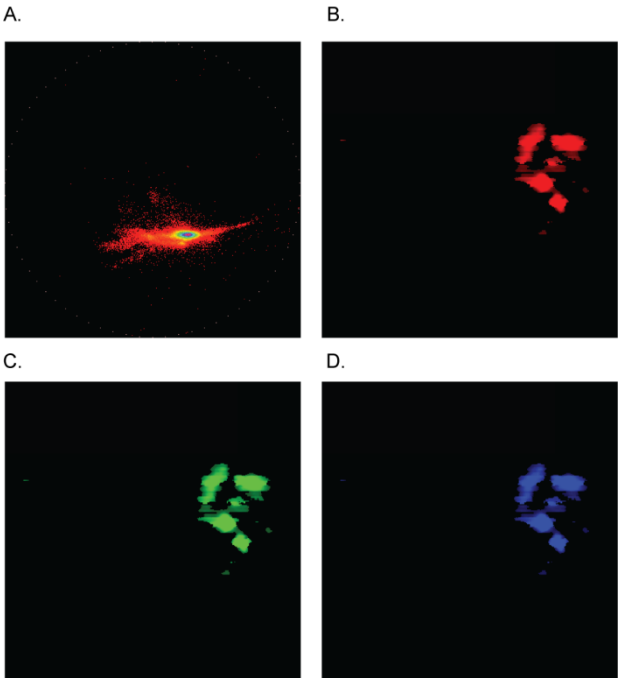

Figure 5-4: Results of spectral phasor analysis from a single three-color IMS snapshot. (A) Spectral phasor plot of an image of co-transfected cAMP biosensor ^{T}-Epac-^{VV} (mTurquoise and cpVenus-Venus) and $[Ca^{2+}]_i$ sensor GCaMP5G (cpGFP). (B-D) Phasor unmixed RGB images of the cpVenus-Venus (B), cpGFP (C), and mTurquoise (D) signals.

By analyzing the same spectral snapshot collected from the IMS with the traditional linear unmixing and the spectral phasor approach, we find comparable intensities for each FP, as shown in Figure 5-5. Interestingly, the spectral profile identified by the phasor analysis more closely resembles the expected spectra than that from the raw lambda stack. This demonstrates one of the significant advantages to natively identifying the spectral components in an image for quantitative analysis. The reference spectra, which are typically collected from single transfections of individual FPs, can introduce artefacts that may reduce the accuracy of linear unmixing. For example, the environmental constraints of the FPs within the biosensors may be different enough than for the individual FPs to affect the unmixing results. The reference spectra utilized by the spectral phasor analysis are provided by the phasor algorithm itself, which solves the possible problem of environmental artifacts and obviates the need to

collect separate reference spectra experimentally. Recent improvements in the spectral phasor analysis have been implemented by the addition of the second harmonic, which expands the number of spectra that can be distinguished from each pixel in an image (Cutrale, Salih et al. 2013). In future, this method of data analysis may well replace the standard linear unmixing and we hope to apply it to the dual-FRET data described in Chapter 4 and to data collected in ongoing hyperspectral imaging studies.

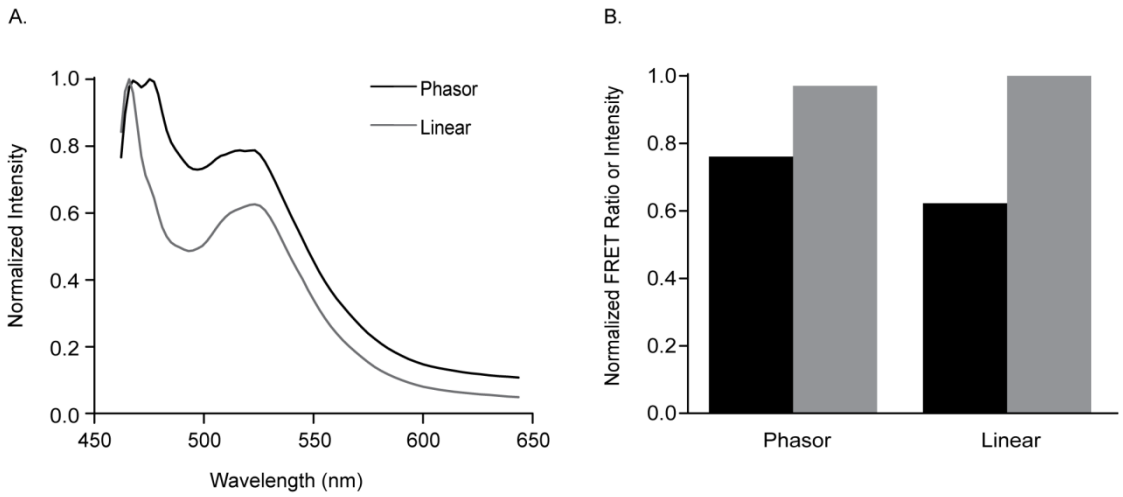

Figure 5-5: Comparison of linear unmixing and spectral phasor analysis. (A) Normalized spectra from a single IMS snapshot (same as Figure 5-4) measured from the remapped lambda stack (gray) and the spectral phasor ImageJ plugin (black). (B) Normalized intensity of GCaMP5G from (A) in gray bars and normalized FRET ratio of ^{T}-Epac-^{VV} in black bars.

REFERENCES

Ahmad, F., R. Lindh, et al. (2009). "Differential regulation of adipocyte PDE3B in distinct membrane compartments by insulin and the beta3-adrenergic receptor agonist CL316243: effects of caveolin-1 knockdown on formation/maintenance of macromolecular signalling complexes." Biochem J **424**(3): 399-410.

Ahren, B. (2000). "Autonomic regulation of islet hormone secretion--implications for health and disease." Diabetologia **43**(4): 393-410.

Ahren, B. (2009). "Islet G protein-coupled receptors as potential targets for treatment of type 2 diabetes." Nat Rev Drug Discov **8**(5): 369-385.

Ahren, B., A. Ar'Rajab, et al. (1991). "Presence of galanin in human pancreatic nerves and inhibition of insulin secretion from isolated human islets." Cell Tissue Res **264**(2): 263-267.

Ahren, B., R. C. Veith, et al. (1987). "Sympathetic nerve stimulation versus pancreatic norepinephrine infusion in the dog: 1). Effects on basal release of insulin and glucagon." Endocrinology **121**(1): 323-331.

Akerboom, J., T. W. Chen, et al. (2012). "Optimization of a GCaMP calcium indicator for neural activity imaging." J Neurosci **32**(40): 13819-13840.

Alves, C., F. Batel-Marques, et al. (2012). "A meta-analysis of serious adverse events reported with exenatide and liraglutide: acute pancreatitis and cancer." Diabetes Res Clin Pract **98**(2): 271-284.

Andersen, D. K., D. Elahi, et al. (1978). "Oral glucose augmentation of insulin secretion. Interactions of gastric inhibitory polypeptide with ambient glucose and insulin levels." J Clin Invest **62**(1): 152-161.

Aoyagi, S. and T. K. Archer (2008). "Dynamics of coactivator recruitment and chromatin modifications during nuclear receptor mediated transcription." Mol Cell Endocrinol **280**(1-2): 1-5.

Archer, T. K., P. Lefebvre, et al. (1992). "Transcription factor loading on the MMTV promoter: a bimodal mechanism for promoter activation." Science **255**(5051): 1573-1576.

Asahara, S., Y. Shibutani, et al. (2013). "Ras-related C3 botulinum toxin substrate 1 (RAC1) regulates glucose-stimulated insulin secretion via modulation of F-actin." Diabetologia **56**(5): 1088-1097.

Bachmann, V. A., A. Riml, et al. (2013). "Reciprocal regulation of PKA and Rac signaling." Proc Natl Acad Sci U S A **110**(21): 8531-8536.

Baier, A., V. N. Ndoh, et al. (2014). "Rac1 and Rac2 control distinct events during antigen-stimulated mast cell exocytosis." J Leukoc Biol.

Baird, G. S., D. A. Zacharias, et al. (1999). Circular permutation and receptor insertion within green fluorescent proteins. Proc Natl Acad Sci U S A. **96:** 11241-11246.

Bedard, N., N. Hagen, et al. (2012). "Image mapping spectrometry: calibration and characterization." Opt Eng **51**(11).

Bedard, N., N. Hagen, et al. (2012). "Image mapping spectrometry: calibration and characterization." Optical Engineering **in review**

Beebe, S. J., J. B. Redmon, et al. (1985). "Discriminative insulin antagonism of stimulatory effects of various cAMP analogs on adipocyte lipolysis and hepatocyte glycogenolysis." J Biol Chem **260**(29): 15781-15788.

Bell, G. I., R. F. Santerre, et al. (1983). "Hamster preproglucagon contains the sequence of glucagon and two related peptides." Nature **302**(5910): 716-718.

Benninger, R. K., W. S. Head, et al. (2011). "Gap junctions and other mechanisms of cell-cell communication regulate basal insulin secretion in the pancreatic islet." J Physiol **589**(Pt 22): 5453-5466.

Berg, J., Y. P. Hung, et al. (2009). "A genetically encoded fluorescent reporter of ATP:ADP ratio." Nat Methods **6**(2): 161-166.

Berg, J. M., Tymoczko, J.L., Stryer, L. (2002). Biochemistry, W H Freeman.
Birukova, A. A., T. Zagranichnaya, et al. (2007). "Prostaglandins PGE(2) and PGI(2) promote endothelial barrier enhancement via PKA- and Epac1/Rap1-dependent Rac activation." Exp Cell Res **313**(11): 2504-2520.
Bliss, M. (1997). "The discovery of insulin: the inside story." Publ Am Inst Hist Pharm **16**: 93-99.
Boden, G. (1997). "Role of fatty acids in the pathogenesis of insulin resistance and NIDDM." Diabetes **46**(1): 3-10.
Boden, G. and G. I. Shulman (2002). "Free fatty acids in obesity and type 2 diabetes: defining their role in the development of insulin resistance and beta-cell dysfunction." Eur J Clin Invest **32 Suppl 3**: 14-23.
Boehning, D., R. L. Patterson, et al. (2003). "Cytochrome c binds to inositol (1,4,5) trisphosphate receptors, amplifying calcium-dependent apoptosis." Nat Cell Biol **5**(12): 1051-1061.
Bonner-Weir, S. and L. Orci (1982). "New perspectives on the microvasculature of the islets of Langerhans in the rat." Diabetes **31**(10): 883-889.
Bramswig, N. C., L. J. Everett, et al. (2013). "Epigenomic plasticity enables human pancreatic alpha to beta cell reprogramming." J Clin Invest **123**(3): 1275-1284.
Brissova, M., M. J. Fowler, et al. (2005). "Assessment of human pancreatic islet architecture and composition by laser scanning confocal microscopy." J Histochem Cytochem **53**(9): 1087-1097.
Broccolini, A., E. Ricci, et al. (2004). "Insulin-like growth factor I in inclusion-body myositis and human muscle cultures." J Neuropathol Exp Neurol **63**(6): 650-659.
Brock, C., M. Schaefer, et al. (2003). "Roles of G beta gamma in membrane recruitment and activation of p110 gamma/p101 phosphoinositide 3-kinase gamma." J Cell Biol **160**(1): 89-99.
Brunicardi, F. C., R. Kleinman, et al. (2001). "Immunoneutralization of somatostatin, insulin, and glucagon causes alterations in islet cell secretion in the isolated perfused human pancreas." Pancreas **23**(3): 302-308.
Butler, A. E., J. Janson, et al. (2003). "Beta-cell deficit and increased beta-cell apoptosis in humans with type 2 diabetes." Diabetes **52**(1): 102-110.
Butler, A. E., J. Janson, et al. (2003). "Increased beta-cell apoptosis prevents adaptive increase in beta-cell mass in mouse model of type 2 diabetes: evidence for role of islet amyloid formation rather than direct action of amyloid." Diabetes **52**(9): 2304-2314.
Cabrera, O., D. M. Berman, et al. (2006). "The unique cytoarchitecture of human pancreatic islets has implications for islet cell function." Proc Natl Acad Sci U S A **103**(7): 2334-2339.
Campbell, C. E., M. Piper, et al. (2008). "The transcription factor Nfix is essential for normal brain development." BMC Dev Biol **8**(1): 52.
Carroll, J. S., X. S. Liu, et al. (2005). "Chromosome-wide mapping of estrogen receptor binding reveals long-range regulation requiring the forkhead protein FoxA1." Cell **122**(1): 33-43.
Carroll, J. S., C. A. Meyer, et al. (2006). "Genome-wide analysis of estrogen receptor binding sites." Nat Genet **38**(11): 1289-1297.
Cawthorn, E. G. and C. B. Chan (1991). "Effect of pertussis toxin on islet insulin secretion in obese (fa/fa) Zucker rats." Mol Cell Endocrinol **75**(3): 197-204.
Cejvan, K., D. H. Coy, et al. (2003). "Intra-islet somatostatin regulates glucagon release via type 2 somatostatin receptors in rats." Diabetes **52**(5): 1176-1181.
Chen, J. and C. G. Ostenson (2004). "Glucagon release is regulated by tyrosine phosphatase and PI3-kinase activity." Biochem Biophys Res Commun **325**(2): 555-560.
Chen, L., J. Philippe, et al. (2011). "Glucagon responses of isolated alpha cells to glucose, insulin, somatostatin, and leptin." Endocr Pract **17**(5): 819-825.
Cheng-Xue, R., A. Gomez-Ruiz, et al. (2013). "Tolbutamide Controls Glucagon Release From Mouse Islets Differently Than Glucose: Involvement of KATP Channels From Both alpha-Cells and delta-Cells." Diabetes **62**(5): 1612-1622.

Cheng, H., S. G. Straub, et al. (2003). "Protein acylation in the inhibition of insulin secretion by norepinephrine, somatostatin, galanin, and PGE2." Am J Physiol Endocrinol Metab **285**(2): E287-294.
Cherrington, A. D. (2005). "The role of hepatic insulin receptors in the regulation of glucose production." J Clin Invest **115**(5): 1136-1139.
Choi, Y. H., S. Park, et al. (2006). "Alterations in regulation of energy homeostasis in cyclic nucleotide phosphodiesterase 3B-null mice." J Clin Invest **116**(12): 3240-3251.
Christensen, M., J. I. Bagger, et al. (2011). "The alpha-cell as target for type 2 diabetes therapy." Rev Diabet Stud **8**(3): 369-381.
Christensen, M., F. K. Knop, et al. (2011). "Lixisenatide for type 2 diabetes mellitus." Expert Opin Investig Drugs **20**(4): 549-557.
Christensen, M., L. Vedtofte, et al. (2011). "Glucose-dependent insulinotropic polypeptide: a bifunctional glucose-dependent regulator of glucagon and insulin secretion in humans." Diabetes **60**(12): 3103-3109.
Cirillo, L. A., F. R. Lin, et al. (2002). "Opening of compacted chromatin by early developmental transcription factors HNF3 (FoxA) and GATA-4." Mol Cell **9**(2): 279-289.
Cirulli, V., D. Baetens, et al. (1994). "Expression of neural cell adhesion molecule (N-CAM) in rat islets and its role in islet cell type segregation." J Cell Sci **107 (Pt 6)**: 1429-1436.
Cryer, P. E. (2002). "Hypoglycaemia: the limiting factor in the glycaemic management of Type I and Type II diabetes." Diabetologia **45**(7): 937-948.
Cuthbertson, D., K. Smith, et al. (2005). "Anabolic signaling deficits underlie amino acid resistance of wasting, aging muscle." FASEB J **19**(3): 422-424.
Cutrale, F., A. Salih, et al. (2013). "Spectral Phasor approach for fingerprinting of photo-activatable fluorescent proteins Dronpa, Kaede and KikGR." Method Appl Fluoresc **1**(3): 35001.
Dai, C., M. Brissova, et al. (2012). "Islet-enriched gene expression and glucose-induced insulin secretion in human and mouse islets." Diabetologia **55**(3): 707-718.
De Marinis, Y. Z., A. Salehi, et al. (2010). "GLP-1 inhibits and adrenaline stimulates glucagon release by differential modulation of N- and L-type Ca2+ channel-dependent exocytosis." Cell Metab **11**(6): 543-553.
de Rooij, J., F. J. Zwartkruis, et al. (1998). Epac is a Rap1 guanine-nucleotide-exchange factor directly activated by cyclic AMP. Nature. **396:** 474-477.
Deconinck, J. F., F. A. Van Assche, et al. (1972). "The ultrastructure of the human pancreatic islets. II. The islets of neonates." Diabetologia **8**(5): 326-333.
DeFronzo, R. A., T. Okerson, et al. (2008). "Effects of exenatide versus sitagliptin on postprandial glucose, insulin and glucagon secretion, gastric emptying, and caloric intake: a randomized, cross-over study." Curr Med Res Opin **24**(10): 2943-2952.
DeFronzo, R. A. and D. Tripathy (2009). "Skeletal muscle insulin resistance is the primary defect in type 2 diabetes." Diabetes Care **32 Suppl 2**: S157-163.
Degerman, E., F. Ahmad, et al. (2011). "From PDE3B to the regulation of energy homeostasis." Curr Opin Pharmacol **11**(6): 676-682.
Degn, K. B., C. B. Juhl, et al. (2004). "One week's treatment with the long-acting glucagon-like peptide 1 derivative liraglutide (NN2211) markedly improves 24-h glycemia and alpha- and beta-cell function and reduces endogenous glucose release in patients with type 2 diabetes." Diabetes **53**(5): 1187-1194.
DeGraff, D. J., X. Yu, et al. (2008). The role of Foxa proteins in the regulation of androgen receptor activity. Androgen Action in Prostate Cancer. D. J. Tindall and J. L. Mohler.
Denton, J. S. and D. A. Jacobson (2012). "Channeling dysglycemia: ion-channel variations perturbing glucose homeostasis." Trends Endocrinol Metab **23**(1): 41-48.
Diao, J., Z. Asghar, et al. (2005). "Glucose-regulated glucagon secretion requires insulin receptor expression in pancreatic alpha-cells." J Biol Chem **280**(39): 33487-33496.
Dillon, J. S., M. Lu, et al. (2005). "The recombinant rat glucagon-like peptide-1 receptor, expressed in an alpha-cell line, is coupled to adenylyl cyclase activation and intracellular calcium release." Exp Clin Endocrinol Diabetes **113**(3): 182-189.

Donath, M. Y., J. A. Ehses, et al. (2005). "Mechanisms of beta-cell death in type 2 diabetes." Diabetes **54 Suppl 2**: S108-113.
Dorrell, C., J. Schug, et al. (2011). "Transcriptomes of the major human pancreatic cell types." Diabetologia **54**(11): 2832-2844.
Dousa, T. P., L. D. Barnes, et al. (1977). "Immunohistochemical localization of 3':5'-cyclic AMP and 3':5'-cyclic GMP in rat renal cortex: effect of parathyroid hormone." Proc Natl Acad Sci U S A **74**(8): 3569-3573.
Driller, K., A. Pagenstecher, et al. (2007). "Nuclear factor I X deficiency causes brain malformation and severe skeletal defects." Mol Cell Biol **27**(10): 3855-3867.
Drucker, D. J. and M. A. Nauck (2006). "The incretin system: glucagon-like peptide-1 receptor agonists and dipeptidyl peptidase-4 inhibitors in type 2 diabetes." Lancet **368**(9548): 1696-1705.
Dunning, B. E., B. Ahren, et al. (1986). "Galanin: a novel pancreatic neuropeptide." Am J Physiol **251**(1 Pt 1): E127-133.
Dyachok, O., O. Idevall-Hagren, et al. (2008). "Glucose-induced cyclic AMP oscillations regulate pulsatile insulin secretion." Cell Metab **8**(1): 26-37.
Dyachok, O., Y. Isakov, et al. (2006). "Oscillations of cyclic AMP in hormone-stimulated insulin-secreting beta-cells." Nature **439**(7074): 349-352.
Dyachok, O., J. Sagetorp, et al. (2006). "cAMP oscillations restrict protein kinase A redistribution in insulin-secreting cells." Biochem Soc Trans **34**(Pt 4): 498-501.
Edgerton, D. S., K. M. Johnson, et al. (2009). "Current strategies for the inhibition of hepatic glucose production in type 2 diabetes." Front Biosci (Landmark Ed) **14**: 1169-1181.
Eeckhoute, J., J. S. Carroll, et al. (2006). "A cell-type-specific transcriptional network required for estrogen regulation of cyclin D1 and cell cycle progression in breast cancer." Genes Dev **20**(18): 2513-2526.
Eizirik, D. L., M. Sammeth, et al. (2012). "The human pancreatic islet transcriptome: expression of candidate genes for type 1 diabetes and the impact of pro-inflammatory cytokines." PLoS Genet **8**(3): e1002552.
Elchebly, M., P. Payette, et al. (1999). "Increased insulin sensitivity and obesity resistance in mice lacking the protein tyrosine phosphatase-1B gene." Science **283**(5407): 1544-1548.
Elliott, A. D., L. Gao, et al. (2012). "Real-time hyperspectral fluorescence imaging of pancreatic beta-cell dynamics with the image mapping spectrometer." J Cell Sci **125**(Pt 20): 4833-4840.
Farilla, L., H. Hui, et al. (2002). "Glucagon-like peptide-1 promotes islet cell growth and inhibits apoptosis in Zucker diabetic rats." Endocrinology **143**(11): 4397-4408.
Fereidouni, F., A. N. Bader, et al. (2012). "Spectral phasor analysis allows rapid and reliable unmixing of fluorescence microscopy spectral images." Optics Express **20**(12): 12729-12741.
Ferris, D. G., R. A. Lawhead, et al. (2001). "Multimodal hyperspectral imaging for the noninvasive diagnosis of cervical neoplasia." J Low Genit Tract Dis **5**(2): 65-72.
Franklin, I., J. Gromada, et al. (2005). "Beta-cell secretory products activate alpha-cell ATP-dependent potassium channels to inhibit glucagon release." Diabetes **54**(6): 1808-1815.
Gao, L., N. Bedard, et al. (2011). "Depth-resolved image mapping spectrometer (IMS) with structured illumination." Optics Express **19**(18): 17439-17452.
Gao, L., R. T. Kester, et al. (2009). Compact Image Slicing Spectrometer (ISS) for hyperspectral fluorescence microscopy. Optics Express. **17:** 12293-12308.
Gao, L. A., R. T. Kester, et al. (2010). "Snapshot Image Mapping Spectrometer (IMS) with high sampling density for hyperspectral microscopy." Optics Express **18**(14): 14330-14344.
Gao, N., K. Ishii, et al. (2005). "Forkhead box A1 regulates prostate ductal morphogenesis and promotes epithelial cell maturation." Development **132**(15): 3431-3443.
Gao, N., J. Zhang, et al. (2003). "The role of hepatocyte nuclear factor-3 alpha (Forkhead Box A1) and androgen receptor in transcriptional regulation of prostatic genes." Mol Endocrinol **17**(8): 1484-1507.

Gao, Y., J. B. Dickerson, et al. (2004). "Rational design and characterization of a Rac GTPase-specific small molecule inhibitor." Proc Natl Acad Sci U S A **101**(20): 7618-7623.
Garg, R., W. Chen, et al. (2010). "Acute pancreatitis in type 2 diabetes treated with exenatide or sitagliptin: a retrospective observational pharmacy claims analysis." Diabetes Care **33**(11): 2349-2354.
Gerich, J. E., M. Lorenzi, et al. (1974). "Effects of somatostatin on plasma glucose and glucagon levels in human diabetes mellitus. Pathophysiologic and therapeutic implications." N Engl J Med **291**(11): 544-547.
Gierer, A. (1974). "Molecular models and combinatorial principles in cell differentiation and morphogenesis." Cold Spring Harb Symp Quant Biol **38**: 951-961.
Gilman, A. G. (1987). "G proteins: transducers of receptor-generated signals." Annu Rev Biochem **56**: 615-649.
Goedhart, J., L. van Weeren, et al. (2010). Bright cyan fluorescent protein variants identified by fluorescence lifetime screening. Nat Methods. **7:** 137-139.
Goldberg, I. J., R. H. Eckel, et al. (2009). "Regulation of fatty acid uptake into tissues: lipoprotein lipase- and CD36-mediated pathways." J Lipid Res **50 Suppl**: S86-90.
Gopel, S. O., T. Kanno, et al. (2000). "Regulation of glucagon release in mouse -cells by KATP channels and inactivation of TTX-sensitive Na+ channels." J Physiol **528**(Pt 3): 509-520.
Goto, A., M. Hoshino, et al. (2011). "Phosphorylation of STEF/Tiam2 by protein kinase A is critical for Rac1 activation and neurite outgrowth in dibutyryl cAMP-treated PC12D cells." Mol Biol Cell **22**(10): 1780-1790.
Gould, G. W. and G. D. Holman (1993). "The glucose transporter family: structure, function and tissue-specific expression." Biochem J **295 (Pt 2)**: 329-341.
Graham, J. R., I. de Pater, et al. (1995). "The fragment R collision: W. M. Keck telescope observations of SL9." Science **267**(5202): 1320-1323.
Greene, R. M., J. L. Shanfeld, et al. (1980). "Immunohistochemical localization of cyclic AMP in the developing rodent secondary palate." J Embryol Exp Morphol **60**: 271-281.
Greiner, T. U., G. Kesavan, et al. (2009). "Rac1 regulates pancreatic islet morphogenesis." BMC Dev Biol **9**: 2.
Gromada, J., K. Bokvist, et al. (1997). "Adrenaline stimulates glucagon secretion in pancreatic A-cells by increasing the Ca2+ current and the number of granules close to the L-type Ca2+ channels." J Gen Physiol **110**(3): 217-228.
Gromada, J., I. Franklin, et al. (2007). "Alpha-cells of the endocrine pancreas: 35 years of research but the enigma remains." Endocr Rev **28**(1): 84-116.
Gromada, J., M. Hoy, et al. (2001). "Somatostatin inhibits exocytosis in rat pancreatic alpha-cells by G(i2)-dependent activation of calcineurin and depriming of secretory granules." J Physiol **535**(Pt 2): 519-532.
Gromada, J., M. Hoy, et al. (2001). "Gi2 proteins couple somatostatin receptors to low-conductance K+ channels in rat pancreatic alpha-cells." Pflugers Arch **442**(1): 19-26.
Gromada, J., X. Ma, et al. (2004). "ATP-sensitive K+ channel-dependent regulation of glucagon release and electrical activity by glucose in wild-type and SUR1-/- mouse alpha-cells." Diabetes **53 Suppl 3**: S181-189.
Grunder, A., T. T. Ebel, et al. (2002). "Nuclear factor I-B (Nfib) deficient mice have severe lung hypoplasia." Mech Dev **112**(1-2): 69-77.
Gu, Y., M. D. Filippi, et al. (2003). "Hematopoietic cell regulation by Rac1 and Rac2 guanosine triphosphatases." Science **302**(5644): 445-449.
Guo, S., C. Dai, et al. (2013). "Inactivation of specific beta cell transcription factors in type 2 diabetes." J Clin Invest.
Gustafsson, M. G. (2000). "Surpassing the lateral resolution limit by a factor of two using structured illumination microscopy." J Microsc **198**(Pt 2): 82-87.
Haataja, L., J. Groffen, et al. (1997). "Characterization of RAC3, a novel member of the Rho family." J Biol Chem **272**(33): 20384-20388.
Hacker, G. (2000). "The morphology of apoptosis." Cell Tissue Res **301**(1): 5-17.

Hall, A. (1998). "Rho GTPases and the actin cytoskeleton." Science **279**(5350): 509-514.
Hamaguchi, K. and E. H. Leiter (1990). "Comparison of cytokine effects on mouse pancreatic alpha-cell and beta-cell lines. Viability, secretory function, and MHC antigen expression." Diabetes **39**(4): 415-425.
Hara, M., X. Wang, et al. (2003). "Transgenic mice with green fluorescent protein-labeled pancreatic beta -cells." Am J Physiol Endocrinol Metab **284**(1): E177-183.
Hatakeyama, H., N. Takahashi, et al. (2007). "Two cAMP-dependent pathways differentially regulate exocytosis of large dense-core and small vesicles in mouse beta-cells." J Physiol **582**(Pt 3): 1087-1098.
Hauge-Evans, A. C., R. L. Anderson, et al. (2012). "Delta cell secretory responses to insulin secretagogues are not mediated indirectly by insulin." Diabetologia **55**(7): 1995-2004.
Hauge-Evans, A. C., A. J. King, et al. (2009). "Somatostatin secreted by islet delta-cells fulfills multiple roles as a paracrine regulator of islet function." Diabetes **58**(2): 403-411.
Hauge-Evans, A. C., A. J. King, et al. (2010). "A role for islet somatostatin in mediating sympathetic regulation of glucagon secretion." Islets **2**(6): 341-344.
Head, W. S., M. L. Orseth, et al. (2012). "Connexin-36 gap junctions regulate in vivo first- and second-phase insulin secretion dynamics and glucose tolerance in the conscious mouse." Diabetes **61**(7): 1700-1707.
Heasman, S. J. and A. J. Ridley (2008). "Mammalian Rho GTPases: new insights into their functions from in vivo studies." Nat Rev Mol Cell Biol **9**(9): 690-701.
Heimann, E., H. A. Jones, et al. (2010). "Expression and regulation of cyclic nucleotide phosphodiesterases in human and rat pancreatic islets." PLoS One **5**(12): e14191.
Heimberg, H., A. De Vos, et al. (1996). "The glucose sensor protein glucokinase is expressed in glucagon-producing alpha-cells." Proc Natl Acad Sci U S A **93**(14): 7036-7041.
Heimberg, H., A. De Vos, et al. (1995). "Differences in glucose transporter gene expression between rat pancreatic alpha- and beta-cells are correlated to differences in glucose transport but not in glucose utilization." J Biol Chem **270**(15): 8971-8975.
Hellman, B., A. Salehi, et al. (2009). "Glucose generates coincident insulin and somatostatin pulses and antisynchronous glucagon pulses from human pancreatic islets." Endocrinology **150**(12): 5334-5340.
Holz, G. G., E. Heart, et al. (2008). "Synchronizing Ca2+ and cAMP oscillations in pancreatic beta-cells: a role for glucose metabolism and GLP-1 receptors? Focus on "regulation of cAMP dynamics by Ca2+ and G protein-coupled receptors in the pancreatic beta-cell: a computational approach"." Am J Physiol Cell Physiol **294**(1): C4-6.
Idevall-Hagren, O., S. Barg, et al. (2010). "cAMP mediators of pulsatile insulin secretion from glucose-stimulated single beta-cells." J Biol Chem **285**(30): 23007-23018.
Imazu, M., W. G. Strickland, et al. (1984). "Phosphorylation and inactivation of liver glycogen synthase by liver protein kinases." J Biol Chem **259**(3): 1813-1821.
Imazu, M., W. G. Strickland, et al. (1984). "Multiple phosphorylation of rat-liver glycogen synthase by protein kinases." Biochim Biophys Acta **789**(3): 285-293.
Iozzo, P., T. Pratipanawatr, et al. (2001). "Physiological hyperinsulinemia impairs insulin-stimulated glycogen synthase activity and glycogen synthesis." Am J Physiol Endocrinol Metab **280**(5): E712-719.
Ishihara, H., P. Maechler, et al. (2003). "Islet beta-cell secretion determines glucagon release from neighbouring alpha-cells." Nat Cell Biol **5**(4): 330-335.
Jansson, L. and C. Hellerstrom (1983). "Stimulation by glucose of the blood flow to the pancreatic islets of the rat." Diabetologia **25**(1): 45-50.
Jarrousse, C. and G. Rosselin (1975). "Regulation by glucose and cyclic nucleotides of the glucagon and insulin release induced by amino acids." Diabete Metab **1**(3): 135-142.
Jia, L., B. P. Berman, et al. (2008). "Genomic androgen receptor-occupied regions with different functions, defined by histone acetylation, coregulators and transcriptional capacity." PLoS One **3**(11): e3645.

Kailey, B., M. van de Bunt, et al. (2012). "SSTR2 is the functionally dominant somatostatin receptor in human pancreatic beta- and alpha-cells." Am J Physiol Endocrinol Metab **303**(9): E1107-1116.
Kalwat, M. A. and D. C. Thurmond (2013). "Signaling mechanisms of glucose-induced F-actin remodeling in pancreatic islet beta cells." Exp Mol Med **45**: e37.
Kalwat, M. A., S. M. Yoder, et al. (2013). "A p21-activated kinase (PAK1) signaling cascade coordinately regulates F-actin remodeling and insulin granule exocytosis in pancreatic beta cells." Biochem Pharmacol **85**(6): 808-816.
Kandpal, L. M., H. Lee, et al. (2013). "Hyperspectral reflectance imaging technique for visualization of moisture distribution in cooked chicken breast." Sensors (Basel) **13**(10): 13289-13300.
Kaneko, K., T. Shirotani, et al. (1999). "Insulin inhibits glucagon secretion by the activation of PI3-kinase in In-R1-G9 cells." Diabetes Res Clin Pract **44**(2): 83-92.
Kawamori, D. and R. N. Kulkarni (2009). "Insulin modulation of glucagon secretion: the role of insulin and other factors in the regulation of glucagon secretion." Islets **1**(3): 276-279.
Kawamori, D., A. J. Kurpad, et al. (2009). "Insulin signaling in alpha cells modulates glucagon secretion in vivo." Cell Metab **9**(4): 350-361.
Keller, P. J., A. D. Schmidt, et al. (2010). "Fast, high-contrast imaging of animal development with scanned light sheet-based structured-illumination microscopy." Nat Methods **7**(8): 637-642.
Kepner, E. M., S. M. Yoder, et al. (2011). "Cool-1/betaPIX functions as a guanine nucleotide exchange factor in the cycling of Cdc42 to regulate insulin secretion." Am J Physiol Endocrinol Metab **301**(6): E1072-1080.
Kersten, S. (2001). "Mechanisms of nutritional and hormonal regulation of lipogenesis." EMBO Rep **2**(4): 282-286.
Kester, R. T., N. Bedard, et al. (2011). "Real-time snapshot hyperspectral imaging endoscope." Journal of Biomedical Optics **16**(5): 056005.
Kielgast, U., T. Krarup, et al. (2011). "Four weeks of treatment with liraglutide reduces insulin dose without loss of glycemic control in type 1 diabetic patients with and without residual beta-cell function." Diabetes Care **34**(7): 1463-1468.
Kilimnik, G., J. Jo, et al. (2012). "Quantification of islet size and architecture." Islets **4**(2): 167-172.
Kilimnik, G., A. Kim, et al. (2009). "Quantification of pancreatic islet distribution in situ in mice." Am J Physiol Endocrinol Metab **297**(6): E1331-1338.
Kim, A., K. Miller, et al. (2009). "Islet architecture: A comparative study." Islets **1**(2): 129-136.
Kimball, C. P. and J. R. Murlin (1923). "Aqueous extracts of pancreas III. Some precipitation reactions of insulin." J Biol Chem **58**(1): 337-348.
Kimple, A. J., D. E. Bosch, et al. (2011). "Regulators of G-protein signaling and their Galpha substrates: promises and challenges in their use as drug discovery targets." Pharmacol Rev **63**(3): 728-749.
Klarenbeek, J. B., J. Goedhart, et al. (2011). "A mTurquoise-based cAMP sensor for both FLIM and ratiometric read-out has improved dynamic range." PLoS One **6**(4): e19170.
Kohn, A. D., S. A. Summers, et al. (1996). "Expression of a constitutively active Akt Ser/Thr kinase in 3T3-L1 adipocytes stimulates glucose uptake and glucose transporter 4 translocation." J Biol Chem **271**(49): 31372-31378.
Konstantinova, I., G. Nikolova, et al. (2007). "EphA-Ephrin-A-mediated beta cell communication regulates insulin secretion from pancreatic islets." Cell **129**(2): 359-370.
Koska, J., A. DelParigi, et al. (2004). "Pancreatic polypeptide is involved in the regulation of body weight in pima Indian male subjects." Diabetes **53**(12): 3091-3096.
Kremers, G. J., Gilbert, S.G., Cranfill, P.J., Davidson, M.W., Piston, D.W. (2011). "Fluorescent proteins at a glance." JCS **124**: 157-160.
Kulkarni, R. N., J. C. Bruning, et al. (1999). "Tissue-specific knockout of the insulin receptor in pancreatic beta cells creates an insulin secretory defect similar to that in type 2 diabetes." Cell **96**(3): 329-339.

Kulkarni, R. N., Z. L. Wang, et al. (2000). "Glibenclamide but not other sulphonylureas stimulates release of neuropeptide Y from perifused rat islets and hamster insulinoma cells." J Endocrinol **165**(2): 509-518.
Kumagai, A. K., Y. S. Kang, et al. (1995). "Upregulation of blood-brain barrier GLUT1 glucose transporter protein and mRNA in experimental chronic hypoglycemia." Diabetes **44**(12): 1399-1404.
Kumar, U., R. Sasi, et al. (1999). "Subtype-selective expression of the five somatostatin receptors (hSSTR1-5) in human pancreatic islet cells: a quantitative double-label immunohistochemical analysis." Diabetes **48**(1): 77-85.
Kurose, T., Y. Seino, et al. (1990). "Mechanism of sympathetic neural regulation of insulin, somatostatin, and glucagon secretion." Am J Physiol **258**(1 Pt 1): E220-227.
Kurose, T., K. Tsuda, et al. (1992). "Glucagon, insulin and somatostatin secretion in response to sympathetic neural activation in streptozotocin-induced diabetic rats. A study with the isolated perfused rat pancreas in vitro." Diabetologia **35**(11): 1035-1041.
Lam, A. J., F. St-Pierre, et al. (2012). "Improving FRET dynamic range with bright green and red fluorescent proteins." Nat Methods **9**(10): 1005-1012.
Landa, L. R., Jr., M. Harbeck, et al. (2005). "Interplay of Ca2+ and cAMP signaling in the insulin-secreting MIN6 beta-cell line." J Biol Chem **280**(35): 31294-31302.
Lavis, L. D. and R. T. Raines (2008). "Bright ideas for chemical biology." Acs Chemical Biology **3**(3): 142-155.
Le Marchand, S. J. and D. W. Piston (2010). "Glucose suppression of glucagon secretion: metabolic and calcium responses from alpha-cells in intact mouse pancreatic islets." J Biol Chem **285**(19): 14389-14398.
Le Marchand, S. J. and D. W. Piston (2012). "Glucose decouples intracellular Ca2+ activity from glucagon secretion in mouse pancreatic islet alpha-cells." PLoS One **7**(10): e47084.
Leavens, K. F. and M. J. Birnbaum (2011). "Insulin signaling to hepatic lipid metabolism in health and disease." Crit Rev Biochem Mol Biol **46**(3): 200-215.
Lee, J. K., S. Lu, et al. (2010). "Real-Time dynamics of Ca2+, caspase-3/7, and morphological changes in retinal ganglion cell apoptosis under elevated pressure." PLoS One **5**(10): e13437.
Leevers, S. J. (2001). "Growth control: invertebrate insulin surprises!" Curr Biol **11**(6): R209-212.
Leung, Y. M., I. Ahmed, et al. (2005). "Electrophysiological characterization of pancreatic islet cells in the mouse insulin promoter-green fluorescent protein mouse." Endocrinology **146**(11): 4766-4775.
Li, G., R. Margueron, et al. "Highly compacted chromatin formed in vitro reflects the dynamics of transcription activation in vivo." Mol Cell **38**(1): 41-53.
Li, J., R. Luo, et al. (2004). "Novel regulation by Rac1 of glucose- and forskolin-induced insulin secretion in INS-1 beta-cells." Am J Physiol Endocrinol Metab **286**(5): E818-827.
Li, N., B. Li, et al. (2012). "NADPH oxidase NOX2 defines a new antagonistic role for reactive oxygen species and cAMP/PKA in the regulation of insulin secretion." Diabetes **61**(11): 2842-2850.
Liljenquist, J. E., J. D. Bomboy, et al. (1974). "Effect of glucagon on net splanchnic cyclic AMP production in normal and diabetic men." J Clin Invest **53**(1): 198-204.
Liljenquist, J. E., J. D. Bomboy, et al. (1974). "Effects of glucagon on lipolysis and ketogenesis in normal and diabetic men." J Clin Invest **53**(1): 190-197.
Limaye, V. S., S. Lester, et al. (2010). "Idiopathic inflammatory myositis is associated with a high incidence of hypertension and diabetes mellitus." Int J Rheum Dis **13**(2): 132-137.
Lin, M. Z., Miyawaki, A., Tsien, R.Y. (2010). "Fluorescent proteins illuminate cell biology." Nat. Rev. Mol Cell Biol **11**(10).
Lindskog, S., B. E. Dunning, et al. (1990). "Galanin of the homologous species inhibits insulin secretion in the rat and in the pig." Acta Physiol Scand **139**(4): 591-596.
Liu, Y. J., E. Vieira, et al. (2004). "A store-operated mechanism determines the activity of the electrically excitable glucagon-secreting pancreatic alpha-cell." Cell Calcium **35**(4): 357-365.

Lopez-Menduina, M., A. I. Martin, et al. (2010). "Systemic IGF-I administration attenuates the inhibitory effect of chronic arthritis on gastrocnemius mass and decreases atrogin-1 and IGFBP-3." Am J Physiol Regul Integr Comp Physiol **299**(2): R541-551.
Luche, H., O. Weber, et al. (2007). "Faithful activation of an extra-bright red fluorescent protein in "knock-in" Cre-reporter mice ideally suited for lineage tracing studies." Eur J Immunol **37**(1): 43-53.
Luciani, D. S., K. S. Gwiazda, et al. (2009). "Roles of IP3R and RyR Ca2+ channels in endoplasmic reticulum stress and beta-cell death." Diabetes **58**(2): 422-432.
Lupien, M., J. Eeckhoute, et al. (2008). "FoxA1 translates epigenetic signatures into enhancer-driven lineage-specific transcription." Cell **132**(6): 958-970.
Lynn, F. C., N. Pamir, et al. (2001). "Defective glucose-dependent insulinotropic polypeptide receptor expression in diabetic fatty Zucker rats." Diabetes **50**(5): 1004-1011.
Ma, X., Y. Zhang, et al. (2005). "Glucagon stimulates exocytosis in mouse and rat pancreatic alpha-cells by binding to glucagon receptors." Mol Endocrinol **19**(1): 198-212.
MacDonald, P. E., Y. Z. De Marinis, et al. (2007). "A K ATP channel-dependent pathway within alpha cells regulates glucagon release from both rodent and human islets of Langerhans." PLoS Biol **5**(6): e143.
Madsbad, S. (2009). "Exenatide and liraglutide: different approaches to develop GLP-1 receptor agonists (incretin mimetics)--preclinical and clinical results." Best Pract Res Clin Endocrinol Metab **23**(4): 463-477.
Marks, V., K. S. Tan, et al. (1990). "Intra-islet cellular interrelationships." Biochem Soc Trans **18**(1): 103-104.
Maruyama, H., A. Hisatomi, et al. (1984). "Insulin within islets is a physiologic glucagon release inhibitor." J Clin Invest **74**(6): 2296-2299.
Mathis, D., L. Vence, et al. (2001). "beta-Cell death during progression to diabetes." Nature **414**(6865): 792-798.
Matsuoka, H., Y. Kosai, et al. (2002). "Single-cell viability assessment with a novel spectro-imaging system." J Biotechnol **94**(3): 299-308.
Matusik, R. J., R. J. Jin, et al. (2008). "Prostate epithelial cell fate." Differentiation; research in biological diversity **76**(6): 682-698.
Mauriege, P., W. M. Klein Kranenbarg, et al. (1996). "Insulin and glucagon responses to adrenaline infusion in abdominal obese men." Int J Obes Relat Metab Disord **20**(7): 668-676.
McCulloch, L. J., M. van de Bunt, et al. (2011). "GLUT2 (SLC2A2) is not the principal glucose transporter in human pancreatic beta cells: implications for understanding genetic association signals at this locus." Mol Genet Metab **104**(4): 648-653.
Michael, M. D., R. N. Kulkarni, et al. (2000). "Loss of insulin signaling in hepatocytes leads to severe insulin resistance and progressive hepatic dysfunction." Mol Cell **6**(1): 87-97.
Miller, R. A., Q. Chu, et al. (2013). "Biguanides suppress hepatic glucagon signalling by decreasing production of cyclic AMP." Nature **494**(7436): 256-260.
Mirosevich, J., N. Gao, et al. (2006). "Expression and role of Foxa proteins in prostate cancer." Prostate **66**(10): 1013-1028.
Momboisse, F., S. Ory, et al. (2010). "The Rho guanine nucleotide exchange factors Intersectin 1L and beta-Pix control calcium-regulated exocytosis in neuroendocrine PC12 cells." Cell Mol Neurobiol **30**(8): 1327-1333.
Morgan, D. G., R. N. Kulkarni, et al. (1998). "Inhibition of glucose stimulated insulin secretion by neuropeptide Y is mediated via the Y1 receptor and inhibition of adenylyl cyclase in RIN 5AH rat insulinoma cells." Diabetologia **41**(12): 1482-1491.
Motta, P. M., G. Macchiarelli, et al. (1997). "Histology of the exocrine pancreas." Microsc Res Tech **37**(5-6): 384-398.
Mounier, C. and B. I. Posner (2006). "Transcriptional regulation by insulin: from the receptor to the gene." Can J Physiol Pharmacol **84**(7): 713-724.
Muller, D., G. C. Huang, et al. (2007). "Gene expression heterogeneity in human islet endocrine cells in vitro: the insulin signalling cascade." Diabetologia **50**(6): 1239-1242.

Murtagh, J., F. Martin, et al. (2003). "The Nuclear Factor I (NFI) gene family in mammary gland development and function." J Mammary Gland Biol Neoplasia **8**(2): 241-254.
Nagai, T. and A. Miyawaki (2004). "A high-throughput method for development of FRET-based indicators for proteolysis." Biochem Biophys Res Commun **319**(1): 72-77.
Nagai, T., A. Sawano, et al. (2001). "Circularly permuted green fluorescent proteins engineered to sense Ca2+." Proc Natl Acad Sci U S A **98**(6): 3197-3202.
Neves, S. R., P. T. Ram, et al. (2002). "G protein pathways." Science **296**(5573): 1636-1639.
Newgard, C. B. and J. D. McGarry (1995). "Metabolic coupling factors in pancreatic beta-cell signal transduction." Annu Rev Biochem **64**: 689-719.
Nicolson, T. J., E. A. Bellomo, et al. (2009). "Insulin storage and glucose homeostasis in mice null for the granule zinc transporter ZnT8 and studies of the type 2 diabetes-associated variants." Diabetes **58**(9): 2070-2083.
Nie, J., B. N. Lilley, et al. (2013). "SAD-A potentiates glucose-stimulated insulin secretion as a mediator of glucagon-like peptide 1 response in pancreatic beta cells." Mol Cell Biol **33**(13): 2527-2534.
Nie, J., C. Sun, et al. (2012). "Synapses of amphids defective (SAD-A) kinase promotes glucose-stimulated insulin secretion through activation of p21-activated kinase (PAK1) in pancreatic beta-Cells." J Biol Chem **287**(31): 26435-26444.
Norquay, L. D., X. Yang, et al. (2006). "Hepatocyte nuclear factor-3alpha binding at P sequences of the human growth hormone locus is associated with pituitary repressor function." Mol Endocrinol **20**(3): 598-607.
Noyes, B. E., F. N. Katz, et al. (1995). "Identification and expression of the Drosophila adipokinetic hormone gene." Mol Cell Endocrinol **109**(2): 133-141.
Nyman, L. R., E. Ford, et al. (2010). "Glucose-dependent blood flow dynamics in murine pancreatic islets in vivo." Am J Physiol Endocrinol Metab **298**(4): E807-814.
Nyman, L. R., K. S. Wells, et al. (2008). "Real-time, multidimensional in vivo imaging used to investigate blood flow in mouse pancreatic islets." J Clin Invest **118**(11): 3790-3797.
Olsen, H. L., S. Theander, et al. (2005). "Glucose stimulates glucagon release in single rat alpha-cells by mechanisms that mirror the stimulus-secretion coupling in beta-cells." Endocrinology **146**(11): 4861-4870.
Ong, S. H. and A. L. Steiner (1977). "Localization of cyclic GMP and cyclic AMP in cardiac and skeletal muscle: immunocytochemical demonstration." Science **195**(4274): 183-185.
Ortez, R. A. (1978). "A semi quantitative method for cyclic nucleotide localization by immunocytochemistry and its application in determining the distribution of cyclic AMP in lungs of normal and pertussis-vaccinated mice following histamine or epinephrine challenge." J Cyclic Nucleotide Res **4**(4): 233-244.
Pederson, R. A. and J. C. Brown (1978). "Interaction of gastric inhibitory polypeptide, glucose, and arginine on insulin and glucagon secretion from the perfused rat pancreas." Endocrinology **103**(2): 610-615.
Pinaud, F., X. Michalet, et al. (2006). "Advances in fluorescence imaging with quantum dot bio-probes." Biomaterials **27**(9): 1679-1687.
Piston, D. W. and G. J. Kremers (2007). "Fluorescent protein FRET: the good, the bad and the ugly." Trends Biochem Sci **32**(9): 407-414.
Powers, A. C., S. Efrat, et al. (1990). "Proglucagon processing similar to normal islets in pancreatic alpha-like cell line derived from transgenic mouse tumor." Diabetes **39**(4): 406-414.
Poykko, S. M., O. Ukkola, et al. (2005). "The negative association between plasma ghrelin and IGF-I is modified by obesity, insulin resistance and type 2 diabetes." Diabetologia **48**(2): 309-316.
Prevention, C. f. D. C. a. (2011). National Diabetes Fact Sheet: national estimates and general information on diabetes and prediabetes in the United States. Atlanta, GA. Department of Health and Human Services, Centers for Disease Control and Prevention.
Pyne, N. J. and B. L. Furman (2003). "Cyclic nucleotide phosphodiesterases in pancreatic islets." Diabetologia **46**(9): 1179-1189.

Quesada, I., M. G. Todorova, et al. (2006). "Glucose induces opposite intracellular Ca2+ concentration oscillatory patterns in identified alpha- and beta-cells within intact human islets of Langerhans." Diabetes **55**(9): 2463-2469.
Quesada, I., M. G. Todorova, et al. (2006). "Different metabolic responses in alpha-, beta-, and delta-cells of the islet of Langerhans monitored by redox confocal microscopy." Biophys J **90**(7): 2641-2650.
Quesada, I., E. Tuduri, et al. (2008). "Physiology of the pancreatic alpha-cell and glucagon secretion: role in glucose homeostasis and diabetes." J Endocrinol **199**(1): 5-19.
Quoix, N., R. Cheng-Xue, et al. (2009). "Glucose and pharmacological modulators of ATP-sensitive K+ channels control [Ca2+]c by different mechanisms in isolated mouse alpha-cells." Diabetes **58**(2): 412-421.
Ramracheya, R., C. Ward, et al. (2010). "Membrane potential-dependent inactivation of voltage-gated ion channels in alpha-cells inhibits glucagon secretion from human islets." Diabetes **59**(9): 2198-2208.
Ravier, M. A., M. Guldenagel, et al. (2005). "Loss of connexin36 channels alters beta-cell coupling, islet synchronization of glucose-induced Ca2+ and insulin oscillations, and basal insulin release." Diabetes **54**(6): 1798-1807.
Ravier, M. A. and G. A. Rutter (2005). "Glucose or insulin, but not zinc ions, inhibit glucagon secretion from mouse pancreatic alpha-cells." Diabetes **54**(6): 1789-1797.
Rhodes, C. J. and P. A. Halban (1987). "Newly synthesized proinsulin/insulin and stored insulin are released from pancreatic B cells predominantly via a regulated, rather than a constitutive, pathway." J Cell Biol **105**(1): 145-153.
Rizzo, M. A., M. W. Davidson, et al. (2009). "Fluorescent Protein Tracking and Detection: Fluorescent Protein Structure and Color Variants." Cold Spring Harbor Protocols **2009**(12): pdb.top63.
Rizzo, M. A. and D. W. Piston (2005). "High-contrast imaging of fluorescent protein FRET by fluorescence polarization microscopy." Biophys J **88**(2): L14-16.
Rizzo, M. A., G. Springer, et al. (2006). "Optimization of pairings and detection conditions for measurement of FRET between cyan and yellow fluorescent proteins." Microsc Microanal **12**(3): 238-254.
Robertson, R. P., J. Harmon, et al. (2003). "Glucose toxicity in beta-cells: type 2 diabetes, good radicals gone bad, and the glutathione connection." Diabetes **52**(3): 581-587.
Rocheleau, J. V., G. M. Walker, et al. (2004). "Microfluidic glucose stimulation reveals limited coordination of intracellular Ca2+ activity oscillations in pancreatic islets." Proc Natl Acad Sci U S A **101**(35): 12899-12903.
Rodriguez-Diaz, R., R. Dando, et al. (2011). "Alpha cells secrete acetylcholine as a non-neuronal paracrine signal priming beta cell function in humans." Nat Med **17**(7): 888-892.
Rorsman, P., S. A. Salehi, et al. (2008). "K(ATP)-channels and glucose-regulated glucagon secretion." Trends Endocrinol Metab **19**(8): 277-284.
Ross-Innes, C. S., R. Stark, et al. (2012). "Differential oestrogen receptor binding is associated with clinical outcome in breast cancer." Nature **481**(7381): 389-393.
Salehi, A., E. Vieira, et al. (2006). "Paradoxical stimulation of glucagon secretion by high glucose concentrations." Diabetes **55**(8): 2318-2323.
Schlegel, N. and J. Waschke (2009). "VASP is involved in cAMP-mediated Rac 1 activation in microvascular endothelial cells." Am J Physiol Cell Physiol **296**(3): C453-462.
Schuit, F., A. De Vos, et al. (1997). "Metabolic fate of glucose in purified islet cells. Glucose-regulated anaplerosis in beta cells." J Biol Chem **272**(30): 18572-18579.
Schuit, F. C., M. P. Derde, et al. (1989). "Sensitivity of rat pancreatic A and B cells to somatostatin." Diabetologia **32**(3): 207-212.
Schwetz, T. A., A. Ustione, et al. (2013). "Neuropeptide Y and somatostatin inhibit insulin secretion through different mechanisms." Am J Physiol Endocrinol Metab **304**(2): E211-221.
Seidner, G., M. G. Alvarez, et al. (1998). "GLUT-1 deficiency syndrome caused by haploinsufficiency of the blood-brain barrier hexose carrier." Nat Genet **18**(2): 188-191.

Sekine, N., V. Cirulli, et al. (1994). "Low lactate dehydrogenase and high mitochondrial glycerol phosphate dehydrogenase in pancreatic beta-cells. Potential role in nutrient sensing." J Biol Chem **269**(7): 4895-4902.
Sharma, N. L., C. E. Massie, et al. (2013). "The androgen receptor induces a distinct transcriptional program in castration-resistant prostate cancer in man." Cancer cell **23**(1): 35-47.
Shibutani, Y., S. Asahara, et al. (2013). "Constitutive activation of Rac1 in pancreatic beta cells facilitates F-actin depolymerization but exerts no influence on the increase of pancreatic beta cell mass and facilitation of insulin secretion." Kobe J Med Sci **59**(3): E72-80.
Shiota, C., J. V. Rocheleau, et al. (2005). "Impaired glucagon secretory responses in mice lacking the type 1 sulfonylurea receptor." Am J Physiol Endocrinol Metab **289**(4): E570-577.
Singh, S., H. Y. Chang, et al. (2013). "Glucagonlike peptide 1-based therapies and risk of hospitalization for acute pancreatitis in type 2 diabetes mellitus: a population-based matched case-control study." JAMA Intern Med **173**(7): 534-539.
Soriano, P. (1999). "Generalized lacZ expression with the ROSA26 Cre reporter strain." Nat Genet **21**(1): 70-71.
Spector, A. A. (1975). "Fatty acid binding to plasma albumin." J Lipid Res **16**(3): 165-179.
Starke, A., T. Imamura, et al. (1987). "Relationship of glucagon suppression by insulin and somatostatin to the ambient glucose concentration." J Clin Invest **79**(1): 20-24.
Steele-Perkins, G., K. G. Butz, et al. (2003). "Essential role for NFI-C/CTF transcription-replication factor in tooth root development." Mol Cell Biol **23**(3): 1075-1084.
Strowski, M. Z., R. M. Parmar, et al. (2000). "Somatostatin inhibits insulin and glucagon secretion via two receptors subtypes: an in vitro study of pancreatic islets from somatostatin receptor 2 knockout mice." Endocrinology **141**(1): 111-117.
Syeda, K., A. M. Mohammed, et al. (2013). "Glucotoxic conditions induce endoplasmic reticulum stress to cause caspase 3 mediated lamin B degradation in pancreatic beta-cells: protection by nifedipine." Biochem Pharmacol **86**(9): 1338-1346.
Taniguchi, C. M., B. Emanuelli, et al. (2006). "Critical nodes in signalling pathways: insights into insulin action." Nat Rev Mol Cell Biol **7**(2): 85-96.
Taylor, C. R. and R. M. Levenson (2006). "Quantification of immunohistochemistry--issues concerning methods, utility and semiquantitative assessment II." Histopathology **49**(4): 411-424.
Theodorakis, M. J., O. Carlson, et al. (2004). "Elevated plasma glucose-dependent insulinotropic polypeptide associates with hyperinsulinemia in impaired glucose tolerance." Diabetes Care **27**(7): 1692-1698.
Thiebaud, D., E. Jacot, et al. (1982). "The effect of graded doses of insulin on total glucose uptake, glucose oxidation, and glucose storage in man." Diabetes **31**(11): 957-963.
Tian, G., S. Sandler, et al. (2011). "Glucose- and hormone-induced cAMP oscillations in alpha- and beta-cells within intact pancreatic islets." Diabetes **60**(5): 1535-1543.
Tian, L., S. A. Hires, et al. (2009). "Imaging neural activity in worms, flies and mice with improved GCaMP calcium indicators." Nat Methods **6**(12): 875-881.
Tolman, K. G., V. Fonseca, et al. (2007). "Spectrum of liver disease in type 2 diabetes and management of patients with diabetes and liver disease." Diabetes Care **30**(3): 734-743.
Tornehave, D., P. Kristensen, et al. (2008). "Expression of the GLP-1 receptor in mouse, rat, and human pancreas." J Histochem Cytochem **56**(9): 841-851.
Truong, T. V., W. Supatto, et al. (2011). "Deep and fast live imaging with two-photon scanned light-sheet microscopy." Nat Methods **8**(9): 757-760.
Tschritter, O., M. Stumvoll, et al. (2002). "The prevalent Glu23Lys polymorphism in the potassium inward rectifier 6.2 (KIR6.2) gene is associated with impaired glucagon suppression in response to hyperglycemia." Diabetes **51**(9): 2854-2860.
Tuduri, E., E. Filiputti, et al. (2008). "Inhibition of Ca2+ signaling and glucagon secretion in mouse pancreatic alpha-cells by extracellular ATP and purinergic receptors." Am J Physiol Endocrinol Metab **294**(5): E952-960.

Unger, R. H. and A. D. Cherrington (2012). "Glucagonocentric restructuring of diabetes: a pathophysiologic and therapeutic makeover." J Clin Invest **122**(1): 4-12.
Unger, R. H. and L. Orci (1975). "The essential role of glucagon in the pathogenesis of diabetes mellitus." Lancet **1**(7897): 14-16.
Unger, R. H. and L. Orci (2010). "Paracrinology of islets and the paracrinopathy of diabetes." Proceedings of the National Academy of Sciences of the United States of America **107**(37): 16009-16012.
van de Schepop, H. A., J. S. de Jong, et al. (1996). "Counting of apoptotic cells: a methodological study in invasive breast cancer." Clin Mol Pathol **49**(4): M214-217.
Veluthakal, R., S. V. Madathilparambil, et al. (2009). "Regulatory roles for Tiam1, a guanine nucleotide exchange factor for Rac1, in glucose-stimulated insulin secretion in pancreatic beta-cells." Biochem Pharmacol **77**(1): 101-113.
Vieira, E., A. Salehi, et al. (2007). "Glucose inhibits glucagon secretion by a direct effect on mouse pancreatic alpha cells." Diabetologia **50**(2): 370-379.
Vikram, A. and G. Jena (2010). "S961, an insulin receptor antagonist causes hyperinsulinemia, insulin-resistance and depletion of energy stores in rats." Biochem Biophys Res Commun **398**(2): 260-265.
Wang, Q., W. Li, et al. (2007). "A hierarchical network of transcription factors governs androgen receptor-dependent prostate cancer growth." Mol Cell **27**(3): 380-392.
Wang, Q., B. Shui, et al. (2008). "Structural basis for calcium sensing by GCaMP2." Structure **16**(12): 1817-1827.
Wang, Z., E. Oh, et al. (2007). "Glucose-stimulated Cdc42 signaling is essential for the second phase of insulin secretion." J Biol Chem **282**(13): 9536-9546.
Watanabe, K., K. Kobayashi, et al. (2013). "Sitagliptin improves postprandial hyperglycemia by inhibiting glucagon secretion in Werner syndrome with diabetes." Diabetes Care **36**(8): e119.
Wong, Y. W., C. Schulze, et al. (2007). "Gene expression analysis of nuclear factor I-A deficient mice indicates delayed brain maturation." Genome Biol **8**(5): R72.
Wraith, J. E. (1989). "Diagnosis and management of inborn errors of metabolism." Arch Dis Child **64**(10 Spec No): 1410-1415.
Wu, Y., P. Wawrzusin, et al. (2013). "Spatially isotropic four-dimensional imaging with dual-view plane illumination microscopy." Nat Biotechnol **31**(11): 1032-1038.
Wu, Y. I., D. Frey, et al. (2009). "A genetically encoded photoactivatable Rac controls the motility of living cells." Nature **461**(7260): 104-108.
Xu, E., M. Kumar, et al. (2006). "Intra-islet insulin suppresses glucagon release via GABA-GABAA receptor system." Cell Metab **3**(1): 47-58.
Yajima, H., M. Komatsu, et al. (2001). "Norepinephrine inhibits glucose-stimulated, Ca2+-independent insulin release independently from its action on adenylyl cyclase." Endocr J **48**(6): 647-654.
Yoshimoto, Y., Y. Fukuyama, et al. (1999). "Somatostatin induces hyperpolarization in pancreatic islet alpha cells by activating a G protein-gated K+ channel." FEBS Lett **444**(2-3): 265-269.
Yu, Y. H. and H. N. Ginsberg (2005). "Adipocyte signaling and lipid homeostasis: sequelae of insulin-resistant adipose tissue." Circ Res **96**(10): 1042-1052.
Yue, J. T., E. Burdett, et al. (2012). "Somatostatin receptor type 2 antagonism improves glucagon and corticosterone counterregulatory responses to hypoglycemia in streptozotocin-induced diabetic rats." Diabetes **61**(1): 197-207.
Zariwala, H. A., B. G. Borghuis, et al. (2012). "A Cre-dependent GCaMP3 reporter mouse for neuronal imaging in vivo." J Neurosci **32**(9): 3131-3141.
Zhang, C. L., M. Katoh, et al. (2009). "The cAMP sensor Epac2 is a direct target of antidiabetic sulfonylurea drugs." Science **325**(5940): 607-610.
Zhang, M., H. Q. Zhang, et al. (2000). "Effect of Bcl-2 and caspase-3 on calcium distribution in apoptosis of HL-60 cells." Cell Res **10**(3): 213-220.
Zhang, Q., R. Ramracheya, et al. (2013). "Role of KATP channels in glucose-regulated glucagon secretion and impaired counterregulation in type 2 diabetes." Cell Metab **18**(6): 871-882.

Zimmermann, T. (2005). "Spectral imaging and linear unmixing in light microscopy." Adv Biochem Eng Biotechnol **95**: 245-265.
Zmuda-Trzebiatowska, E., A. Oknianska, et al. (2006). "Role of PDE3B in insulin-induced glucose uptake, GLUT-4 translocation and lipogenesis in primary rat adipocytes." Cell Signal **18**(3): 382-390.